MITIGATION OF EARTHQUAKE INDUCED GEOTECHNICAL HAZARDS USING TIRE WASTE-SAND MIXTURES

by

Korhan Adır

B.S., Civil Engineering, Boğaziçi University, 2008

Submitted to the Kandilli Observatory and Earthquake

Research Institute in partial fulfillment of

the requirements for the degree of

Master of Science

Graduate Program in Earthquake Engineering

Boğaziçi University

2013

MITIGATION OF EARTHQUAKE INDUCED GEOTECHNICAL HAZARDS USING TIRE WASTE-SAND MIXTURES

APPROVED BY:

Assoc. Prof. Dr. Ayse Edinçliler .....

(Thesis Supervisor)

Prof. Dr. Mustafa Erdik .....

Prof. Dr. Ayfer Erken .....

DATE OF APPROVAL: 07.06.2013

ACKNOWLEDGEMENTS

Foremost, I would like to thank my thesis supervisor Assoc. Prof. Dr. Ayşe Edinçliler, for her continuous support from the beginning of my masters' education at the first place, and for her guidance during my thesis study.

I would like to thank my committee members Prof. Dr. Mustafa Erdik, and Prof. Dr. Ayfer Erken for their contributions and guidances.

I would like to thank Prof. Dr. Hing-Ho Tsang for his great supports.

Finally, I would like to thank all of my family and friends who stood behind me during my study.

ABSTRACT

MITIGATION OF EARTHQUAKE INDUCED GEOTECHNICAL HAZARDS USING TIRE WASTE-SAND MIXTURES

Seismic Isolation Systems are among tools to achieve advanced earthquake-resistant designs, developed in last century. Commonly, the applications are seen in cases which it is aimed to stabilize structures considered to have critical and expensive content in front of a strong ground motion. Recently, an alternative technique for seismic protection had been proposed involving mixing soil with tire waste and so improving the mixture's dynamic properties, than placing it around structures foundations. This soil improvement called as Geotechnical Seismic Isolation (GSI) is supposed to improve especially damping property. It is claimed that, when placed to underlying soil layer of a structure subject to seismic movement, it would level down the soil's seismic movement transmittancy.

This study investigates the applicability of GSI with numerical analysis. Reprocessed Tire Waste-Sand Mixtures (TWSM) from Tire Buffings and Tire Crumbs; of which, mechanical and dynamic properties were revealed for different mixing proportions; are chosen as GSI material alternatives. A finite element program developed as a plug-in on QUAD4M, Equivalent Linear Analysis (ELA) Software, able to model structure-subsoil system is used to perform numerical analyses with the TWSM experimental data. In the results of numerical analyses, TWSM use as GSI material is examined regarding the effect of structure's number of storey, weight ratio of tire crumb over TWSM, different earthquake records, changing TWSM layer thickness, and pile foundation.

During analysis, different earthquake records have been applied to TWSM-structure systems differed in reinforced concrete structure rise (low-medium), and soil layer; different depths of TWSM and pile foundation. Reduction of acceleration motions of rigid structure and inter-storey drift are selected as performance indicators. Results are investigated to reveal the effect of TW inclusion to earthquake induced soil standing under a low-medium rise structure and to comment the functionality of the use of improved soil as geotechnical seismic isolation.

ÖZET

DEPREM SIRASINDA OLUŞAN GEOTEKNİK HASARLARIN ATIK-LASTİK KUM KARIŞIMLARI KULLANILARAK AZALTILMASI

Sismik izolasyon, geçen yüzyılın başından itibaren gelişmekte olan ileri seviyede depreme dayanıklı yapı tasarımı tekniklerinden biridir. Temelde; yapının sismik aktiviteler karşısında indirgenmiş yapısal sismik tepkiler vermesini amaçlamaktadır. Genel olarak, olası deprem hareketi sonucunda kritik performans gösterecek ya da deprem riskinin minimumda tutulması gerekli yapılarda uygulamaları görülmektedir. Yakın dönemde, atık lastik karıştırılarak dinamik özellikleri iyileştirilmiş zeminin, bina temelinin etrafına yerleştirilmesi alternatif bir sismik izolasyon tekniği olarak önerilmiştir. Sözü edilen iyileştirmede, zeminin özellikle sönüm kapasitesinin artacağı ve bu sayede sismik hareket geçirgenliğinin azalacağı varsayılmaktadır. Bu çalışma yukarıda kısaca anlatılmış alternatif geoteknik sismik izolasyon tekniğinin geçerliliğini, sismik performans yönünden incelemektedir.

Atık lastiğin tekrar işlenmesi ile elde edilmiş malzeme, Silivri Kumu olarak bilinen kum numunesine karıştırılmıştır. Bu sayede elde edilen lastik-kum karışımı laboratuarda bir dizi testten geçirilmiş ve mekanik özellikleri saptanmıştır. Daha da önemlisi dinamik laboratuar testleri ile kayma modülü ve sönüm oranı bulunmuştur. Statik ve dinamik özellikleri saptanan lastik atık-kum karışımı, QUAD4M üzerine kurulu bilgisayar programı yolu ile nümerik analizleri gerçekleştirilmiştir. Bu analizler; farklı deprem kayıtları ve az-orta katlı betonarme binalar kullanılarak çeşitlendirilmiştir. Analiz sonuçları; yapıya gelen ivmelerin, çatı, temel ve birinci kat kaymalarının zaman grafiklerini içermektedir. Yukarıda anlatılan atık lastik-kum karışımının, binaların temelinin altına yerleştirilip geoteknik sismik izolasyon malzemesi olarak kullanılması, nümerik analiz sonuçlarındaki sismik performans kriterlerine göre incelenmiştir.

TABLE OF CONTENTS

ACKNOWLEDGEMENTS iii

ABSTRACT iv

ÖZET v

LIST OF FIGURES x

LIST OF TABLES xv

LIST OF SYMBOLS xvii

LIST OF ACRONYMS/ABBREVIATIONS xix

1. INTRODUCTION 1

1.1. General 2

1.2. Problem Statement 3

1.3. Objective of the Thesis 3

1.4. Organization of Thesis 4

2. SCRAP TIRES AND THEIR APPLICATIONS 5

2.1. General Information 5

2.2. Material Properties 8

2.2.1. Different Particulate Rubbers 8

2.2.2. Physical and Mechanical Properties 8

2.2.3. Dynamic Properties 12

2.2.4. Chemical Properties 14

2.2.5. Constructional Aspects 15

2.3. Tire Waste Utilization Fields 17

2.3.1. Ground Rubber Applications 18

2.3.2. Civil Engineering Applications 18

2.3.3. Rubber-Soil Mixture Use as Base Isolation Material 21

3. SEISMIC BASE ISOLATION SYSTEMS 23
3.1. Basic Approach and Purposes 23
3.2. A Glance to Applications Following Chronology 25
3.2.1. Sliding Bearings 26
3.2.2. Elastomeric Bearings 31
3.3. Recent Investigations 38
3.3.1. Geosynthetic Material as Base Isolation 38
3.3.2. Numerical Analyses of Improved Soils with Rubbers as Base Isolation 48
4. THE NUMERICAL MODELING THEORY 52
4.1. Modeling in Engineering and Different Modeling Techniques 52
4.2. Physical (Scale) Modeling 56
4.2.1. Centrifuge Model Tests 57
4.2.2. Shaking Table Model Tests 59
4.3. Numerical Modeling and QUAD4M 61
4.3.1. Equivalent Linear Approach (ELA) 62
4.3.2. Finite Element Method, the Theory 64
4.3.3. Soil Modeling 65
4.3.4. Super Structure Modeling 66
4.3.5. Time Domain Motion Equation 68
4.3.6. Damping Matrix 68
4.3.7. Global Matrices 70
4.3.8. Soil – Structure Interaction 70
4.3.9. Transmitting Boundary 72
4.3.10. Time Integration, Newmark Family Method 73
4.3.11. Trapezoidal Rule 74
4.4. Experimental and Numerical Modeling Applications 75

5. STUDY PROGRAM 79
5.1. General Information 79
5.2. TWSM Static and Dynamic Properties Evaluation 80
5.2.1. Static Properties of TWSM 81
5.2.2. Dynamic Properties of TWSM 90
5.2.3. Modulus and Damping Characteristics of TWSM 91
5.2.4. Normalized Shear Modulus (G / G_{max}) 98
5.3. Proper GSI Material Selection and adoption to Numerical Analysis 101
5.3.1. Possible Methodologies to Extrapolate Data, Hyperbolic Model 102
5.3.2. Elongated Curve Plots, Comparison in the Darendeli Model 106
5.4. Adapting Structures in Numerical Analysis 111
5.4.1. Setting and Adapting Soil Sample Data for Numerical Analysis 114
5.4.2. Choosing Earthquake Records for Numerical Analysis 115
5.5. Numerical Analyses Study Program 116
6. NUMERICAL RESULTS 120
6.1. Brief Information on Numerical Analysis with QUAD4M 120
6.2. Case 1; TCS30 as GSI Material Underneath a 4-storey Reinforced Concrete Building 121
6.3. Case 2; TCS10 as GSI Material Underneath an 8-storey Reinforced Concrete Building 122
6.4. Case 3; TCS20 as GSI Material Underneath an 8-storey Reinforced Concrete Building 125
6.5. Case 4; TCS30 as GSI Material Underneath an 8-storey Reinforced Concrete Building 128
6.6. Case 5; TCS30 as GSI Material Underneath an 8-storey Structure with Pile ... 131
6.7. Case 6; TCS30 as GSI Material Underneath a 12-storey Structure with Pile ... 133
6.8. Case 7; TCS30 as GSI Material Underneath a 12-storey Structure with Pile ... 134

6.9. Case 8; TCS30 as GSI Material Underneath an 18-storey Structure with Pile. 135

6.10. Numerical Analyses Results, Discussions 136

7. CONCLUSION AND RECOMMENDATIONS 147

REFERENCES 137

LIST OF FIGURES

Figure 2.1. An example of tire waste stockpile. 5

Figure 2.2. U.S. scrap tire management trends, 2005-2009 (RMA, 2009). 6

Figure 2.3. Millions of scrap tires remaining in U.S. stockpiles, 1990-2009 (RMA, 2009). 7

Figure 2.4. Recycle, reuse or disposal alternatives for scrap tires (UNCTAD secretariat and OECD, 1998). 7

Figure 2.5. Typical shapes of different processed used tires (not to scale) (Edinçliler *et al.*, 2010). 8

Figure 2.6. Compaction test results (Moo-Young *et al.*, 2003). 10

Figure 2.7. Modulus of elasticity vs. confining pressure of sand, tire chip and 50 per cent by volume mixture (Masad *et al.*, 1996). 13

Figure 2.8. Scrap tire market trends, 2005-2009 (RMA, 2009). 18

Figure 2.9. Central governmental building 7.280 m2 building area, 13 floors (Kasumigaseki, Japan, 2002). 21

Figure 2.10. Figurative picture of base isolation with rubber-soil mixture. 22

Figure 3.1. Fixed base and isolated structure response (Kelly *et al.*, 1998). 24

Figure 3.2. Fixed base and isolated structure response (Kelly *et al.*, 1998). 25

Figure 3.3. Diagram of R-FBI (Mostaghel and Khodaverdian, 1987). 27

Figure 3.4. Schematic diagram of SR-F base isolator (Lin Su *et al.*, 1991). 28

Figure 3.5. Teflon disc bearing design (1 in. = 25.4 mm) (Constantinou *et al.*, 1991). . 30

Figure 3.6. Design of isolation rubber bearing (Zhou Fu-Lin *et al.*, 2005). 36

Figure 3.7. Isolation rubber bearing installation (Zhou Fu-Lin *et al.*, 2005). 37

Figure 3.8. Total number of seismically isolated buildings between 1991 – 2006 in Italy (Martinelli *et al.*, 2006). 38

Figure 3.9. Seismic response of a typical building (a) founded on soil, (b) with base isolation, (c) with geosynthetic foundation isolation (Yegian *et al.,* 1994). 40

Figure 3.10. Test results of a rigid block on geotextile interface under earthquake excitation (Northridge Earthquake, 1994) (Yegian *et al.*, 2004). 42

Figure 3.11. Fixed-base isolated structure peak drifts (Yegian *et al.*, 2004).....43

Figure 3.12. Detailed results for cylindrical geosynthetic liner (Yegian *et al.*, 2005). 44

Figure 3.13. Detailed results for trapezoidal geosynthetic liner (Yegian *et al.*, 2005).....45

Figure 3.14. Schematic drawing of the proposed seismic isolation method using a layer of rubber-soil mixture (Tsang *et al*, 2007). 49

Figure 3.15. Finite element model of the geotechnical seismic isolation system with the use of granulated rubber-soil mixtures (Tsang *et al*, 2009). 50

Figure 4.1. Tire chip-seal construction (Wood, 2004). 53

Figure 4.2. Reflective practice loop (Blockley, 1992). 55

Figure 4.3. Beam centrifuge test machine. 58

Figure 4.4. Drum centrifuge test machine. 59

Figure 4.5. Shaking table test machine. 60

Figure 4.6. Laminar shear box (Ueng *et al.*, 2006). 61

Figure 4.7. Iteration toward strain-compatible G and D in equivalent linear analysis (Xuan *et al.*, 2009). 64

Figure 4.8. The finite element model (Xuan *et al.*, 2009). 65

Figure 4.9. The element stiffness matrix. 66

Figure 4.10. The transform matrix.....67

Figure 5.1. TBS D (per cent) vs. γ (per cent) and G (MPa) vs. γ (per cent) curves (Yıldız, 2012). 94

Figure 5.2. TCS D (per cent) vs. γ (per cent) and G (MPa) vs. γ (per cent) curves (Yıldız, 2012). 95

Figure 5.3. D (per cent) vs. γ (per cent) and G (MPa) vs. γ (per cent) curves under 100 kPa σ' (Yıldız, 2012). 97

Figure 5.4. D (per cent) vs. γ (per cent) curves under all levels of σ' relying on CTT series (Yıldız, 2012). 97

Figure 5.5. G/G_{max} curves of samples vs. Darendeli Model, **σ'**=40 kPa. 99

Figure 5.6. G/G_{max} curves of samples vs. Darendeli Model, **σ'**=100 kPa. 100

Figure 5.7. G/G_{max} curves of samples vs. Darendeli Model, **σ'**=200 kPa. 100

Figure 5.8. Reference shear strain. 103

Figure 5.9. Relation between damping ratio and shear modulus ratio. 106

Figure 5.10. Hyperbolic model of G/G_{max} curves and Darendeli Model, σ'=40 kPa. 107

Figure 5.11. Hyperbolic Model of D curves, σ'=40 kPa. 108

Figure 5.12. Hyperbolic model of G/G_{max} curves and the Darendeli Model. 108

Figure 5.13. Hyperbolic model of D curves, σ'=100 kPa. 109

Figure 5.14. Hyperbolic model of G/G_{max} curves and the Darendeli Model. 109

Figure 5.15. Hyperbolic Model of D curves, σ'=200 kPa. 110

Figure 5.16. Soil – structure system, foundation without pile. 112

Figure 5.17. Soil – structure system, foundation with pile. 112

Figure 5.18. Horizontal and vertical response spectra of the above stated earthquake motions. 116

Figure 6.1. Numerical analysis results for case 1 under EQD. 121

Figure 6.2. Numerical analysis results for case 2 under EQE. 123

Figure 6.3. Numerical analysis results for case 2 under EQN. 124

Figure 6.4. Numerical analysis results for case 2 under EQD. 124

Figure 6.5. Numerical analysis results for case 3 under EQD. 127

Figure 6.6. Numerical analysis results for case 3 under EQN. 127

Figure 6.7. Numerical analysis results for case 3 under EQE. 128

Figure 6.8. Numerical analysis results for case 4 under EQE. 130

Figure 6.9. Numerical analysis results for case 3 under EQN. 130

Figure 6.10. Numerical analysis results for case 3 under EQD. 131

Figure 6.11. Numerical analysis results for case 5 under EQD. 132

Figure 6.12. Numerical analysis results for case 6 under EQD. 133

Figure 6.13. Numerical analysis results for case 7 under EQD. 135

Figure 6.14. Numerical analysis results for case eight under EQD. 136

LIST OF TABLES

Table 2.1. Specific gravity and water absortion values (Moo-Young *et al.*, 2003). 9

Table 2.2. Unit weights of scrap tire (WSDOT Report, 2003). 11

Table 2.3. TOC, pH, and turbidity results (Moo-Young *et al.*, 2003). 15

Table 3.1. Base-isolated buildings in California: new construction and seismic retrofit projects (Kelly *et al.*, 1998)..... 33

Table 3.2. Civil buildings and industrial plants provided with antiseismic devices in Italy. Reproduced by permission of GLIS (Martelli *et al.*, 1998). 34

Table 3.3. Base-isolated buildings in Russia and other former USSR countries in 1996 (Martelli *et al.*, 1998). 35

Table 4.1. Characteristics of well-known members of the Newmark family methods (Hughes, 1987). 74

Table 5.1. CBR test results (Çağatay,2008). 82

Table 5.2. DST summary of TWSM (Çagatay, 2008). 83

Table 5.3. Quick triaxial compression test results (Çagatay, 2008)..... 86

Table 5.4. Summary of consolidated drained triaxial tests (Çagatay, 2008). 88

Table 5.5. Specimen physical properties and CTT program (Yıldız, 2012). 93

Table 5.6. Details of earthquake strong-motion data used in the parametric study. ... 116

Table 5.7. Details of earthquake strong-motion data used in the parametric study. ... 117

Table 6.1. Variable inputs used in the parametric study. 139

Table 6.2. Reduction of maximum horizontal peak strain of structure over subsoil. . 143

Table 6.3. Numerical analyses result summary..... 144

Table 6. 4. Numerical analyses comparison with literature. 145

LIST OF SYMBOLS

A	Area of cross section
c	Cohesion of material
C*u*	Coefficient of uniformity
C*c*	Coefficient of concavity
E	Modulus of elasticity
f	Frequency
G	Shear modulus
G_{max}	Maxiumu shear modulus
I	Moment of inertia
L	Length
m	Mass of body
r	Radius
T_i	1st mode of an isolated structure
T_f	1st mode of a fixed base structure
$Ü_g$	Input earthquake
v	velocity (constant)
v_s	shear wave velocity
V_p, V_s	Primary and secondary wave velocity
W_i, W_j	Weight coefficients
ρ	Unit weight of material
γ	Shear strain
γ_{eff}^{1}	Efficient shear strain
б,σ	Mean pressure

σ'	Effective confining pressure
D	Damping ratio
τ	Shear stress
μ	Surface friction coefficient
ω	Angular velocity
[B]	Strain displacement transformation matrix
[C]	Stress-strain matrix
[J]	Jacobian operator matrix
[K]	Element stiffness matrix
[L]	Length matrix
[M]	Mass matrix
[T]	Transformation function matrix
[t]	Time matrix
[ξ]	Damping matrix
R	External force vector
U	Displacement vector
$\mathring{U}$	Velocity vector
$\ddot{U}$	Acceleration vector

LIST OF ACRONYMS / ABBREVIATIONS

ASTM	American society of testing materials
CDTT	Consolidated drained triaxial test
CBR	California bearing ratio
CTT	Cyclic triaxial test
DST	Direct shear test
EDF	Electricité de France
EERC	Earthquake engineering research center
ELA	Equivalent linear analysis
EPA	Environmental protection agency
EQD	Düzce 1997 Earthquake
EQE	El Salvador 2001 Earthquake
EQN	Northridge 1994 Earthquake
FEM	Finite element method
FPS	Friction pendulum system
GLIS	Italian working group on seismic isolation
GSI	Geotechnical seismic isolation
LASDER	Association of rubber industrialists of Turkey
NS	Structure's storey number
QTCT	Quick triaxial compression test
RCT	Resonant column test
RMA	Rubber manufacturers association
R-FBI	Resilient-friction base isolation

R-O	Ramberg-Osgood model
S	Sand
SBI	Seismic base isolation
SIM	Seismic isolation method
SP	Poorly graded sand
SR-F	Sliding resilient-friction base isolation system
TASS	TAISEI shake suppression system
TB	Tire buffings material
TB1	Tire buffings with sizes between 2mm and 4mm
TB2	Tire buffings with the sizes greater than 4mm
TBS	Tire buffings sand mixture
TC	Tire crumbs material
TCS	Tire crumb sand mixture
TW	Tire waste
TWSM	Tire waste sand mixture
UCS	Unified classification system
1-D	One dimensional
2-D	Two dimensional
3-D	Three dimensional

1. INTRODUCTION

This study investigates possible use of Tire Waste Sand Mixtures (TWSM) as Geotechnical Seismic Isolation (GSI) material with numerical analyses. In literature, it exist previous studies with numerical analyses on similar subject but with shredded rubber and soil mixture (RSM) placed underneath different structures' foundations (Tsang *et al.*, 2007; 2009; 2012). All of them were performed with experimental data obtained by Feng and Sutter (2000), in Resonant column tests (RCT) applied on RSM composed from sand and tire shreds. All of the former studies on the mitigation of earthquake hazards using RSM included the use of only one type of tire rubber as GSI material.

As priorly stated (Masad *et al.*, 1996; Edinçliler *et al.*, 2004), RSM static and dynamic properties are influenced by type of rubber, rubber aspect ratio, rubber/sand ratio in the mixture, sand unit weight, confining pressure, other sand and rubber characteristics, and environmental, experimental conditions. Accordingly, a series of laboratory tests is conducted under different normal/confining stresses. During experiments, two different types of tire wastes, fiber shaped tire buffings (TB) and granulated tire crumbs (TC) were mixed with sand in variable ratios to determine the soil properties of the TWSM (Yıldız, 2012; Çağatay, 2008). Furthermore, cyclic triaxial tests (CTT) were executed with same composite material under three different confining pressures (Yıldız, 2012). In this comparative study the static and dynamic test data of TB-Sand (TBS) and TC-Sand (TCS) mixtures with different mixing ratios have been evaluated regarding their dynamic properties to be used as GSI material under low to medium rise reinforced concrete structures. Following, the selected TWSM data is used in numerical simulations with QUAD4M; a dynamic, time domain, equivalent linear, two-dimensional finite element software; capable to do equivalent linear analysis of a soil profile.

This study concerns use of tire crumbs-sand mixtures as GSI around the foundation of low-medium rise structures, under different earthquake ground excitations. The following parts cover present TWSMs' static and dynamic properties evaluation, deciding

to proper GSI material accordingly, input preparation for numerical modeling with QUAD4M and evaluation and discussion of the numerical analyses.

1.1. General

Tire wastes (TW) are evaluated in many different engineering applications due to their convenient engineering properties such as thermal insulation, permeability, compressibility, stiffness and also high damping. A further reason to such convenience is their differentiated sizes and shapes.

In literature, TW were used in geotechnical applications as lightweight fill, embankment fill, and retaining wall backfill recently, a new Seismic Isolation Method (SIM) proposed to use TWSM as GSI material due to its enhanced damping and stiffness properties compared to sand itself. This comparative study investigates numerically the usability of the same methodology in a case of a potential TWSM replacement with sand under low to medium rise structures. In this manner, numerical analyses are conducted with software developed on QUAD4M (Tsang *et al.*, 2010). The behavior of TWSM is measured when used as soil layer placed around a structure's foundation against induced strong earthquake motions. To determine the effect of TWSM on the seismic performance of the structure, different cases were modeled. RSM samples with best damping and stiffness performance were chosen among the available data obtained after experimental studies.

In the model studies, six performance criteria is considered: different earthquake scenarios, number of storey, TWSM layer depth, confining pressure, rubber percentage in TWSM, foundation with/out pile. In total, eight different soil and structure models were analyzed. Results involved first floor inter-story drift; horizontal accelerations at roof and foundation base mid points. Use of TWSM as GSI material, for seismic base isolation is investigated with the analyses of the results considering performance criteria.

1.2. Problem Statement

The basic approach underlying seismic base isolation (SBI) methodology is to reduce the earthquake–generated devastating forces acting upon fixed base structures. Conventional SBI techniques involve different isolation systems such as elastomeric and rubber bearings. Recent studies in literature propose also use of rubber soil mixtures or geosynthetics as geotechnical seismic isolation (GSI) material alternative to SBI. This study concerns the numerical analyses of interacted tire rubber - soil mixture layers underneath reinforced concrete structures subject to strong earthquake movement excitations. Analyses involve a variety of structures differentiated from low to medium rise. Furthermore, soil layers are modeled with TWSM material based on a series of statical and dynamic tests conducted; which is a first time in literature. Numerical results are evaluated regarding the seismic performance of TWSM. It is investigated if TWSM have dynamic properties adequate against strong ground motion excitations as GSI material.

1.3. Objective of the Thesis

This study presents the preliminary research works on a potential seismic isolation method to dissipate earthquake energy, thus reducing structural response and minimizing the potential damage. It is mainly concentrated on potential use of TWSM as GSI material to mitigate earthquake hazardous effects. For this purpose, TWSM samples with best damping and stiffness performance are chosen among the available data obtained after experimental studies. A series of numerical analyses are evaluated on TWSM layer - structure interaction systems with a software based on QUAD4M. Different TWSM subsoil layers; in terms of Tire Waste – Sand mixing proportions; are placed beneath structures, which are differentiated with number of stories and piles under foundations. Their behavior is interpreted in terms of first floor inter-story drift; horizontal accelerations at roof and foundation base mid points, and structural fundamental period change. Effect of TWSM subsoil on the seismic performance of structures was determined. These deductions are reviewed to determine potential use of TWSM as GSI material for foundation isolation.

1.4. Organization of Thesis

This thesis starts with general information about rubber soil mixture's engineering properties and seismic base isolation. The following section continues with detailed explanation of numerical modeling technique subject to study. Further, numerical analysis program is given. Finally, the results are cited with summary information and conclusion of whole study in last section.

2. SCRAP TIRES AND THEIR APPLICATIONS

2.1. General Information

Tire waste (TW) accumulation rises from several industries such as construction, automobile and increasing with each passing day. It is considered a global problem. In 2009, Rubber Manufacturers of Association (RMA) cited that approximately 5.170 thousand tons of tires were generated in the U.S. By comparison, in 2009, 85 per cent of tires by weight were consumed whereas this number was only 11 per cent in 1990 (Figure 2.1). Coming up with the environmental concerns, this situation procreated an intensive solid waste disposal matter. By the way, according to the Association of Rubber Industrialists of Turkey (LASDER, 2007), annual TW generation is 180.000 tons (RMA).



Figure 2.1. An example of tire waste stockpile.

Accumulated tire wastes in stockpile as shown in Figure 2.2, can be seed of large tire fires that can smolder for several weeks or even months, sometimes with dramatic effect on the surrounding environment. Furthermore, tire waste stockpiles are breeding grounds for mosquitoes since they may hold water for long periods of time due to their shapes, providing excellent site for mosquito larvae development. Tire stocks transportation had also contributed to the introduction of non-native mosquito species that are more difficult to control and are spreading more disease. Therefore, recycling and re-use of scrap tires is an eminent methodology aimed and tried to be achieved in many engineering disciplines. Scrap tires are consumed by a variety of markets summarized in Figure 2.4, including tire-

derived fuel, civil engineering and ground rubber applications, as well as other smaller markets and legal landfilling. Still, the accumulated amount of tire wastes is increasing because of the growing population, demand on tires and also their short service lives. Especially, some of the developed countries focused on some regulations like recycling and reuse of tire wastes as construction material in order to prevent environmental pollution. Even though the amount of scrap tire stockpiles increases each year, reused and recycled amount of scrap tires increases, too. The variation of number of scrap tires in stockpiles between 1990 and 2009 is demonstrated in Figure 2.3.

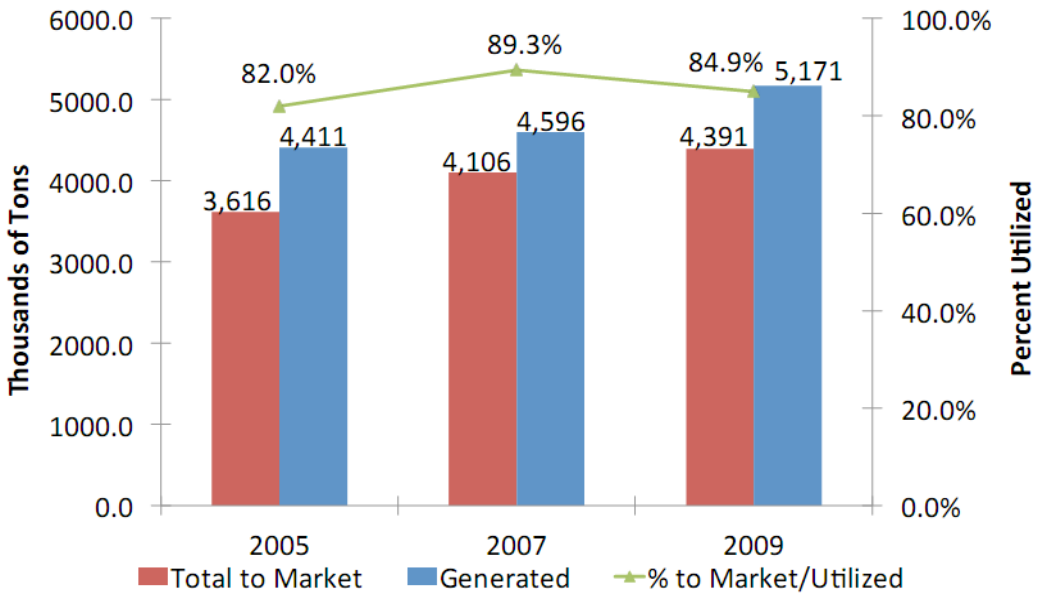

Figure 2.2. U.S. scrap tire management trends, 2005-2009 (RMA, 2009).

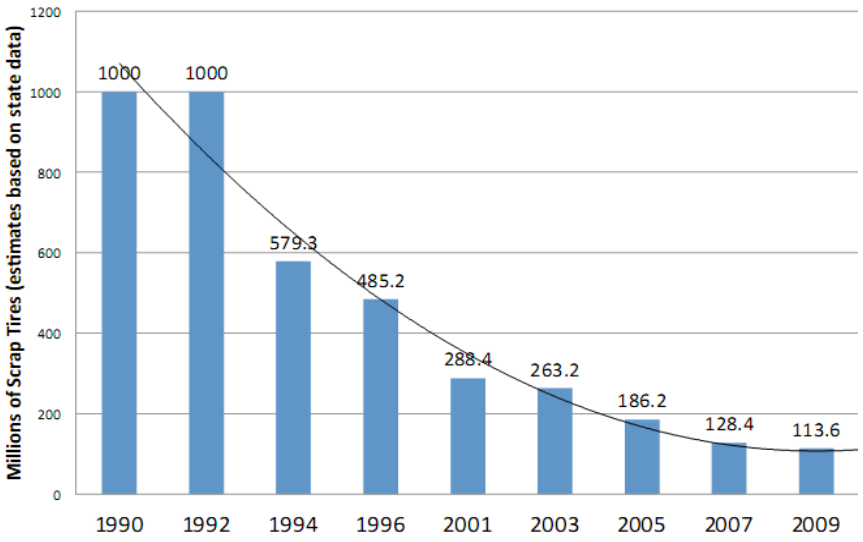

Figure 2.3. Millions of scrap tires remaining in U.S. stockpiles, 1990-2009 (RMA, 2009).

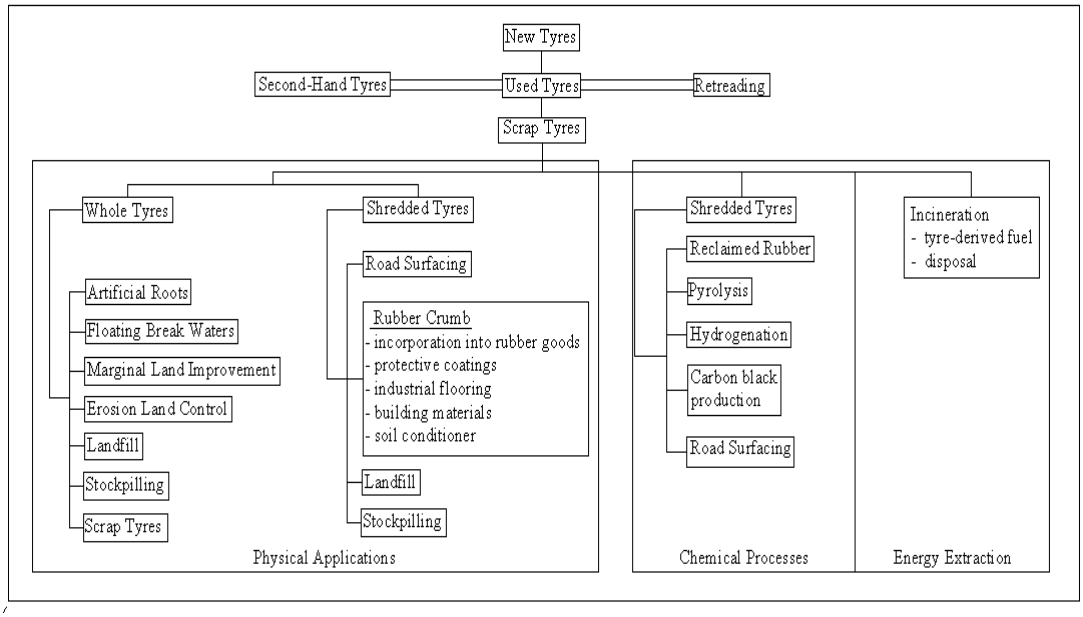

Figure 2.4. Recycle, reuse or disposal alternatives for scrap tires (UNCTAD secretariat and OECD, 1998).

2.2. Material Properties

2.2.1. Different Particulate Rubbers

Scrap tires can be managed as whole, slit, shred, chip, ground, or crumb rubber according to transformation by means of a mechanical size reduction process into a collection of particles, with or without a coating of a partitioning agent to prevent agglomeration during production, transportation, or storage. As shown in Figure 2.5, few types of processed used tires are used in civil engineering applications (Edinçliler *et al.*, 2010).



Figure 2.5. Typical shapes of different processed used tires (not to scale) (Edinçliler *et al.*, 2010).

2.2.2. Physical and Mechanical Properties

Studies on physical and chemical properties of tire shreds demonstrated that specific gravity was independent of change in size of tire. On the other hand, as the tire shred size increased, the hydraulic conductivity increased from 0,2 to 0,85 cm/s. Increasing the compaction energy had little effect on the final compaction density. The angle of friction

and cohesion ranged from 15˚ to 32˚ and 349 N/m^2 to 394 N/m^2 respectively. As the particle size of tire shreds increased, the shear strength of the scrap tire increased. Moreover, as the tire shred size increased, compressibility increased (Humphrey *et al.*, 1997; Moo-Young *et al.*, 2003).

The water absorption of the tire shreds ranged from six per cent, seven to per cent, which are similar to the results reported by other researchers (Humphrey and Manion, 1992). The specific gravity of tire shreds tested ranged from 1,06 to 1,12. These values are shown in Table 2.1.

Table 2.1. Specific gravity and water absortion values (Moo-Young *et al.*, 2003).

Tire Size (mm)	Specific Gravity	Water Absorption (%)
<50	1,10	6,70
50 - 100	1,10	6,95
100 - 200	1,06	7,10
200 - 300	1,10	7,00

Compaction tests were performed on tire shreds and tire chips using a 30.48 cm compaction mold with a modified compaction hammer and a 222 N weight dropped from 91.4 cm (Moo-Young *et al.*, 2003) (Figure 2.6). The test results for the compaction of tire shreds at various particle sizes and the dry maximum unit weight is shown in Figure 2.8. The modified compaction hammer using 60 per cent compaction energy produced similar results to the 222 N weight using 100 per cent compaction energy. It was reported that the compaction energy has only a small effect on the resulting dry unit weight.

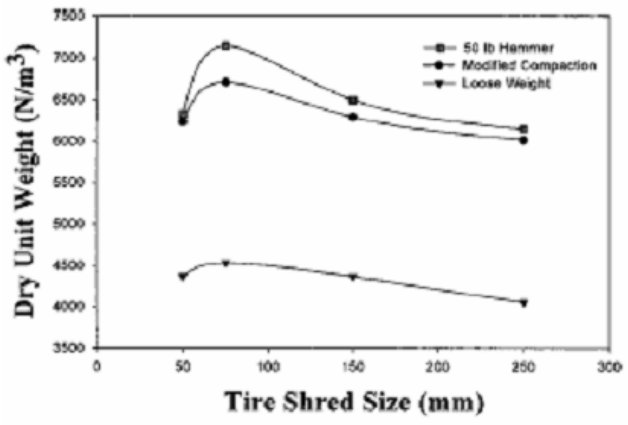

Figure 2.6. Compaction test results (Moo-Young *et al.*, 2003).

The specific gravity of tire chips is expected to be in the 1.1 to 1.3 range, with higher specific gravity values for chips containing steel belts.

Depending on the size of the tire material, unit weights can range from as low as 25 lb/ft^3 to as high as 53 lb/ft^3. The coarser the size of the scrap tire particle, the lower the compacted unit weight (Table 2.2). Limited direct shear testing of tire material has been performed using a specially designed large-scale direct shear testing apparatus. The friction angle of tire material ranged from 19° to 25°. Cohesion values range from 7.6 kPa to 11.5 kPa. Tire chips with a greater amount of exposed steel belts tend to have a higher angle of internal friction. Tire shreds or chips are much more compressible during the initial stages of loading than soils. Final loading cycles normally result in significantly less compressibility of the tire shreds or chips. Higher amounts of exposed steel belts appear to result in higher compressibility, especially during the first loading cycle. The values of Young's modulus for tire chips range from 770 kPa to 1250 kPa. Therefore, at least 0.9 m of conventional soil is required to be placed on top of a layer of tire chips in order to prevent or minimize surface deflections. Although scrap tire particles (shreds or chips) are not capable of spontaneous combustion, it does appear to be possible that, under certain circumstances, an initial exothermic reaction may occur within a tire shred or tire chip embankment or backfill that could eventually raise the temperature within the fill to a point where ignition could possibly occur. Although the shear strength characteristics of tire

chips vary according to the size and shape of the chips, internal friction angles were between to range from 190 to 260 while cohesion values ranged from 4.3 kPa to 11.5 kPa (WSDOT Report, 2003).

Table 2.2. Unit weights of scrap tire (WSDOT Report, 2003).

Unit Weight (lb/ft^3)	Compaction Method	Particle Size	Reference
Laboratory Compaction			
35.1 - 37.3	Modified	12 mm max.	Cecich *et al.*, 1996.
31.5 - 37.5		38 mm max.	Benda, 1995.
41	Modified		Humphrey and Manion,1992.
40	Standard		
40	60% Standard		
38.6 - 40.1	60% Standard		Humphrey , *et. al.*, 1993.
27.5 - 31.3	Shaken/vibrated in mold		Westerberg and Mascik, 2001.
43.0	Modified	400 to 50 mm	Moo-Young, *et al.*, 2001.
28.6	Loose		
31.3		D_{50} = 30 mm	Newcomb and Drescher, 1994.
42.8 - 46.9	Standard	16 mm max.	Youwai and Bergado, 2003.
25	Loose	5 to 25 mm	Ahmed and Lovell, 1993.
35	Modified		
In-Place or Field Compacted			
43.1 - 44.3	Walk behind, vibratory tamping foot roller compactor, static weight 2600 lb.	1.5 to 3 in 38 to 76 mm	Tweedie, Humphrey and Sandford, 1998.
33 45 53	In trucks D-8 Dozer 5.5 ft Surcharge		Upton and Machan, 1993.
42.3 - 47.6	1152 lb/ft^2 Surcharge		Benda, 1995.
31.3 - 43.8	626 - 1044 lb/ft^2 8354 lb/ft^2		Westerberg and Mascik, 2001.
38	20000 lb smooth, steel wheel roller; then loaded with up to 5 ft of fill and 8 ft of surcharge that remained for 4 mo.	4.75 to 300 mm	Dickson, Dwyer and Humphrey, 2001.

2.2.3. Dynamic Properties

To describe mechanical properties of Tire Shreds or Chips it is stated that they are light-weighted, highly compressible under low pressure materials (Humphrey *et al.*, 1997; Moo-Young *et al.*, 2003). Further investigations were deduced below instructions which leaded to analyze their high damping characteristics.

Humphrey and Manion (1992) studied waste tires with a compacted dry unit weight of 40 pcf (0.64 Mg/m3) and a specific gravity of 1.05. Compressibility tests showed that tire chips were very compressible at low stresses but that compressibility decreased significantly at higher stresses. The coefficient of lateral earth pressure at rest was about 0.40 at low stresses and about 0.94 at high stresses. Preliminary finite element studies were showed the importance of the thickness and modulus of elasticity.

Humphrey *et al.* (1993) investigated the allowability of tire chips use as backfill for retaining wall. The compressibility tests showed that tire chips are highly compressible on initial loading but that compressibility on subsequent unloading/reloading cycles is less. Tire chips had low unit weight, moderate shear strength.

Masad *et al.* (1996) realized experiences regarding the engineering properties of Ottawa sand, and a mixture of 50 per cent Ottawa sand and 50 per cent shredded tires by volume (70 per cent Ottawa sand and 30 per cent shredded tires by weight). The data indicated that the modulus values of the tire chips or the 50/50 blend are considerably lower than those values obtained for the Ottawa sand. Furthermore, the modulus of elasticity increased as confining pressure increased (Figure 2.7).

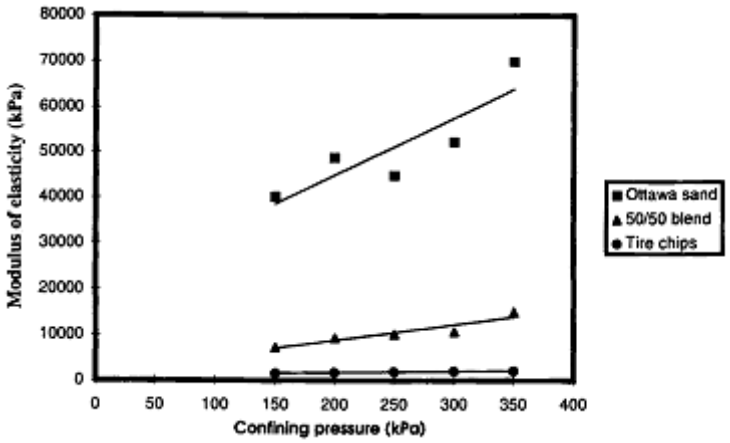

Figure 2.7. Modulus of elasticity vs. confining pressure of sand, tire chip and 50 per cent by volume mixture (Masad *et al.*, 1996).

Feng and Sutter (2000) performed Resonant Column Tests to soil mixture prepared with Ottawa Sand and Tire Rubber to evaluate dynamic properties as shear modulus G, and damping ratio, D. When the volume of rubber in a mixture were treated as voids, the Gmax could be estimated from Hardin's equation (1968), when given a known percentage of tire inclusion and air void for a rubber/soil mixture, the maximum shear modulus of the mixture could be estimated. Behavior of RSM was identified as close to a cohesive soil.

Similar investigations were handled not with Tire Wastes but, likely having parallel properties, Geosynthetic Polymers placed on top of soil layer under structure foundation base relying on the experimental results of cyclic tests that they had conducted (Yegian *et al.*, 1998; 2005). They had deduced that Ultrahigh Molecular Weight Polyethylene/nonwoven geotextile interface between foundation and top of soil layer worked as dynamic excitation isolator. Through slip deformations geosynthetics reduced seismic energy.

Hyde *et al.* (2007) conducted cyclic triaxial compression tests on sand-tire chips mixtures of ratios 100:0, 99:1, 97.5:2.5, 95:5, and 85:15, by solid volume. Tested sand was

silica sand having D50 of 0.7 mm, brown colour, sub-rounded to sub-angular grains. CT0515 tire chips were obtained commercially. Tests were conducted on Undrained Condition, cylindrical specimen 100 mm D, 200 mm H. Resultantly, the mixtures did not show a clear sign of improvement in terms of liquefaction resistance except for the 99/1 mixtures. However, since only one size of tyre chips were tested; it was urged for further study using other factors, e.g., size, shape, and materials.

Senetakis *et al.* (2009; 2012) investigated evolutions of gravel, and sands' dynamic properties after rubber inclusion on laboratory conditions with resonant column tests (RCT). They observed that results are influenced by the relative size of soil versus rubber particles, the confining pressure, and rubber content in mixtures, the grain-size characteristics and dynamic properties of the physical portion of the mixtures. They deduced that increase in mean confining pressure, results in more linear behavior at same shear strain amplitude. At low amplitude RCT; significant reduction in shear stiffness of Rubber Soil Mixtures (RSM) as percentage of rubber increases. Contrarily, Dmin increases as Rubber presence in RSM augmented by weight. At high amplitude RCT; D – log (shear strain) curves of clean sand and RSM tend to converge with increase in Rubber percentage. Furthermore, they deduced also that low amplitude G and D curves of sand/rubber mixtures are slightly affected by moisture content.

2.2.4. Chemical Properties

Scrap tire material is not reactive under normal environmental conditions. The principal chemical component of tires is a blend of natural and synthetic rubber but additional components include carbon black, sulfur, polymers, oil, paraffin, pigments, fabrics, and bead or belt materials. Chemical analysis of tire shreds was conducted to illustrate how properties such as total organic carbon, pH, and turbidity change with tire size. Table 2.3 shows the results of chemical analysis. As tire shred size increases, the results illustrated a decrease in total organic carbon (TOC) and turbidity. Total organic carbon is the total amount of organic carbon molecules in the material, and turbidity is the

amount of solid particles that are suspended in water. The pH also showed a slight decrease as tire size increased (Moo-Young *et al.*, 2003).

Table 2.3. TOC, pH, and turbidity results (Moo-Young *et al.*, 2003).

Tire size (mm)	TOC (ppm)	pH	Turbidity (NTU)
<50	22.7	6.97	234
50–100	17.4	6.98	202
100–200	14.5	6.96	251
200–300	3.1	6.95	99

2.2.5. Constructional Aspects

Tire shreds have a compacted dry density that is one-third to one-half of the compacted dry density of typical soil. This makes them an attractive lightweight fill for embankment construction on weak, compressible soils where slope stability or excessive settlement is a concern.

The thermal resistivity of tire shreds is approximately eight times greater than for typical granular soil. For this reason, tire shreds can be used as a 150 to 450-mm thick insulating layer to limit the depth of frost penetration beneath roads. This reduces frost heave in the winter and improves subgrade support during the spring thaw. In addition, tire shreds can be used as backfill around basements to limit heat lost through basement walls, thereby reducing heating costs.

The low-compacted dry density, high-hydraulic conductivity, and low-thermal conductivity makes tire shreds very attractive for use as retaining wall backfill. Lateral earth pressures for tire shred backfill can be about 50 per cent of values obtained for soil backfill. Tire shreds also can be used as backfill for geosynthetic-reinforced retaining walls.

The high hydraulic conductivity of tire shreds, generally greater than one cm/s, makes them suitable for many drainage applications, including French drains, drainage layers in landfill liner and covers systems, and leach fields for on-site sewage disposal systems.

Tire shreds with a maximum size of 75 mm or 300 mm generally are placed in 300-mm thick lifts and compacted by a tracked bulldozer, sheepsfoot roller, or smooth drum vibratory roller with a minimum operating weight of 90 kN. Rough shreds generally are placed in 900-mm thick lifts and compacted by a tracked bulldozer. For most applications, a minimum of six passes of the compaction equipment should be used.

Tire shreds should be covered with a sufficient thickness of soil to limit deflections of overlying pavement caused by traffic loading. Soil covers thicknesses as low as 0.8 m may be suitable for roads with light traffic. For roads with heavy traffic, one to two m of soil cover may be required. For unpaved applications, 0.3 to 0.5 m of soil cover may be suitable depending on the traffic loading. The designer should assess the actual thickness of soil cover needed based on the loading conditions, tire-shred layer thickness, pavement thickness, and other conditions as appropriate for particular project. Regardless of the application, the tire shreds should be covered with soil to prevent contact between the public and the tire shreds, which may have exposed steel belts.

In applications where pavement will be placed over the tire shred layer and in drainage applications, the tire shred layer should be wrapped completely in a layer of nonwoven or woven geotextile to minimize infiltration of soil particles into the voids between the tire shreds.

Whole tires and tire sidewalls that have been cut from the tire carcass can be used to construct retaining walls and bound together to form drainage culverts.

Tire shred fills should be designed to minimize the possibility of an internal heating reaction. Possible causes of the reaction are oxidation of the exposed steel belts and oxidation of the rubber. Microbes may play a role in both reactions. Although details of the reaction are under study, the following factors are thought to create conditions favorable for oxidation of exposed steel, or rubber, or both; free access to air; free access to water; retention of heat caused by the high insulating value of tire shreds in combination with a large fill thickness; large amounts of exposed steel belts; smaller tire shred sizes and excessive amounts of granulated rubber particles; and, the presence of inorganic and organic nutrients that would enhance microbial action as stated in ASTM D6270-08 (2012).

2.3. Tire Waste Utilization Fields

Refocusing on annual scrap tire production in United States, the largest portions of scrap tires being used are burned for tire derived fuel (~48 per cent), civil engineering applications (~32 per cent) and ground rubber (12 per cent). Figure 2.8 shows the increasing tendency of scrap tire market trend between the years of 2005 and 2009 (RMA, 2009).

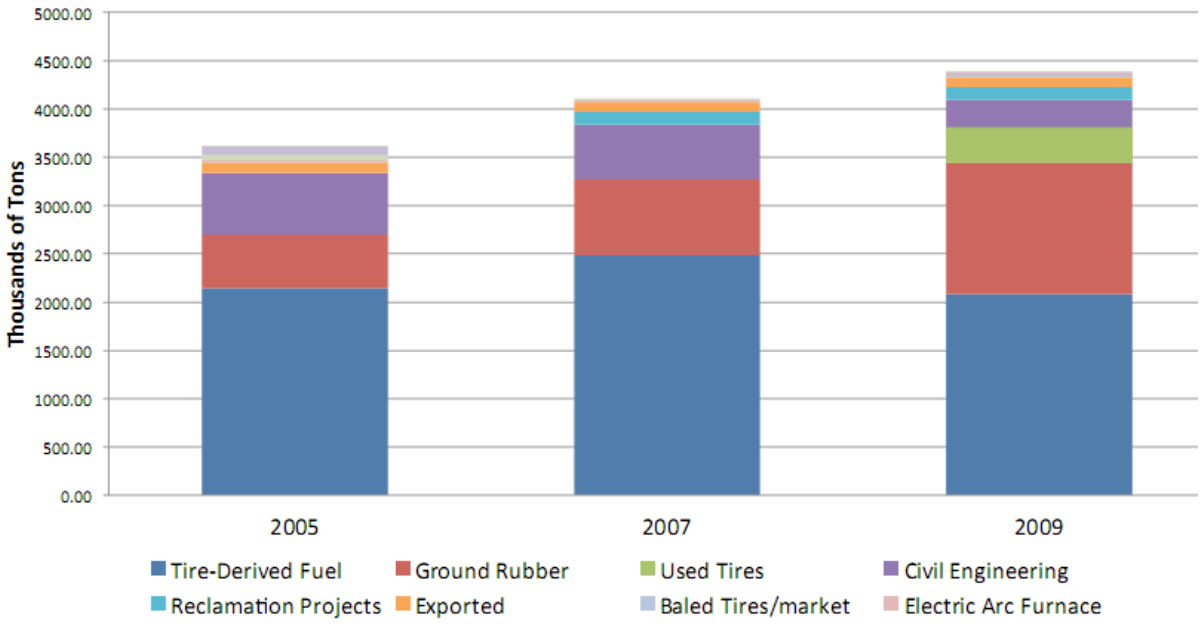

Figure 2.8. Scrap tire market trends, 2005-2009 (RMA, 2009).

2.3.1. Ground Rubber Applications

Ground tire rubber is used in rubber products (such as floor mats, carpet padding, and vehicle mud guards), plastic products and as a fine aggregate addition (dry process) in asphalt friction courses.

Some of the applications are; ground cover under playground equipment, running track material, sports and playing fields, ground tire rubber blended with asphalt for road construction, molded rubber products, brake pads and brake shoes, additive to injection molded and extruded plastics, automotive parts, agricultural and horticultural applications/soil amendments, horse arena footing.

2.3.2. Civil Engineering Applications

They were mainly used in landfill construction and operations, cap closures, alternate daily covers, leachate collection systems, gas venting systems, septic system drain fields,

subgrade fill and embankments, backfill for walls and bridge abutments, subgrade insulation for roads, vibration dampening layers (RMA, 2009).

If used as landfill, in slope stability, embankment applications; rubber can enhance geotechnical and drainage performance of soil depending on the degree of compaction of soil-tire mixture. Tire waste and soil mixtures relatively low to medium tire waste content by weight ranged between 35 per cent - 55 per cent displays increased dynamic behavior, higher shear strength, low to medium compressibility, reduced void ratio and denser solid matrix fabric. Therefore, in the last two decades, scrap tires mixed with soils have been utilized in drainage, thermal-isolation, insulation layer, retaining wall & bridge abutments, conventional fill, and light weight construction applications.

The use of soils locally available at the construction site will usually satisfy design specifications with a significant reduction in construction costs. The filling of the tire with soil can be accomplished even by manual compaction. This type of wall does not require cement or steel (Garga and O'Shaughnessy, 1995).

Edil *et al.* (1994) conducted experiences regarding the engineering properties of shredded scrap tires and soil mixture to research availability to use it for light-weight fill material in highway construction, for drainage material in highway and landfill construction, and for other similar applications. In this context; considering number of ways in which shredded tires can be used in highway construction, as an aggregate replacement in the construction of nonstructural sound-barrier fills, light-weight embankment fills crossing soft or unstable ground, regular fills, retaining-wall backfills, and edge drains; the use of shredded tires in highway applications was considered a potentially significant avenue for putting scrap tires into beneficial reuse.

Again, Masad *et al.* (1996) realized similar laboratory research with Ottawa sand, and a mixture of 50 per cent Ottawa sand and 50 per cent shredded tires by volume (70 per cent Ottawa sand and 30 per cent shredded tires by weight). They concluded the use of

shredded tires/Ottawa sand mixes as a lightweight fill material very promising although the data obtained were limited to the above stated mixture.

Lee *et al.* (1999) used numerical modeling to study the mechanical behavior of shredded tire backfill. The results of the study prove that tire shred-sand mixture is an effective example for backfill material. Bosscher and Edil (1994) found that vertically placed tire shred provide higher shear strength. Also, when pressure caused by water is taken into consideration, to use tire shred in soil mixture will bring advantages by providing good drainage performance.

Bosscher *et al.* (1997) investigated the effect of heavy trucks on embankment constructed with outwash sand and shredded tires. It is claimed that the embankment showed a satisfactory performance. Moreover, Bosscher stated out that over a period of two years the sections constructed with pure tire shreds exercised a smaller amount of settlement than the sections constructed with soil. There are several projects in the world which benefitted from shredded tires at the construction of asphalt pavement in civil engineering applications.

To be able to use TB as an additive for modifying soil property; a large-scale direct shear testing device were used for TB, TB and sand (TBS) shear strength parameters and strain behavior determination. It were experienced that medium dense sand mixed with TB samples demonstrated stiff behavior at low strains, the displacement at failure values were increased by three to seven fold with TB presence in sand. Dynamic triaxial tests were conducted on these samples to determine dynamic shear modulus and damping characteristics under different confining stresses. The dynamic shear modulus of TB had increased by two orders of magnitude when it was mixed with sand. The addition of 10 per cent by weight TB to S decreased the shear modulus, while causing a major increase in damping. As a deduction; use of TB to modify stress - strain behavior under dynamic conditions on sand, was applicable concerning not only experimental results but also economic feasibility (Edinçliler *et al.*, 2004).

2.3.3. Rubber-Soil Mixture Use as Base Isolation Material

In a conventional design, the foundation of the structure rests firmly on the soil. During an earthquake, because of the large friction between the foundation and the underlying soil, the ground motions are fully transmitted to the superstructure (the building above the foundation) To limit the seismic energy transmission to a structure, structural engineers have been developing mechanical devices referred to as base isolators (Figure 2.9). The basic idea of seismic base isolation is to provide a flexible interface between a structure and the ground in order to minimize the lateral load on a superstructure during strong earthquake ground motions. This can be achieved by shifting the fundamental period of the structure to a range outside the periods of earthquake ground motion (Chopra, 2006).

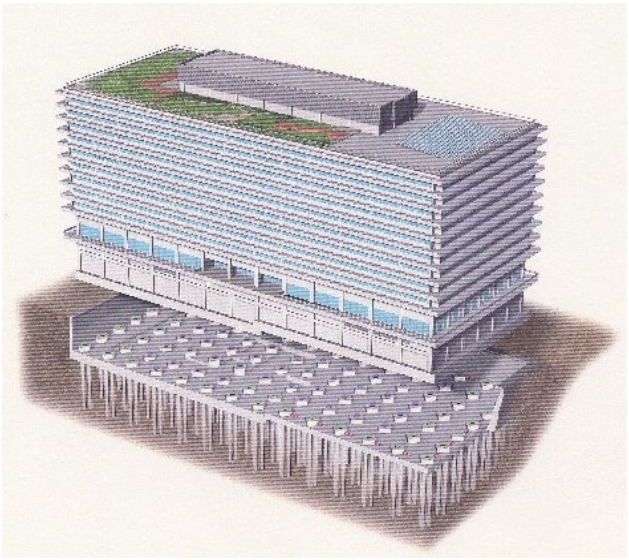

Figure 2.9. Central governmental building 7.280 m2 building area, 13 floors (Kasumigaseki, Japan, 2002).

In New Zealand and Japan isolation systems combine low-damping natural rubber bearings with some form of mechanical damper. These include hydraulic dampers, steel bars, steel coils, or lead plugs within the bearing itself. There are several drawbacks to using dampers for isolating structures: Every type of damper-except the internal lead plug-requires mechanical connectors and routine maintenance, the yielding of metallic dampers introduces a nonlinearity into the response that complicates the analysis of the dynamic

response of the isolated building, and they reduce the degree of isolation by causing response in higher modes (Naeim and Kelly, 1999).

Traditional seismic isolation aims to reduce structural responses under seismic actions, however, due to high cost of implementation, these base isolation techniques are only applied to structures with critical or expensive contents. In view of the lack of low-cost and effective earthquake protection techniques, a promising earthquake protection method involving the use of rubber-soil mixtures around the foundation of structures for reducing structural responses under seismic action has been proposed (Xuan, 2009).

Considering the energy absorption capability, durability material characteristic properties of scrap tires, and their use for base isolation purpose is accepted as an incisive methodology (Figure 2.10).

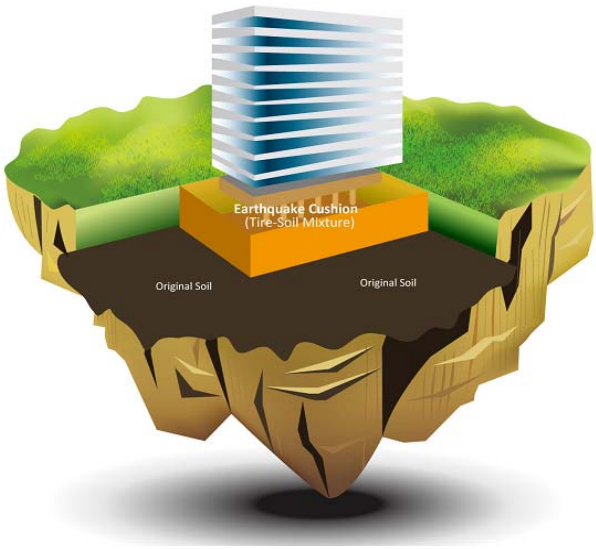

Figure 2.10. Figurative picture of base isolation with rubber-soil mixture (Tsang, 2009).

3. SEISMIC BASE ISOLATION SYSTEMS

3.1. Basic Approach and Purposes

In conventional fixed-base design, efforts to strengthen the structural system to provide superior seismic performance lead to a stiffer structure, and thus will attract more force to the structure and its contents. A fixed-base building tends to amplify the ground motion. In order to minimize this amplification, the structural system must be either extremely rigid or provided with high levels of damping. At best, rigidity leads to the contents of the building experiencing the accelerations of the ground motion which may be too high for sensitive internal equipment and contents. The alternative of providing high levels of damping into the system generally leads to damage of the structural system or to structural forms. Seismic Base Isolation allows a design that can function without damping, yet protects the building and its contents with relatively simple and low cost structural systems. A seismic isolation system may be defined as a flexible or sliding interface positioned between a structure and its foundation, for the purpose of decoupling the horizontal motions of the ground from the horizontal motions of the structure, thereby reducing earthquake damage to the structure and its contents. Seismic isolation can have two effects on the structure seismic response: superstructure lateral forces reduction; lateral displacements concentration at the isolation interface. Figure 4.1 shows two acceleration response spectra: the upper one is for damping in the fixed base structure and the lower one is as in the isolated structure. Lower damping in the isolated structure comes from higher damping provided by the base isolation. The 1st mode period T_f of a fixed base structure is shown by a vertical line on the left; the 1st mode period T_i of the isolated structure is shown by a vertical line on the right. The isolation system lengthens the fundamental period of a structure, and adds damping. These effects reduce structure's acceleration response and lateral forces in the structure (Kelly *et al.*, 1982; 1998).

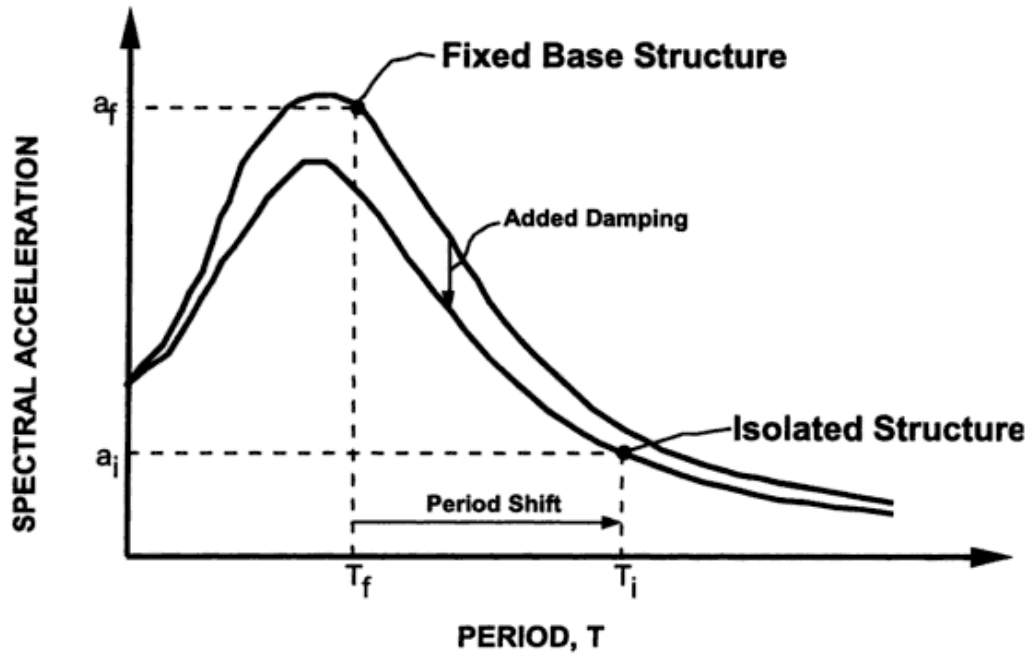

Figure 3.1. Fixed base and isolated structure response (Kelly *et al.*, 1998).

Base Isolation's second effect is illustrated in Figure 4.2. The structure above the isolation system tends to move as a rigid body, and interstroy displacements within the superstructure are greatly reduced. Lateral displacements are concentrated at the isolation interface, and minimized in the superstructure.

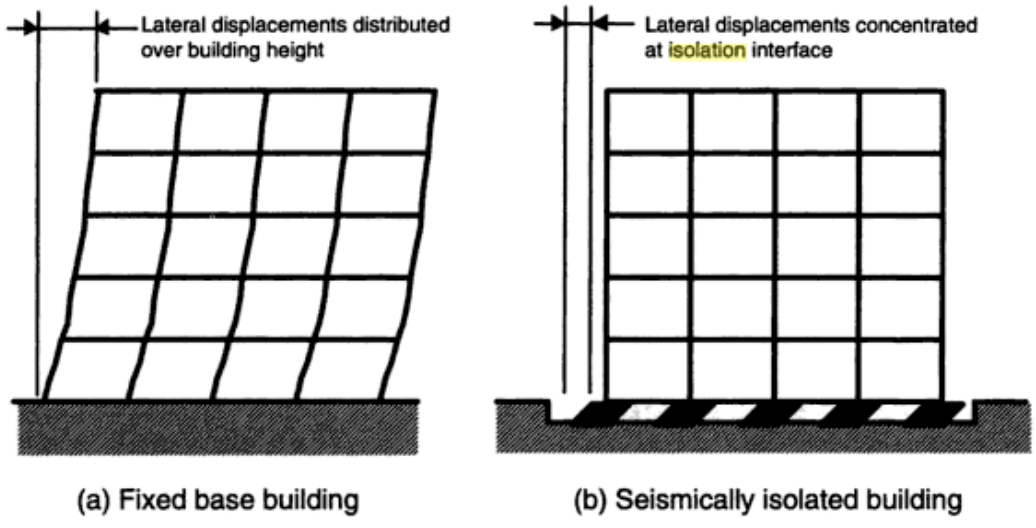

Figure 3.2. Fixed base and isolated structure response (Kelly *et al.*, 1998).

Additionally, base isolation results in ameliorated torsional response, near-fault effects observed; behavior under wear, aging and temperature effects, against overturning pressure.

Summarizing and emphasizing; there are two main purposes of seismic base isolation system:

1. Reduce the fundamental vibration frequency of structure to a value lower than the predominant energy-containing frequencies of earthquake ground motions.

2. Provide a means of energy dissipation so as to reduce the transmitted acceleration to the superstructure.

3.2. A Glance to Applications Following Chronology

One notable historic structure is Frank Lloyd Wright's Imperial Hotel in Tokyo. Completed in 1921, this building was founded on a shallow layer of firm soil which in turn was supported by an underlying layer of mud. Cushioned from devastating ground motion, the hotel survived the 1923 Tokyo earthquake and later Wright wrote in his autobiography of the "merciful provision" of 60 to 70 feet of soft mud below the upper eight foot thick surface soil layer which supported the building (Wright, 1977).

Bridge structures have for a number of years been supported on elastomeric bearings, and as a consequence have already been designed with a flexible mount. It is equally possible to support buildings on elastomeric bearings and in excess of 150 examples exist in Europe and Australia, where buildings have been successfully mounted on these pads. Up to date this has been realized primarily for vertical vibration isolation

rather than seismic protection. By increasing the thickness of the bearing, additional lateral flexibility and period shift can be attained (Stanton and Roeder, 1982).

One of the most effective means of providing a substantial level of additional damping is through hysteretic energy dissipation. The term hysteretic refers to the offset in the loading and unloading curves under cyclic loading. Work done during loading is not completely recovered during unloading and the difference is dissipated as heat. Mechanical devices which use the plastic deformation of either mild steel or lead to achieve this behavior have been developed.

3.2.1. Sliding Bearings

A structure supported entirely by sliding bearings would be experiencing forces at the isolation interface that are always bounded by the mobilized frictional force, regardless of the level of ground acceleration or its frequency content. However, a freely sliding structure would also have large permanent displacements, particularly when the sliding interface is not perfectly leveled. Control of these permanent displacements within acceptable limits is accomplished by the use of recentering devices. Several sliding isolation systems with recentering devices have been proposed.

In 1985, a sliding-elastomer system had been developed under the auspices of Electricite De France (EDF), consisting of steel reinforced neoprene bearing topped by a lead bronze plate which is in frictional contact with stainless steel plate anchored to the structure. The sliding-elastomer base isolator uses essentially an elastomeric bearing and friction couple in series. This system is standardized for nuclear power plants in regions of high seismicity. Comparison of the displacement and acceleration histories shows that the effects of the bi-axial interaction are considerable in the response of buildings isolated by sliding-elastomer bearing under bidirectional motion. In force-displacement hysteresis loops, simulated using visco-plastic model, there is no discontinuity. Therefore, EDF model is suitable for computation of response of the isolated system subjected to bidirectional motion (Gueraud *et al.*, 1985).

The resilient-friction base isolation system (R-FBI) was developed in 1987. It consisted of several teflon layers coated friction plates with a central core of rubber. The rubber provides the restoring force for the system, hence, controls the relative displacement, while energy is dissipated by the friction forces. In a study of a five-story building isolated by the R- FBI system, A natural period of three to 4.5 sec was suggested. Figure 3.3 illustrates the mechanical behavior of the R-FBI system acting in shear (Mostaghel and Khodaverdian, 1987).

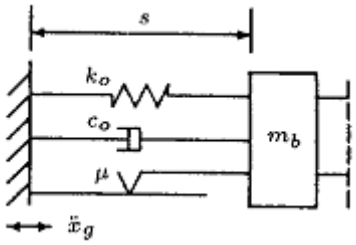

Figure 3.3. Diagram of R-FBI (Mostaghel and Khodaverdian, 1987).

In 1988, the TAISEI shake suppression system (TASS) to reduce horizontal seismic acceleration had been proposed. Slip occurs between sliding bearings and bearing plates and Coulomb damping is generated to absorb seismic energy. The fundamental response characteristics were studied by one-dimensional lumped mass model and detailed response characteristics such as torsional or rocking vibration were analyzed three dimensionally. It was made clear that TASS system has good isolation effects, when input acceleration is 50cm/sec, the response acceleration of a base-isolated building is reduced to 1/2 ~ 1/8 of the non base-isolated one, and the maximum relative displacement of the base is within 30cm, which is adopted as maximum response displacement in the design. The acceleration mitigation effects are not disturbed by vertical and rocking vibration and torsional response scarcely occurs (Kawamura *et al.*, 1988).

Friction pendulum system (FPS) was proposed by Mokha *et al.* (1990a, 199Ia). A shake-table study of the friction-pendulum isolation system, installed in a six-story, quarter-scale, 52-kip model structure, is presented. Two bearing materials are studied, one with a peak friction coefficient of 0.075 and another of 0.095. In both cases, the isolation

system has a rigid-body mode period of one sec. The isolated structure is found to be capable of withstanding strong earthquake forces of different frequency content. In tests with the El Centro earthquake motion (1940), the isolated structure sustains, without any damage, peak ground acceleration six times greater than that it could under fixed-based conditions. It is found that the bearing displacements are low and that the permanent bearing displacements at the end of free vibration are very small; in general, not exceeding six per cent of the bearing designs displacement. The system is shown to have quantifiable properties, and analytical techniques are presented that provide accurate prediction of the response.

Combining the desirable features of the Electricite de France (EDF) base isolator and the resilient-friction base-isolation (R-FBI) system, a modified design for a base isolation system had been proposed as the sliding resilient-friction (SR-F) base-isolation system, for a nonuniform shear beam structure as in Figure 3.5 (Lin Su *et al.*, 1991).

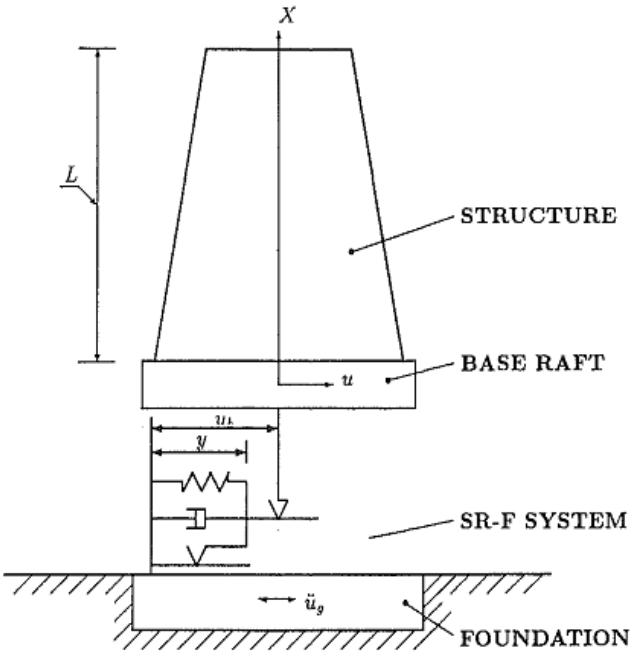

Figure 3.4. Schematic diagram of SR-F base isolator (Lin Su *et al.*, 1991).

Results of numerical simulations under a variety of conditions, parametric studies on the effect of variations in the properties of the SR-F isolator concluded as follows:

The SR-F system is highly effective in reducing the peak acceleration and deflection responses of the structure without generating excessively large base displacements.

The amount of base displacement generated by the SR-F base isolator is, usually, manageable.

Peak deflection and acceleration responses of a structure with the SR-F base isolation system do not vary significantly with severe variations in the intensity of ground acceleration.

The SR-F system is insensitive to long-period contents of the ground acceleration when its natural frequency is away from the excitation frequency.

The SR-F system, which combines the features of the EDF and the R-FBI systems, could become a reliable base isolator for a variety of structures with different seismic protection demands.

A sliding isolation system consisting of Teflon disc bearings and helical steel springs providing bilinear restoring force when deformed in shear had been proposed (Constantinou *et al.*, 1991). The system was tested so that the mobilized peak frictional force was larger by at least a factor of two than the peak restoring force. Under these conditions the system had a low sensitivity to the frequency content of the input. Three groups of tests; one without the steel springs and two with springs of different total stiffness were conducted. During each cases, the mobilized peak frictional forces were larger by at least a factor of two than the developed peak restoring forces in the springs, resulting in systems with weak or no restoring force. The tests demonstrated that:

The system was effective in protecting the structural system above against motions of significantly different frequency content.

In all of the tests the peak model acceleration, peak interstory drift, and peak base shear were practically the same for the same table input. The restoring-force devices (helical springs) served as nothing but displacement-control devices.

The frequency content of the response of the model structure in the three groups of tests was practically unaffected by the stiffness of helical springs. This phenomenon further indicates that the springs were effective only in controlling the bearing displacement, and those they did not contribute to the effectiveness of the isolation system by lengthening the period of the structural system.

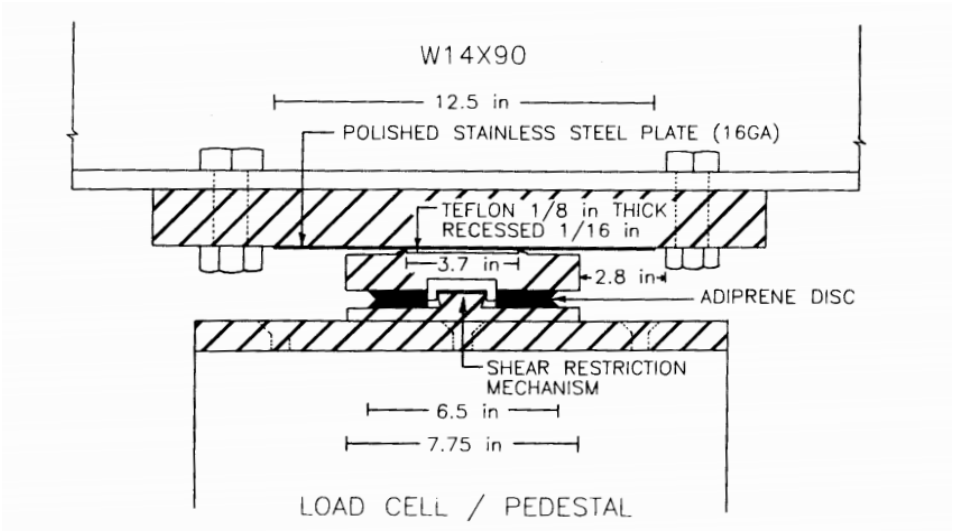

Figure 3.5. Teflon disc bearing design (1 in. = 25.4 mm) (Constantinou *et al.*, 1991).

To summarize, earlier base isolation applications are examples of various sliding bearing techniques. They prohibit the transmission of force across the sliding interface so as to produce the isolation effect. However restoring force devices are needed to be incorporated, otherwise permanent displacements would accumulate to an unacceptable

level. The most practical means of introducing restoring force capacity is through the use of a spherical sliding surface in the friction pendulum (FPS) system bearings. FPS bearings consist of an articulated slider which is faced with bearing material, generally a self-lubricating high bearing capacity composite on a spherical surface. The spherical surface is faced with a polished stainless steel overlay. Restoring force is generated by the rising of the structure along the spherical surface, while energy is dissipated by friction.

3.2.2. Elastomeric Bearings

For the Elastomeric Bearing methodology; the primarily used material was low-damping natural rubber, displaying shear strain in the order of 0.05 or less. Although it was useful in protecting structure with very sensitive contents, additional energy dissipation were desired for the wide application. Notable progress in this direction had been made on the development of lead-rubber bearing and high-damping rubber bearing. Lead Rubber Bearing consists of low-damping natural rubber with a lead core at the center, providing energy absorbing capacity through additional hysteretic damping in the yielding of the lead core that reduces the lateral displacements of isolator especially under ambient vibration. High-Damping Rubber Bearings essentially consists of steel and rubber plates which exhibits equivalent damping ratio of about 0.10 to 0.15 (of critical damping) that build in the alternate layers. It typically presents high-damping capacity, horizontal flexibility, and high vertical stiffness.

The primary applications of elastomeric bearings in United States were the very first demonstration buildings for housing projects that have been completed using natural rubber bearings as the isolation system in Santiago, Chile (Sarrazin and Moroni, 1993) University of Chile in cooperation with the Ministry of Housing and City Planning and the National Scientific and Research Council developed this project involving a four story building supported on high damping rubber isolators and an already nearby built with conventional techniques. Structures had a 10 by six m installation area in plan. Their first floors were made of reinforced concrete, the upper threes of confined masonry; considered as a low cost housing. The isolated building is supported on eight high damping rubber

isolators which rest on foot foundations, connected between them with reinforced concrete beams. The bearings are located on the external perimeter of the building, four at the corners and rest at the middle of the longer sides. The bearings are 31.5 cm diameter by 32 cm height. They were made in a local rubber factory.

The buildings were instrumented with a local network of four digital accelerometers located at the ground under the isolated building, at the bottom slab of the isolated building, at the roof level of the isolated and of the traditional building to observe both structures' responses against earthquakes.

Following, at least 14 earthquakes of different intensities have been registered in a small time period of two years by this recording system ranging from 0.65 to 9.54 cm/sec2 and dominant frequency between two and 20 Hz. Even though mentioned ground motion intensities were small; It had been observed that the isolation were effective in reducing the building peak accelerations. Anyway, since they were made for 50 per cent deformation, with a natural vibration period of the system level approximately two sec.; they were quite stiff during recorded earthquakes. Therefore, the filtering had been supposed to be less effective than predicted with an idea to be designated with larger motions.

In 1998, Kelly *et al.* published the below table displaying a selection of new structures and seismically retrofitted restaurated ones in former decade in California as shown in Table 3.1.

Table 3.1. Base-isolated buildings in California: new construction and seismic retrofit projects (Kelly *et al.*, 1998).

Name of building	Location	Status
Foothill Communities Law and Justice Center	Rancho Cucamonga	New building, completed
USC University Hospital	Los Angeles	New building, completed
Rockwell International Office Bldg	Seal Beach	Retrofit of existing building, completed
County of Los Angeles Fire Command and Control Center	East Los Angeles	New building, completed
Martin Luther King, Jr/Charles Drew Medical Center	Willowbrook	New building, completed
Kaiser Regional Data Center	Corona	New building, completed
Emergency Operations Center	Los Angeles	New building, completed
Veterans Administration Medical Center	Long Beach	Retrofit of existing building, completed
Los Angeles City Hall	Los Angeles	Retrofit of existing building, in design development, construction scheduled for near future
County of San Bernardino Medical Center	Colton	New building, near completion
Caltrans Traffic Management Center	Kearny Mesa	New building, near completion
Hoag Memorial Hospital Nursing Tower	Newport Beach	Retrofit of existing building, beginning construction
City and County of San Francisco 911 Center	San Francisco	New building, under construction
County of San Diego Emergency Communications Center	San Diego	New building, under construction

Similar review outlining approach to seismic base isolation and application in Europe and also in countries formerly belonging to USSR were published in 1995. The development of the Seismic Isolation systems originated from not only on seismic engineering, but especially on material technologies (in particular, of rubber) and fabrication processes was emphasized. A great impetus to the improvement of Seismic Isolation systems formed by rubber bearings was given in Western Europe (especially in France) by the interest in their application in the nuclear field. It was found that the stringent seismic requirements of nuclear plants could not be satisfied for some sites in the horizontal plane, at least without major modification of the standard design, when using the conventional fixed-base approach. Thus, rubber bearings were the Seismic Isolation devices which have been used to horizontally isolate civil buildings in most European countries. Both natural and synthetic rubbers have been used: some natural rubbers in Italian buildings, whereas synthetic rubbers have mostly been used in French applications (Table 3.2) In the former USSR countries, the seismic isolation approach has usually been quite different and has been consistent with the goal of adopting low-cost isolators. Only four buildings had been isolated by means of steel-laminated rubber bearings at the end of 1996, while the most commonly used Seismic Isolation techniques have so far been those listed in Table 3.3. However, in addition to these low-cost systems, a sophisticated 3-D pneumatic system was developed by the Russian Ministry of Defense, considered for application to nuclear reactors, in conjunction with viscous dampers (Martelli *et al.*, 1998).

Base Isolation is supposed to be a serious concern by civil engineers in People's Republic of China since they are faced with a seriously seismic region of which, over 60 per cent is a seismic area, and about 80 per cent of its large cities located in this area. In 2001, Fu Lin Zhou reclaimed that, from 1991 onwards; being one of most common types of building in China, seven or eight storey reinforced concrete frame houses are frequently built with base isolation. 180 buildings of this type had been built in a decade. Later, the quantity was arised to 500 in following four years (Zhou Fu-Lin *et al.*, 2005).

Type of SI system	Location	Date of construction	Number of buildings
Pendulum suspension and steel springs system	Ashkabad-City (Turkmenistan)	1959	1
Flexible ground-floor columns, in conjuction with energy dissipation switching-off elements and rigid inelestic displacement limiters	North-Baikal, Siberia and Kamchatka (Russia)	1972–1996	125
Pile-in-tube system with switching-off inelastic elements	Tynda, Siberia (Russia)	1989	2
Low-friction teflon/steel supports sliding between the foundations and walls, in conjuction with rigid displacement limiters	Bishkek (Kirgizia) and Kamchatka (Russia)	1984–1990	40
Kinematic (rocking) RC supports consisting of columns with spheric ends, in conjunction with switching-off and dry friction elements	Sebastopol (Ukraine)	1972–1974	3
Rocking upside-down mushroom-type RC supports	Alma-Ata (Kazakhstan) and Kamchatka (Russia)	1979–1989	120
Rocking RC supports consisting of columns with plane ends, in conjunction with displacement limiters and friction surfaces	Buryatia, Caucasus, Siberia (Russia)	1987–1990	8
Steel-laminated rubber bearings	Minsk (Byelorussia) and Tashkent (Uzbekistan) and Vanadzor (Armenia)	1985–1996	4
Total number of applications			303

Table 3.2. Civil buildings and industrial plants provided with antiseismic devices in Italy. Reproduced by permission of GLIS (Martelli *et al.*, 1998).

No	Buildings and plants			Isolators–dissipators–restraints			
	Type	Location	Year	Type	No	Diameter (mm)	Height (mm)
1	New fire station headquarters	Napoli	1981	Mechanical dissipators and isolators	NA	—	—
2	2nd fire station building	Napoli	1985	Neoprene bearings and oleodynamic restraints	24 72	700 —	150 —
3	Hospital	Sora	1988	Friction dissipation	NA	—	—
4	Civic Centre	Monte d'Ago, Ancona	1989	Neoprene bearings	6	900	180
5–9	Telecom Italia Centre of Marche Province	Ancona	1989–92	HDRBs	182 115	600 500	204 204
10	S Giovanni Battista Carife (retrofitting)	Avellino	1990	Oleodynamic restraints	18	—	—
11	CNR Laboratory	Frascati	1990	Mechanical dissipators	NA	—	—
12	Apartment houses (twin-isolated and non-isolated houses)	Squillace Marina (Catanzaro)	1990–92	Rubber bearings HDRBs	14 13 16	400 500 300	205 205 208
13	Navy building	Ancona	1991–92	HDRBs	24 20	600 500	303 303
14	New ENEL headquarters	Napoli	1989–93	Mechanical dissipators and Oleodynamic restraints	142 NA	— —	— —
15	Navy Medical Centre	Augusta (Sicily)	1992–93	HDRBs	16 8	400 500	354 328
16–19	Apartment houses of the Italian Navy	Campo Palma (Augusta, Sicily)	1992–93	HDRBs	48 36 36 16 24 16 16	300 350 400 400 450 450 450	254 294 304 294 306 282 258
20, 21	FIAT industrial buildings	Melfi (PZ) and Prato La Serra (CB)	1993	Oleodynamic restraints	173 NA	— —	— —
22	Sports Hall	Rimini	Completed	Oleodynamic restraints	NA	—	—
23	Faculty of Engineering	Brescia	Completed	Oleodynamic restraints	NA	—	—
24	Department of Mathematics, University of Basilicata	Potenza	1995	HDRBs	89	500–800*	262–278
25–28	Blocks 1–4, Faculty of Agriculture, University of Basilicata	Potenza	1995	HDRBs	132	500–800*	262–278
29, 30	Airport hangars	Bologna and Torino	Completed	Oleodynamic restraints	NA NA	— —	— —
31	Turbine and Thermal Power Cycle Buildings	Montalto Power Station	Completed	Oleodynamic restraints	NA	—	—
32	Large water supply pipe	S Giacomo (Abruzzo)	Completed	Oleodynamic restraints	NA	—	—
33	Standard telephone switchboard houses	In seismic areas	To be constructed	HDRBs	NA	—	—
34	Bell tower	Trignano–RE	In progress	SMA devices	4	—	—
35	Gas-insulated electric substations	ENEL Plants	Designed	HDRB/RBRL/Wire rope	4–8	—	—

Table 3.3. Base-isolated buildings in Russia and other former USSR countries in 1996 (Martelli *et al.*, 1998).

The rubber bearings use as a seismic base isolation in China has been widely spread. Zhou Fu-Lin *et al.* (2005) cited their application areas as follows:

1. New design structures and existed structures;

2. Important buildings and civil buildings especially for house buildings;

3. Both for protecting the building structures and for protecting the facilities inside the buildings;

4. Free architectural design. The seismic isolation rubber bearings system can be used in the buildings with irregular configuration, by putting the isolation layer on the suitable vertical level and by arranging the isolators with different stiffness and damping in plan of isolation layer.

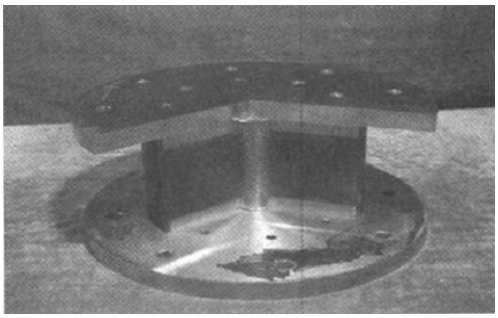

Figure 3.6. Design of isolation rubber bearing (Zhou Fu-Lin *et al.*, 2005).

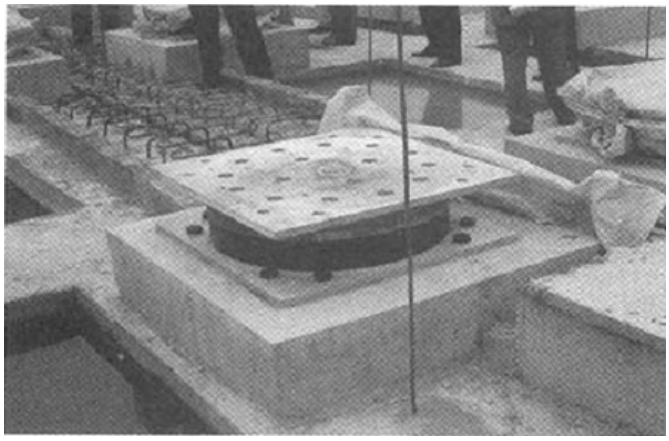

Figure 3.7. Isolation rubber bearing installation (Zhou Fu-Lin *et al.*, 2005).

To be admitted as a seismic base isolation material in China, commonly used rubber bearings inquires various tests including principally 2 kinds of work:

a. Tests of rubber bearing isolators include compression tests (capacities, stiffness), compression-shear cycle loading tests (stiffness, damping ratio and maximum horizontal displacement), low cycle fatigue tests, creep tests and ozone aging tests.

b. Shaking table tests for large scale structural model, including one six stories concrete shear wall-frame model. The results show that the acceleration responses on each stories of structure model are nearly the same. It means that the elements and joints of structure with isolation rubber bearings nearly work within elastic range only. The acceleration response of structure with isolation is only 1/10 ~1/3 of fixed structure. It means the rubber bearing isolation structure is more effective to attenuate the structural response in earthquake than any other methods.

Seismic Isolated Building Design concept was actually globally spreading issue in recent years. Figure 3.8 displays the increase in rate of use in Italy from 1991 up to 2006.

So far described and illustrated with case applications, The Seismic Base Isolation is a present matter of concern for civil engineers especially when working in the regions of

seismic activity. Structural earthquake engineering approach to this problem were mainly placing an interface between structures' foundation and soil layer They aimed to damp the seismic movements coming through soil and to lengthen structures' first modal period of vibration to reduce the possibility to face with a resonance.

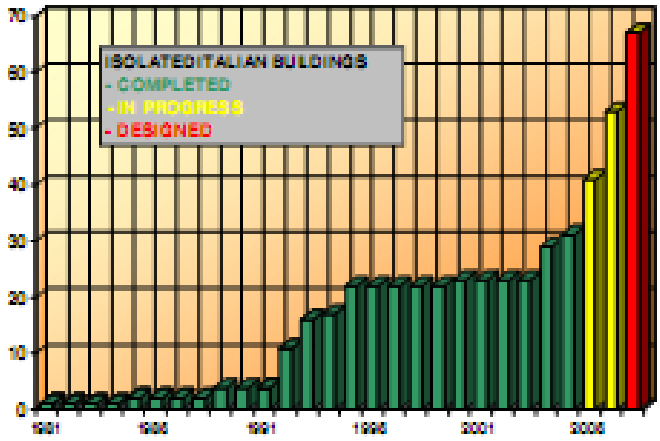

Figure 3.8. Total number of seismically isolated buildings between 1991 – 2006 in Italy (Martinelli *et al.*, 2006).

The geotechnical earthquake engineering point of view for the soil hazard mitigation against earthquakes necessitates soil improvement with several methodologies. In this regard; sharing same concern of developing a proper seismic isolation method for low to medium rise structures with ease of in-situ applications and low costing; several engineers approached lead rubbers too. But, instead of using them as a composite element of foundations; they tried to use scrap rubber tires as a soil improvement material.

3.3. Recent Investigations

3.3.1. Geosynthetic Material as Base Isolation

Geosynthetics are polymeric products; used in many civil engineering applications such as hydraulic, private development of road, dams, canals, landfilling and geotechnical applications such as retaining structures and foundations. Main properties are:

a. Loose soils, fine cohesionless silts, highly turbid liquids, and microorganism laden liquids (farm runoff) can be troublesome with certain designs with geopipes, geonets.

b. Storage and all workmanship must be assured by careful quality control and quality assurance.

c. Geosynthetic designs have usually less cost compared to alternative natural soil designs and also have invariably sustainability (lower CO2 footprint) advantages.

d. Geosynthetic materials have also physical conveniences versus natural soil counterpart. These can be cited as the thinness, light weight on the subgrade, less airspace used, and avoidance of quarried sand, gravel, and clay soil materials.

e. Easier workmanship is significant in comparison to thick soil layers (sands, gravels, or clays) requiring large earthmoving equipment.

f. Design methods are currently available in that many universities are teaching stand-alone courses in geosynthetics or have integrated geosynthetics in traditional geotechnical, Geoenvironmental, and hydraulic engineering courses.

Yegian *et al.* (1994) performed shaking table tests to demonstrate the technical feasibility of using geosynthetics for foundation isolation. Different than the former studies on Base Isolation; they preferred to isolate foundation from soil with geosynthetic materials, instead of enforcing foundation by placing base isolators between foundation and structure itself. Their proposed methodology is illustrated with below Figure 3.9.

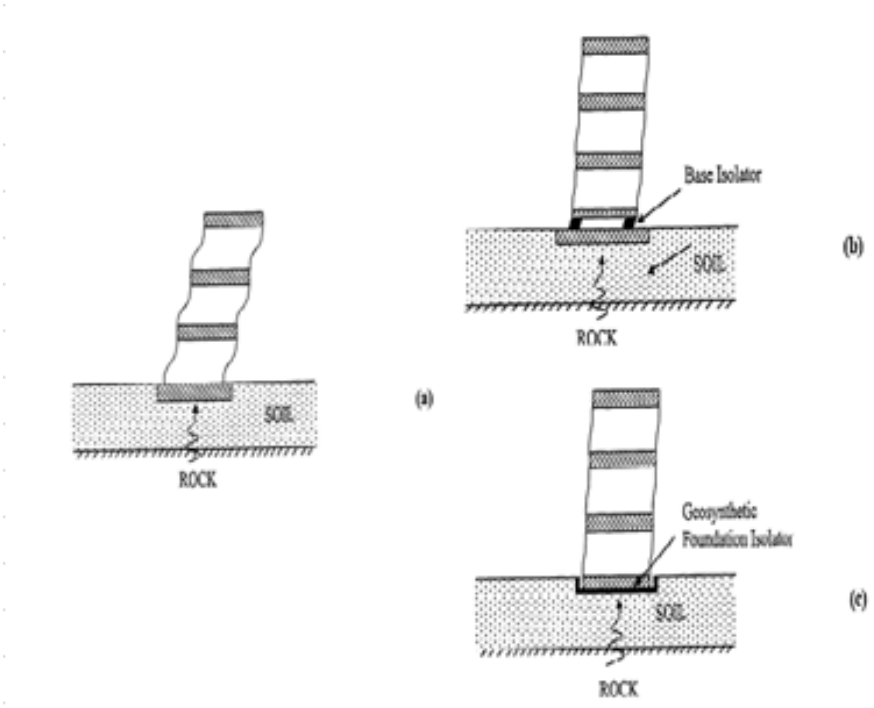

Figure 3.9. Seismic response of a typical building (a) founded on soil, (b) with base isolation, (c) with geosynthetic foundation isolation (Yegian *et al.,* 1994).

Response of a single-storey model to seismic motions was measured by placing on the shaking table. The dynamic interaction between the building top mass and its foundation was observed with three records selected among records from the 1989 Loma Prieta Earthquake based on their frequency contents. Names are: Santa Cruz (with high frequency), Capitola (with intermediate frequency), and Corralitos (with low frequency). Different Tests were carried out by scaling the peak accelerations of the records, and by changing the mass ratios (top mass divided by the total mass) of the building model. The experiments were repeated with and without foundation isolation. The results demonstrated that Ultrahigh Molecular Weight Polyethylene/nonwoven geotextile interface between foundation and top of soil layer works as dynamic excitation isolator. Through slip deformations geosynthetics reduce seismic energy, and the dynamic response of the model structure. At a base acceleration of 0.40 g, the column shear force was 35 per cent of the conventionally model without base isolation.

Later, again Yegian *et al.* (1998) repeated same experience with different accelerometers types; not piezoelectric but capacitive. Yet again they observed that there is a limiting shear stress that can be transmitted through a geomembrane-geotextile interface to the above structure block.

Yegian *et al.* (2004) continued to conduct experiences on same methodology with cyclic loading and shaking table tests. The geotextile component that they use did not change: nonwoven geotextile over ultrahigh molecular weight polyethylene. Results are illustrated with Figure 3.10, Figure 3.11, and Figure 3.12. Properties are indicated as mechanical properties of the foundation isolator:

a. The static friction coefficient between layers of isolation should not be influenced by moisture, temperature, vertical stress and sliding velocity, sliding displacement. It should be slightly greater than dynamic friction coefficient, that is supposed to be 0.05 – 0.15.

b. The geosynthetic interface should possess resistance against long-term creep, biological and chemical effects possibly arising from environment.

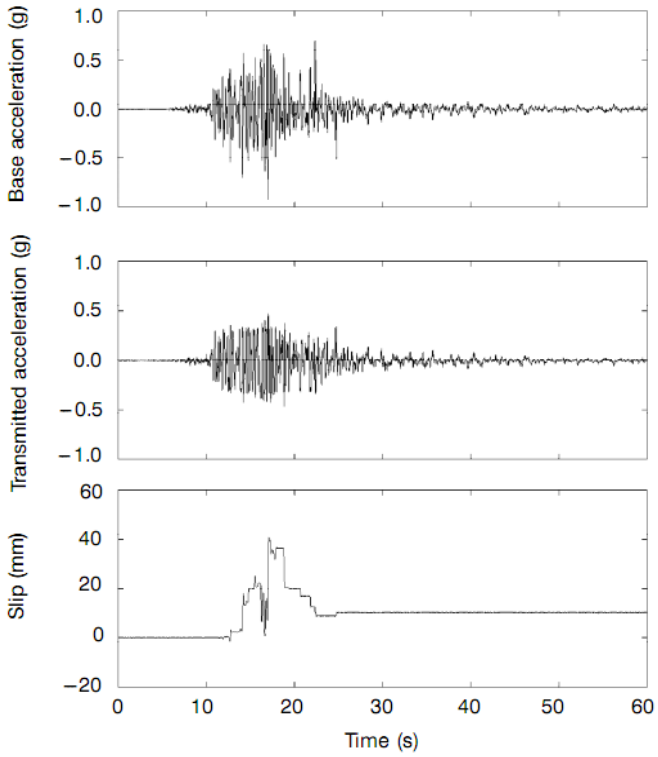

Figure 3.10. Test results of a rigid block on geotextile interface under earthquake excitation (Northridge Earthquake, 1994) (Yegian *et al.*, 2004).

After cyclic loading and shaking model tests conducted, it is deduced that above described soil structure interface component has 0.08 as dynamic friction and 0.11 as static friction coefficients. Furthermore, peak drift comparison in Figure 3.11 is made between non isolated and isolated one-storey structure models on shaking table tests:

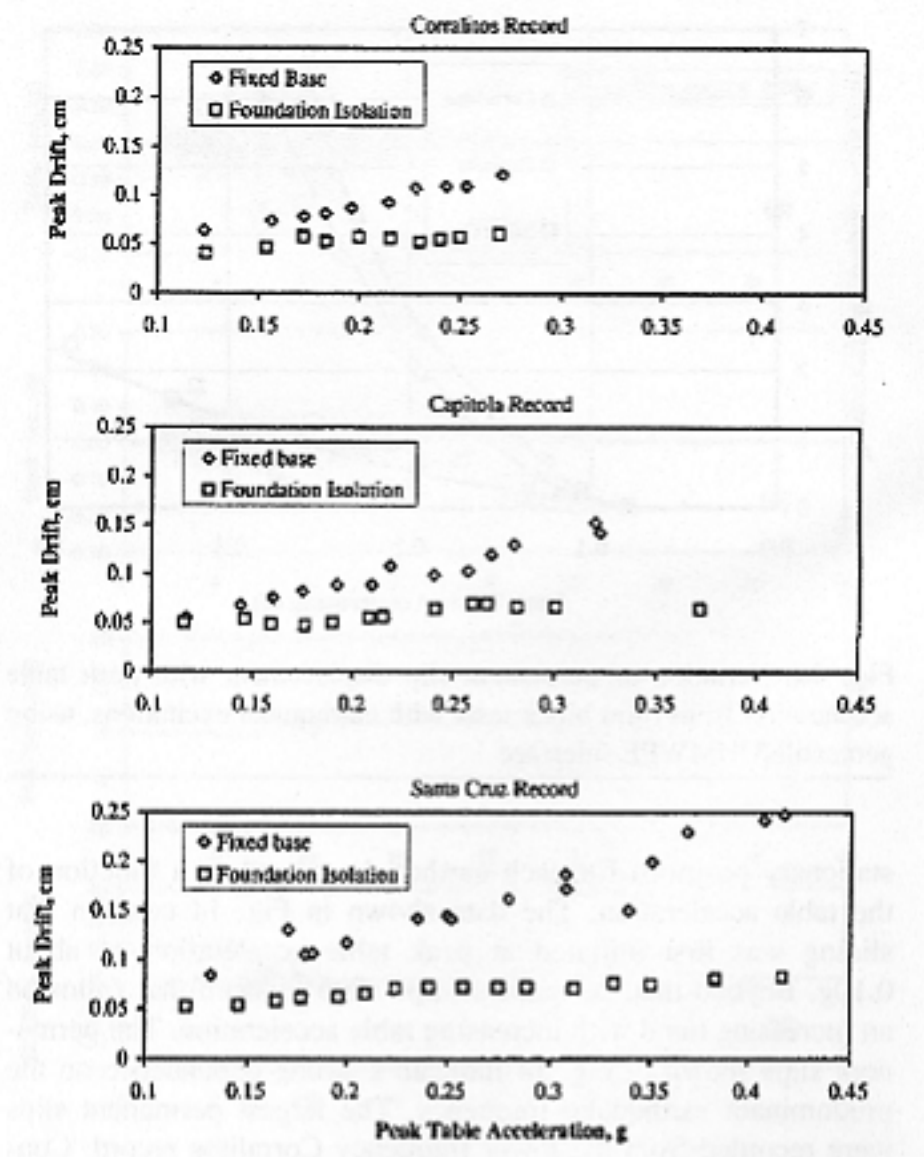

Figure 3.11. Fixed-base isolated structure peak drifts (Yegian *et al.*, 2004).

The study of the interface geometry was investigated (Yegian *et al.*, 2005). Structure isolator geosynthetic component layers in cylindrical, tub, trapezoidal, and compound trapezoidal with reinforced core geometries were separately modeled and their 2-D plain-strain analyses were achieved as illustrated in Figure 3.13. It is deduced that cylindrical and compound trapezoidal types are most effective geosynthetic base isolations.

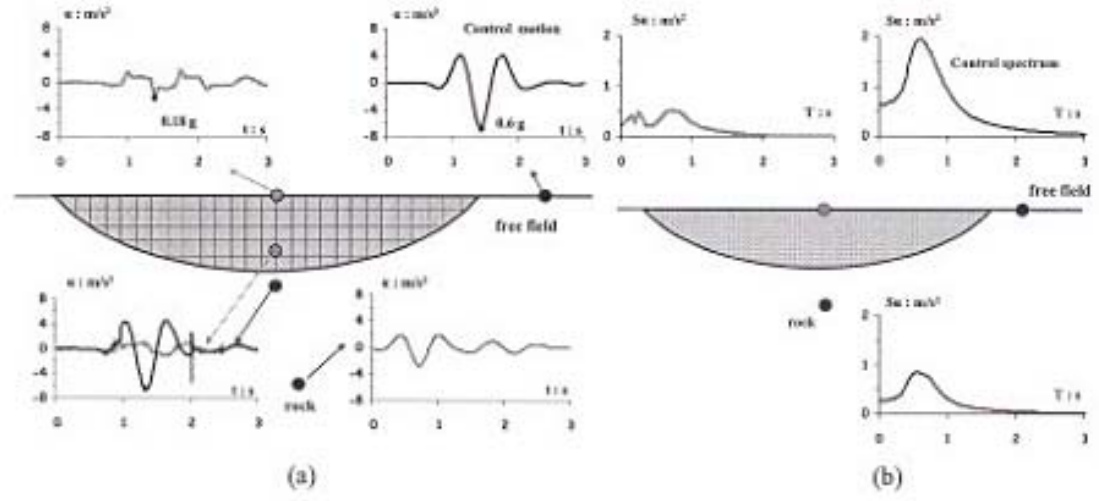

(a) Acceleration time histories, and (b) Response Spectral acceleration for cylindrical liner

(a) Acceleration time histories, (b) Response Spectral Acceleration for cylindrical liner geometry. Control motion : Ricker f_0 = 1 Hz; soft soil profile

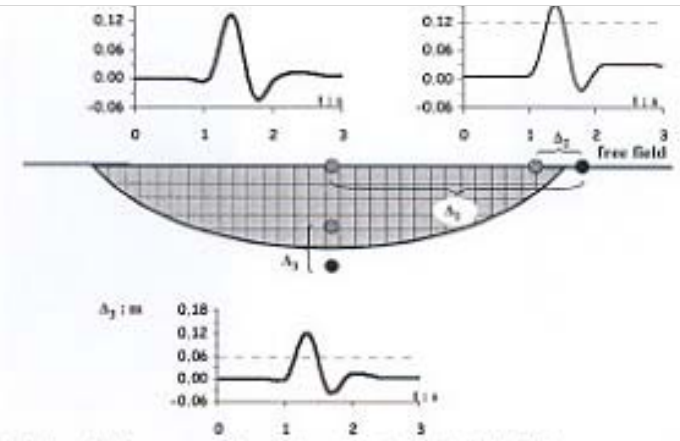

Relative displacement time histories for cylindrical liner geometry. Control motion : Ricker f_0 = 1 Hz, $a_{g_{max}}$ = 0.66 g ; soft soil profile

Relative Displacement time histories for cylindrical liner geometry. Control motion : Ricker f_0 = 1 Hz; soft soil profile

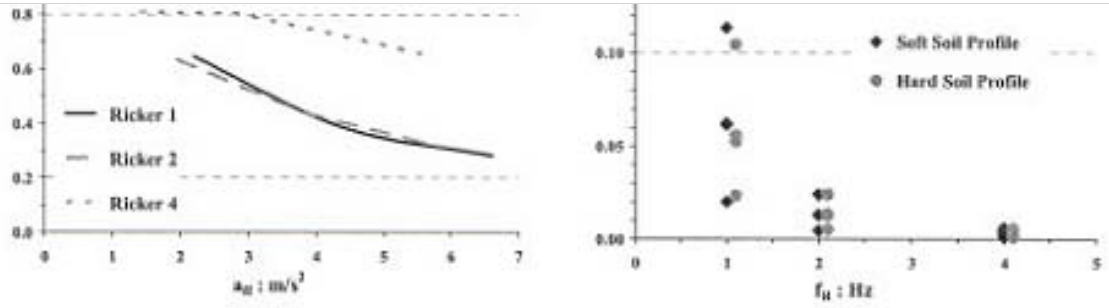

(a) Peak acceleration ratio (Soft soil profile), and (b) maximum slippage at the interface.

(a) Pick acceleration ratio and (b) maximum slippage at the interface

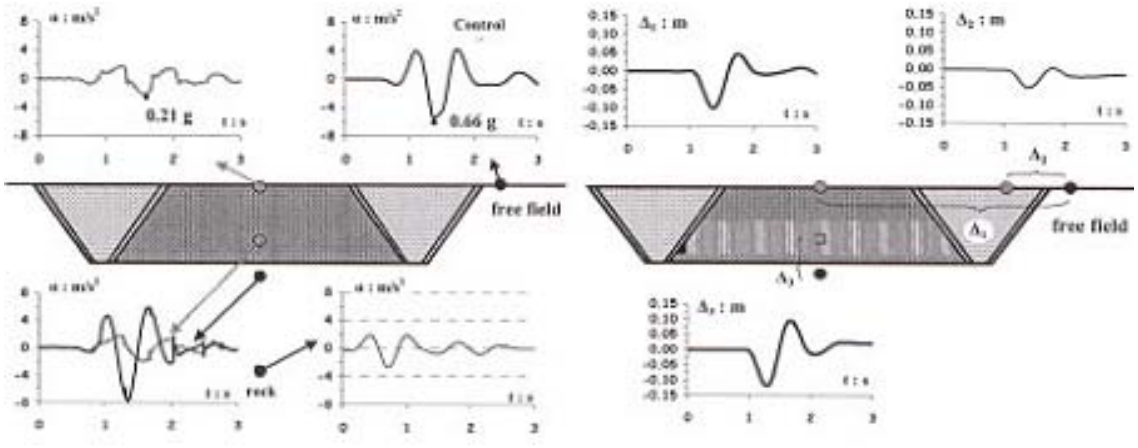

(a) Acceleration time histories, (b) Relative displacement time histories for trapezoidal liner geometry. Control motion : Ricker f_0 = 1 Hz; soft soil profile

Figure 3.13. Detailed results for trapezoidal geosynthetic liner (Yegian *et al.*, 2005).

Feng and Sutter (2000) performed a set of torsional resonant column test to investigate the shear modulus and damping ratio of granulated rubber and sand mixtures. Specimens were constructed using different percentages of granulated tire rubber and Ottawa sand at different percentages. As a result of these set of tests, it is figured out that the shear modulus of the mixtures influenced by the percentage of the rubber inclusion. Damping ratio increased slightly with confinement pressure for the 100 per cent rubber. This can be explained as; under increasing confining stress, the size of interparticle contacts between particles increases significantly due to the presence of rubber. Additionally, the normalized shear modulus reduction for 50 per cent granulated rubber is close to a typical saturated cohesive soil. It is stated that the damping ratio in rubber-sand mixture is due to; (i) the friction particles and (ii) the deformation of particles. The sand particles are very stiff and thus dissipate very little energy in particle deformation. Also, the samples prepared by hand-spooning were less uniform and consequently more sand clusters existed in samples and by the way the rubber dominates the strength behavior of mixture which results with lower shear modulus.

Edinçliler *et al.* (2004) conducted a set of cyclic triaxial test with tire buffings, sand and tire buffing mixtures. Test results demonstrate that the dynamic shear modulus values

for tire buffings are very low when compared to those of sand and tire buffing mixtures. Also, tire buffings added to the medium dense sand changed the deformation behavior and the dynamic behavior of sand–tire buffings mixture. The damping ratio of sand was increased more than threefold by the addition of tire buffings due to the fiber shape of tire buffings.

Ribay *et al.* (2004) carried out a set of laboratory cyclic triaxial and resonant column tests to investigate shear modulus and damping ratio of grouted sand. Different types of grouted sands were investigated. The results of experiments demonstrate that; the shear modulus increase with confining stress and variation of confining stress has a negligible effect on the damping ratio of specimen. Also the shear modulus increases as strain increases. The slight effect of variation in confining stress on damping ratio explained by the limited rotation and particle sliding and restricted mobilization of sliding.

Hyde *et al.,* (2007) investigated the compressibility and liquefaction potential of rubber composite materials. Regarding compressibility, Oedometer Test displayed that a sand mixture containing five per cent tyre chips by solid volume has a similar compressibility to that of pure sand. The compressibility of the mixtures, however, begins to change noticeably when the percentage of tyre chips is increased to 10 per cent and composites with greater than 20 per cent may not be tolerable in geotechnical design, suggesting that the limiting percentage of tyre chips mixed sand should not exceed 20 per cent. To come to a conclusion for the liquefaction potential, the Leighton Buzzard (United Kingdom) Sand and only CT0515 type tyre chips mixtures were subject to Cyclic Triaxial Test in undrained condition. Results demonstrated a more gradual buildup of pore water pressures but an overall reduction in the liquefaction resistance with increasing rubber chip content this time except one per cent rubber, 99 per cent soil mixture.

Lee J. S. *et al.* (2007) studied the load-deformation behavior of rigid-soft granular mixtures using specimens prepared with uniform sand and small rubber particles (D_{sand}/D_{rubber} ~4) at different volume fractions. They deduced following conclusions:

a. Small-, middle-, and large-strain deformation moduli are not linear functions of the volume fraction of rigid particles. A threshold volume fraction separates soft from rigid skeleton conditions. The threshold volume fraction is conning stress dependent.

b. The friction angle increases with sand fraction and no peak strength is apparent in specimens with low sand fraction (sf~0.6).

c. In most cases, load carrying particle chains do not involve soft particles. However, soft particles do participate in preventing the buckling of load carrying chains.

Kim *et al.* (2008) prepared mixtures of small rigid sand particles D_s and large soft rubber particles D_r at different volume fractions and tested small-strain and zero-lateral strain responses (D_r / D_s ~10). Both data sets are simultaneously gathered in an oedometer cell instrumented with bender elements. Results show that:

a. The sand skeleton controls the mixture response when the volume fraction of rubber particles is $V_{rubber} \leq 0.3$, while the rubber skeleton prevails at $V_{rubber} \geq 0.6$. The large size and incompressibility of rubber particles provides high stress-induced stiffness in the sand skeleton near the equatorial plane of rubber particles. The corresponding increase in local small-strain shear modulus G_{max} results in earlier wave arrivals in mixtures with $V_{rubber} \leq 0.3$ than in pure sand, while the quasi-static constrained modulus is highest in pure sand. The constrained modulus and shear wave velocity are power functions of the applied effective stress in all mixtures.

b. The development of internal fabric, particle level processes, and the associated macroscale response of sand rubber mixtures depend on the relative size between the soft rubber chips and the stiff sand particles D_r / D_s and their volume fractions.

Anastasiadis *et al.,* (2009) performed experimental and theoretical studies to investigate dynamic characteristics of soil-rubber mixtures using a fixed-free torsional resonant column device. Specimens were prepared with various percentages of granulated tire rubber and medium poor graded sand. Specimens were tested under 50 and 100 kPa confining pressures. It is concluded that low amplitude resonant column results indicate a significant reduction in shear stiffness of sand/rubber specimens due to contribution of rubber solids on shear stiffness of the sand/rubber matrix. Also, low amplitude damping ratio of sand-rubber mixtures increases significantly with an increase in the percentage of rubber. The dynamic parameters of clean granulated tire rubber are unaffected by confining pressure. Saturated specimens exhibit higher damping ratio at low amplitude shear strains due to the mechanisms of viscous damping observing on saturated specimens. Low amplitude shear modulus is slightly affected by moisture content.

Stimulation to create fields of scrap tire consumption in large amounts in front of augmenting tire waste stockpiles in developed countries of 1990's were reflected on the idea to use waste rubbers when mixed with soil as a lightweight backfill for embankments and other similar structure. That investigation continued to its evaluation with the idea to use scrap rubber as a remedy for earthquake hazardous soils due to rubbers' high damping mechanical properties. This concept is not only supported with above stated experimental findings, but also with numerical simulation applications.

3.3.2. Numerical Analyses of Improved Soils with Rubbers as Base Isolation

With the above mentioned vision of applying seismic isolation technology to public housing, schools and hospitals in developing countries where the replacement cost due to earthquake damage could be significant; Tsang *et al.* (2008) proposed an alternative seismic isolation scheme particularly suitable for developing countries, making use of rubbersoil mixtures.

A series of numerical simulations had been achieved with the proposed scheme in Figure 3.11. The subject building has a typical dimension (10-storey and 40 m width (*w*)) of a residential or office building. Surrounding the footing of a low-rise building, a layer of soil is replaced by soil mixed with a designated proportion of rubber of thickness (*t*) in the order of 10 m. They used QUAD4M as the instrument, a software capable of doing site response analysis with commonly adopted equivalent linear method. The rubber-soil mixture datas were adopted from the study of Feng and Sutter (2000), Vucetic and Dobry (1991).

Tsang *et al.* (2006) claimed that using rubber-soil mixture with above mentioned methodology could greatly reduce the level of horizontal, vertical shaking as well as other well-known seismic isolation systems due to rubber's energy dissipation mechanism, damping properties. They suggested that mixing soil with rubber could decrease its liquefaciton potential, is also safe regarding environmental concerns relying on previous studies; but still, they emphasized that preloading should be applied to rubber soil mixtures due to increasing compressibility to prevent possible excessive settlement.

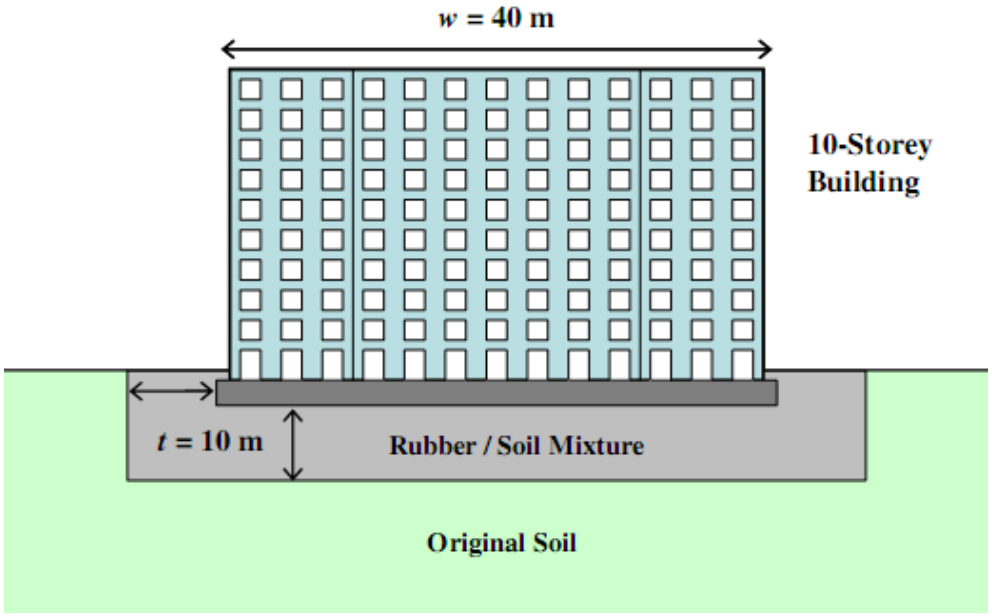

Figure 3.14. Schematic drawing of the proposed seismic isolation method using a layer of rubber-soil mixture (Tsang *et al*, 2007).

Recently; Tsang *et al.* (2009) came up with the idea of adding piling to their previous numerical setup (Figure 3.15). They developed an in-house program adopted by STRAND and QUAD4M. They adopted Feng and Sutter (2000) and Xiong (2010) tested rubber sand mixture samples to their simulation. They introduced percentage reduction in their parametric study.

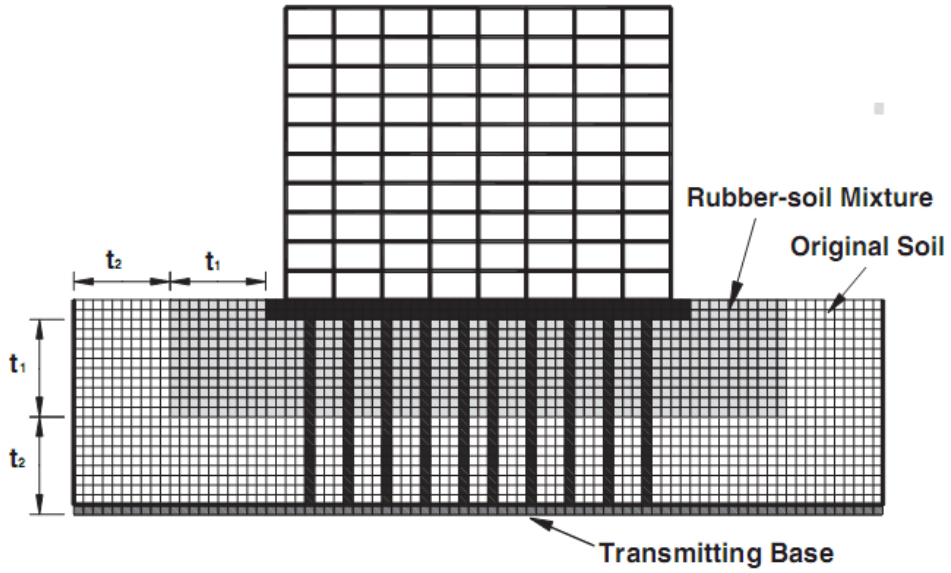

Figure 3.15. Finite element model of the geotechnical seismic isolation system with the use of granulated rubber-soil mixtures (Tsang *et al*, 2009).

Consequently, it is claimed that use of scrap tires as the rubber material could lead to 40–60 per cent response reduction on average in 1st floor drift, roof and horizontal accelerations on average. The results have been found to be the most sensitive to variations in the thickness of the RSM layer. Finally, the correlation between the period lengthening ratio and the reduction effectiveness has been briefly explored. They cited that rubber soil mixture could provide an alternative way of consuming huge stockpiles of scrap tires from all over the world.

4. THE NUMERICAL MODELING THEORY

4.1. Modeling in Engineering and Different Modeling Techniques

Modeling forms an implicit part of all engineering designs but few engineers are aware of the fact that they are making assumptions as part of the modeling or real conditions and consequences of those assumptions. During modeling, many of them may not have stopped to think about implicit approximations and assumptions, still less than the nature of the constitutive models that may have been invoked. Models in engineering are abbreviated representations of real systems, occurring environmental conditions. Therefore its accuracy depends on its promoting the extent. The skill in modeling is to spot the appropriate level of simplification to distinguish the important aspects from these that are not. All models are projections of reality; therefore they always possess a trade-off as to what level of detail is included in the model. Insufficient detailing reserves the risk of missing relevant interactions and the resultant model does not promote understanding. Reverse case makes it too much complicated and actually prevents the development of understanding. Models can't be developed in the context of the entire natural aspects. In a geotechnical model, it is essential to predict the soil behavior in the most appropriate manner available. Most commonly any analysis tries to break down a problem into sufficiently small elements to achieve this rationalization (Wood, 2004).

Theoretically, a proper ground description to determine the behavior of a soil or rock mass and engineering structure should include all properties in the mass including all spatial variations of these properties. To bring it on; it is necessary to divide a mass into assumed homogeneous geotechnical units. Then, a part of the mass in which the mechanical properties of the soil or intact rock material are assumed to be uniform. This includes also direction-dependent features such as discontinuities, of which the orientation and properties are uniform within the same geotechnical unit. Figure 4.1 shows a schematic visualization of a ground mass and its division in geotechnical units. In practice, homogeneity is seldom found and material and discontinuity properties vary within a selected range of values within every unit. The allowable variation of the properties within one geotechnical unit depends on the degree of variability of the properties within a mass

and the context in which the geotechnical unit is used. A ground mass with a large variation of properties over small distances necessarily results in geotechnical units with wider variations in properties. The smaller the allowed variability of the properties means more accurate calculation. Smaller variability of the properties of the geotechnical units involves collecting more data, however, and is thus more costly. The higher accuracy obtained for a calculation based on more data, therefore, has to be balanced against the economic and environmental value of the engineering structure to be built and the possible risks for the engineering structure, environment or human life. The allowable variations within a geotechnical unit for the foundation of a highly sensitive engineering structure will be smaller than for a geotechnical unit in a calculation for the foundation of a standard house. There are no specific standards for dividing a mass into units. It just depends on experience and 'engineering judgment' of geotechnical engineers. However, features such as changes in litho logy, faults, shear zones, etc., are often the boundaries of a geotechnical unit (Hack *et al.*, 2006).

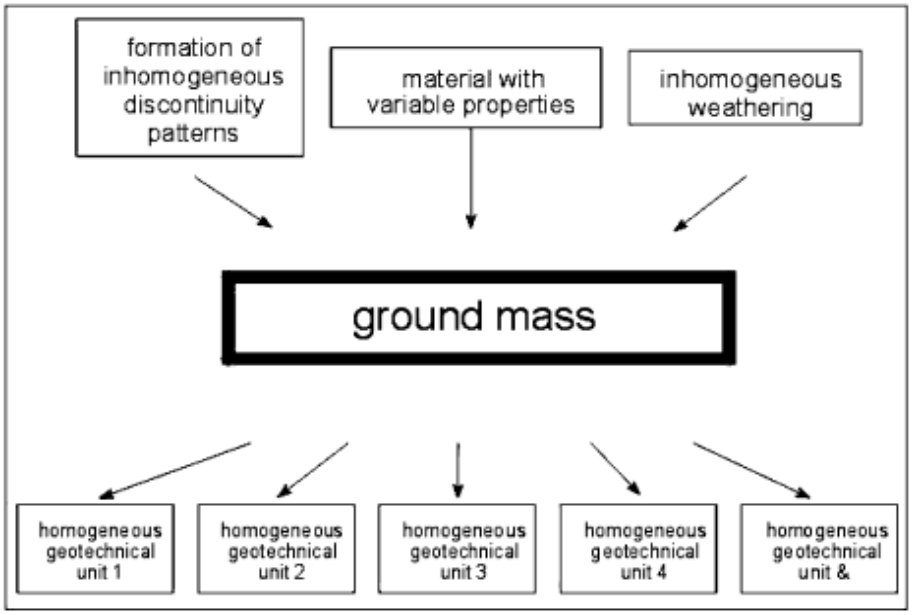

Figure 4.1. Tire chip-seal construction (Wood, 2004).

In traditional methods of design, it has been necessary to neglect or restrict one or more of the soil behaviors in order to make useful estimations with the parameters and methods available. Although each of the methods restricts different requirements, the constitutive behavior is always idealized in a variety of manners, none of which are a true

representation of actual soil behavior. That is why, the ability of full numerical analyses, such as those using the finite element or finite difference method, to represent all of these characteristics, including a wide range of constitutive soil models, which sets it apart as a uniquely powerful tool for the modern engineer. To be benefitted from such methods correctly, it is important to fully understand their specific applications and limitations and their theory. Uncertainty of the model in geo-engineering work should be common practice to make an estimation of the errors in the geotechnical properties of the subsurface and the influence of these errors on the engineering structure to be built in or on it. Different methodologies are applied to give a certain amount of quantification of possible errors in the design of an engineering structure due to uncertainty regarding the subsurface properties. The geotechnical expert knowledge used to make the subsurface model and the division of the subsurface layers in geotechnical units are addressed in only a very rudimentary way or not addressed at all in these analyses. To understand that it is necessary to go back to the basics of geo-engineering. The likelihood of the distribution or the inherent error in estimating a property at a certain location in space is well defined if appropriate statistical routines are used. However, depends on the correctness of the boundaries of the geotechnical units which itself is related to (i) the geology and (ii) the variation in properties allowed for each in geotechnical unit. Geotechnical engineers make use of a main knowledge of the geological environment to which the subsurface geology will adhere. The quality of this information, is essential in the interpretation and it cannot in general, be quantified at present. The establishment of geotechnical units, as well as the definition of their boundaries and the allowed variation of properties within each unit will be based on a balance between improved details against higher costs. It is known that no decent analysis of hazard and risk can be made if the quality of the expert knowledge and the definition of the geotechnical units cannot be quantified. Any up-to-date analysis describes all sorts of uncertainties in measurable properties, but is totally lacking one of these two main parameters governing, to a large extent, the correctness of the subsurface model (Wood, 2004).

For any engineering problem modeling has few aspects closely related to each other; (i) theoretical (mathematical) model, (ii) experimental (physical) model, (iii) numerical model. The first important stage is the theoretical modeling with the correct

formulation. The physical modeling is performed in order to validate theoretical or empirical hypotheses. It can be built in two cases: Full scale and small scale models. In the field of engineering, the scale model is usually smaller than the original and used as a guide of the object in full size. The numerical model which will be conducted has to be synchronized with physical model in order to take similar responses from analysis. In this sense, physical and numerical model can be considered as complementary to each other. Muir *et al.* (2002) stated that the observation forms are indispensable part of the reflective practice loop which underpins engineering and scientific progress during the modeling. It is cited that the modeling chronology is as important as excellent observation (Figure 4.2).

The above methodology is appropriate for the principle geotechnical earthquake engineer problem; soil-structures' dynamic behavior. The correct observation and proper mathematical formulation is the initial problem to solve. For numerical modeling, simulation of the real problem's physics is a must for idealizing the material characterization and the boundary conditions' representation as in mathematical model.

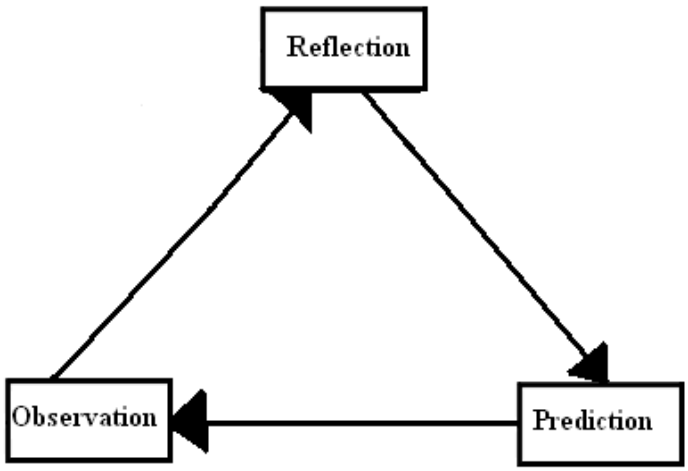

Figure 4.2. Reflective practice loop (Blockley, 1992).

Physical models needs visualization, from examining the model, of information about the thing the model represents. The geometry and the object must be similar in the sense that one is a rescaling of the other. For that reason the scale is an important

characteristic. However, in many cases the similarity is only approximate or even intentionally distorted.

4.2. Physical (Scale) Modeling

Models can be advantageous for studying prototype-scale behavior on a qualitative basis by verifying the assumptions that have been adopted in the theoretical analysis. In absence of former practical experience, it allows unpredictable difficulties to be found and errors to be corrected at relatively low costs. It is also helpful when the mathematical approach does not provide good results or the problem involves so many variables that no analytical solution can be developed (Pinto, 1999).

Full-scale testing is a physical modeling where all features of the prototype being studied and reproduced at full scale. However, it is desired to obtain information about expected patterns of response more rapidly and with closer control over model details than would be possible with full-scale testing. This usually implies that parametric studies should be performed in which key parameters of models are varied in order to discover their effect (Wood, 2004).

Scale models are an excellent tool to study engineering problems since they provide a possible solution for most of the problems posed with full-size testing. Reduced-scale models are versatile, cheaper and easier to construct, and less time is required for instrumentation, and testing. Reduced-scale models can be monitored until failure occurs, which is difficult in full-scale experiments. For quantitative studies, the most important principle is obeying modeling laws. The correct scaling of the influencing parameters is the basis for the reliability of the results. Errors, due to the difficulty of reproducing certain features accurately to scale, or due to factors that have been overlooked when formulating the conditions for modeling, introduce what is commonly called “scale effects” (Pinto, 1999).

If the model is not built at full scale then we must know how to extrapolate the observations that we make at model scale to the prototype scale. If the material behavior is entirely linear and homogeneous for the loads that we apply to the model and expect in the prototype then it may be a simple matter to scale up the model observations and details of the model but, this still depends on the details of the underlying theoretical model. However, if the material behavior is nonlinear or if the structure to be studied contains several materials which interact with each other, then the development of the underlying theoretical model will become more difficult. It then becomes even more vital to consider and understand the nature of the expected behavior so that the details of the model can be correctly established and the rules to be applied for extrapolation of observations are clear (Wood, 2004).

Similarity and dimensional analyses are two analytical methods used for physical modeling. Similarity requirements involve the general equilibrium equations and the stress-strain relationship of the materials. Dimensional analyses allow the different independent variables influencing the phenomenon to be arranged in independent dimensionless combinations that show how the different variables are related to each other (Pinto, 1999).

There are various different ways in which dimensions of variables can be defined but the most commonly used fundamental system reduces everything to combinations of length [L], mass [M], time [t]. Where thermal effects are important then it is necessary also to add in temperature and charge but those additions will not concern us here. For many geotechnical problems we are concerned with forces and stresses rather than masses and the dimension of time only comes in through the conversion of mass to force.

4.2.1. Centrifuge Model Tests

Being the most common physical modeling test, the mechanical principle is; if a body of mass *m* is rotating at constant radius *r* about an axis with steady speed '*v*' then in

order to keep it in that circular orbit it must be subjected to a constant radial centripetal acceleration. In order to produce this acceleration, the body must experience a radial force, mrw^2, directed towards the axis. It is necessary to test the model in a gravitational field n times larger than that of prototype in order to replicate the gravity-induced stresses of a prototype in a 1/n reduced model. A centrifuge is the most convenient tool to make a high acceleration field in a model. This idea was applied for the first time in 1930's, in the field of the geotechnical engineering. Today, centrifuge modeling has become one of the powerful tools for physical modeling. There are two types of centrifuge machine that are in common use: beam and drum (Figure 4.3 and 4.4). In beam centrifuge, the model is rotated about a vertical axis at the end of a strong beam which at its other end carries some sort of a balancing mass or counterweight in order to prevent damaging out of balance rotator forces on the centrifuge bearings. In many beam centrifuges the model is placed on a swinging platform so that the local gravitational acceleration field in the model is always coincident with the model vertical as the centrifuge speed is increased. This has obvious advantages for model preparations. The power of the centrifuge is usually quoted in g-tones a given device may be able to tolerate a larger model but with lower permissible maximum acceleration (Wood, 2004).

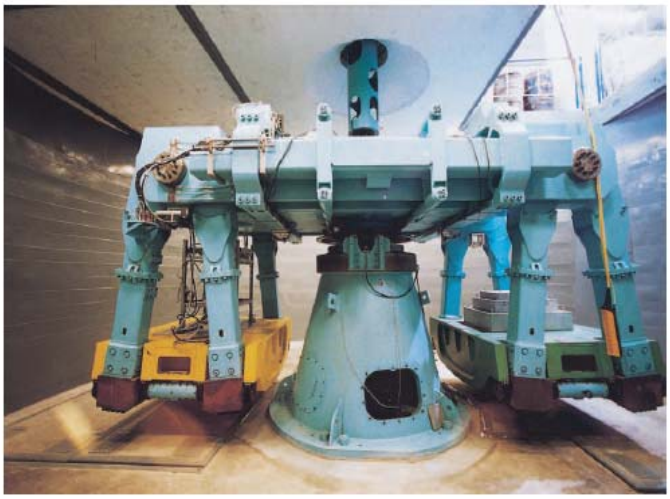

Figure 4.3. Beam centrifuge test machine.

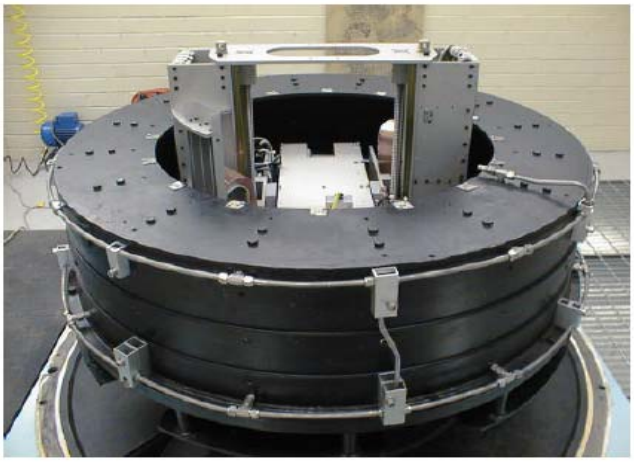

Figure 4.4. Drum centrifuge test machine.

4.2.2. Shaking Table Model Tests

The purpose of the tests is to validate the numerical model or to understand the basic failure mechanisms. They have the advantage of well controlled large amplitude, multi-axis input motions and easier experimental measurements.

Shaking table research has provided valuable insight into liquefaction, post-earthquake settlement, foundation response and lateral earth pressure problems. For the models used in shaking tables, soil can be placed, compacted and instrumented relatively easily. Though higher gravitational stresses cannot be produced in a shaking table test, the contractive behavior associated with high normal stresses at significant depths can be simulated by placing soil very loosely during model preparations (Figure 4.5).



Figure 4.5. Shaking table test machine.

In shaking table tests, the similarity rule in terms of stress and strain against the prototype cannot be satisfied because of the stress dependency of the stress–strain soil behavior. Thus the model tests can be considered to be small prototype test. A number of works have been carried out to understand the failure mechanisms and behavior of earth structures using shaking table tests. Koga and Matsuo (1990) carried out shaking table tests on reduced scale embankment models founded on saturated sandy ground. They investigated the cyclic stress strain behavior of soil in the ground by using the acceleration and pore pressure records. Kokusho (2003) has explained the use of one g shaking table tests in understanding the mechanism of flow failure in liquefied deposits. He retreated that use of torsion simple shear tests, in situ soil investigation, case histories including shaking table tests were essential to understand and develop the lateral flow mechanism during liquefaction. Orense *et al.* (2003) stated the importance of one g shaking table tests in understanding the behavior of underground structures during soil liquefaction. They have reviewed several shaking table test results from different authors on the behavior of buried structures and possible mitigation measures against liquefaction failure using gravel drains. In order to reproduce actual earthquake data, a six degree of freedom shaking table is essential. It is a very complex electro-hydraulic system and requires high maintenance and operational costs. If the response and failure mechanisms are eliminated, single degree of

freedom of shaking tables is sufficient. The increase of payload causes the increase in cost of motion starters.

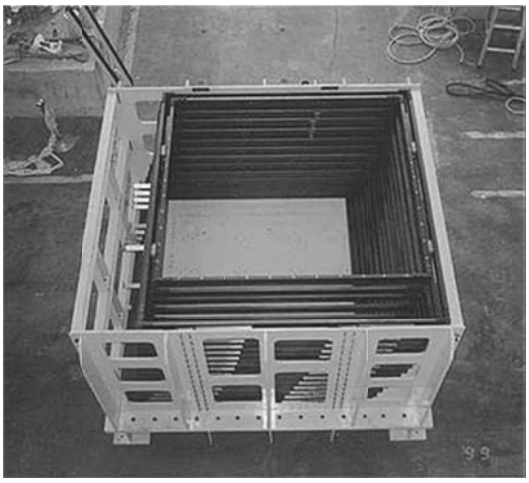

Figure 4.6. Laminar shear box (Ueng *et al.*, 2006).

The physical model tests in geotechnical earthquake engineering have been developed as a method between element and in situ tests. This kind of tests is being used for the study of seismic behavior of level or inclined grounds in liquefiable soils or soft clays, soil-structure systems like shallow or deep foundations, retaining walls and embankments. Using the model test results in controlled conditions considering material type and boundary conditions, we can simply identify the failure mechanisms, optimize the design methods and determine the validity of the constitutive models and analytical methods. The physical model tests in earthquake geotechnical engineering are conducted in 1g gravity field on shaking table, or the augmented gravity field in geotechnical centrifuge. Considering the necessity of correspondence for stress levels in real situation and the model case, use of centrifuge in modeling of earthquake geotechnical problems lead to more applicable results, although there are still some deficiencies and without minimizing the induced errors, the results of centrifuge tests are not reliable (Wood, 2004).

4.3. Numerical Modeling and QUAD4M

In numerical modeling, to understand the controlling physical constraints on each problem is important. To begin, soil mechanical properties characterization and the

boundary conditions must be clarified. Exact, closed-form solutions are in general only obtainable for a rather limited set of conditions. It is always necessary to consider whether the massaging of the problem to fit these constraints removes any key characteristics of the problem. There is the possibility of using numerical techniques when the situation is clearly too great to obtain a solution and when there is an underlying simple and widely accepted theoretical description of the physical conditions.

Numerical solution usually implies the replacement of a continuous description of a problem in which the solution is only obtained at a finite number of points in space and time. The accuracy of the result depends on the quality of the numerical approximation. If key quantities are changing very rapidly with position or with time, it is necessary either to increase the density of the discretization used in the numerical modeling in order to be able to follow the changes or else to incorporate within the numerical description some mathematical interpolation which is able to follow the real variation between discrete modeling points. If the exact answer of a problem is known, it is highly probable to take correct results from a procedure that is developed for numerical solution. In this case, it would be possible to approach to the matter of concern more confidentially (Wood, 2004).

Currently, the finite element method (FEM) is a powerful numerical technique for analyzing problems involving complicated geometries, loadings and material properties and it is widely used by geotechnical earthquake engineers in numerical modeling instruments such as QUAD4M; one of the most commonly used computer program employing the equivalent linear method. It is a dynamic, time domain, equivalent linear, two-dimensional (2-D) FEM software. And the nonlinear characteristics of soils are captured by two strain compatible material parameters; shear modulus G and damping ratio D. QUAD4M and ELA principles is given below in further details (Kavazanjian, 2006; Xuan *et al.*, 2009).

4.3.1. Equivalent Linear Approach (ELA)

It is well known that dynamic properties of soils are significantly dependent on the soil shear strains. Because of the complexity and rare use of full nonlinear analysis,

equivalent linear dynamic analysis is preferred in many engineering problems involving soil dynamics and/or soil structure interaction to investigate shear strain dependent soil dynamic properties. In literature, the equivalent linear approach was first proposed by Idriss and Seed (1990) and elaborated upon by Constantopoulos *et al.* (1973). It uses a damped elastic model whose appropriate properties are obtained iteratively to model the dynamic response of the non linear hysteretic soil.

When used with the finite element method, in each element, the stress-strain properties of the soil are defined by a shear modulus and an equivalent damping ratio which depend on the shear strain in equivalent linear analysis. The variation of the shear modulus and the equivalent damping ratio with regard to shear strain is derived from extensive experiments. The iteration procedure is schematically given in Figure 4.7.

1. Initial estimates of shear modulus G (1) and damping ratio D (1) are made for each element.

2. The estimated G (1) and D (1) are utilized to compute the soil structure system response, including the shear strain time histories of each element.

3. The effective shear strain in each element γ_{eff}^{1} is calculated from the maximum shear strain in the computed response times a reduction factor, which varies from 50 per cent to 70 per cent in earthquake analysis. In this study, 65 per cent is employed.

4. From the effective shear strain γ_{eff} (1), G (2) and D (2) which are compatible with it are obtained and used for the next iteration.

5. Steps two to four are repeated and the parameters are checked until strain compatible values of G and D are obtained.

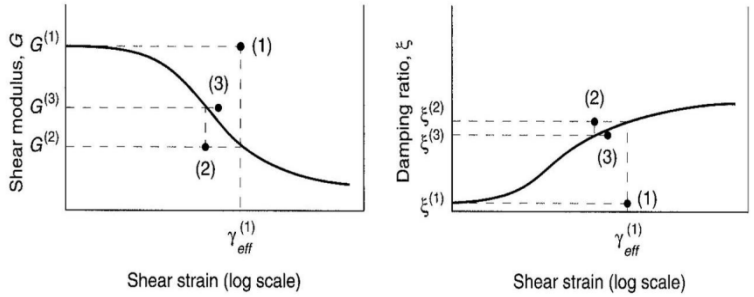

Figure 4.7. Iteration toward strain-compatible G and D in equivalent linear analysis (Xuan *et al.*, 2009).

4.3.2. Finite Element Method, the Theory

For simplicity, three-dimensional (3-D) soil-structure systems are presented by means of either one or two dimensional models (1-D or 2-D). 2-D approximations are well justified and can reliably simulate 3-D conditions especially for structures with cylindrical symmetry, or under plane strain conditions. Thus, a 2-D finite element model as illustrated in Figure 4.8 is formulated to model the soil foundation-structure system.

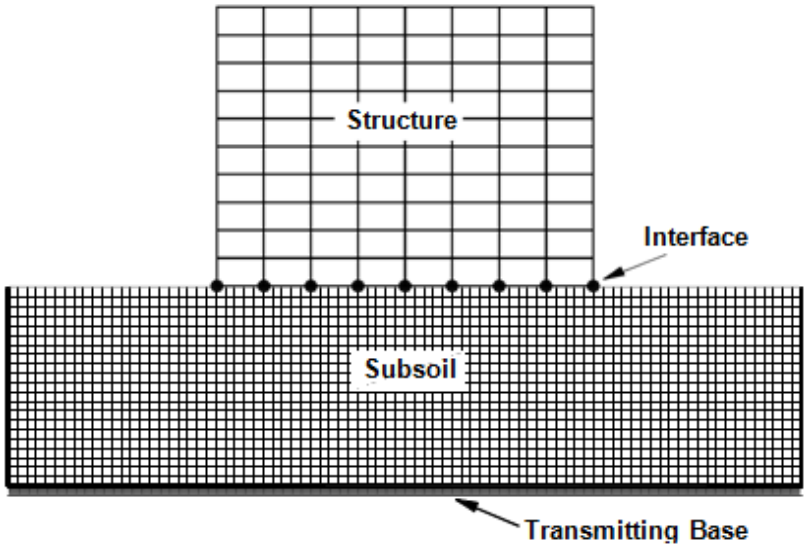

Figure 4.8. The finite element model (Xuan *et al.*, 2009).

4.3.3. Soil Modeling

In QUAD4M, the soil is assumed as a plane strain material in 2-D FEM models. The 4-node plane strain element is utilized to model its properties. The element stiffness matrix is given as:

$$[K]^e = \int \int [B]^T [C] \, [\mathrm{B}] \, \mathrm{dxdy} = \int_{-1}^{1} \int_{-1}^{1} [\mathrm{B}]^T [\mathrm{C}][\mathrm{B}] \, [\mathrm{J}] \, \mathrm{d}\xi \, \mathrm{d}\eta \tag{4.1}$$

in which [B] is the strain-displacement transformation matrix, J is the Jacobian operator relating the natural coordinate derivatives with the local coordinate derivatives, and [C] is stress strain matrix. In a 2-D plane strain problem, [C] is given as:

$$[\mathrm{C}] = \begin{bmatrix} \frac{E(1-\upsilon)}{(1+\upsilon)(1-2\upsilon)} & \frac{\upsilon E}{(1+\upsilon)(1-2\upsilon)} & 0 \\ \frac{\upsilon E}{(1+\upsilon)(1-2\upsilon)} & \frac{E(1-\upsilon)}{(1+\upsilon)(1-2\upsilon)} & 0 \\ 0 & 0 & \frac{E}{(1+2\upsilon)} \end{bmatrix} \tag{4.2}$$

The three-order Gaussian numerical integration procedure in which both the positions of the sampling points and the weights have been optimized is employed for the integration of Equation (4.3).

$$[K]^e = \sum_{i=l}^{3} \sum_{j=1}^{3} [\mathrm{B}]^T [\mathrm{C}] \, [\mathrm{B}] \, [\mathrm{J}] \, \mathrm{W}_i \, \mathrm{W}_j \tag{4.3}$$

Where W_i and W_j are the weight coefficients. The element mass matrix of a 4-node plane strain element is also given as a lumped-mass matrix that will be described in more details further.

$$[M]e = \rho A \setminus 4 * [1\ 1\ 1\ 1\ 1\ 1] \tag{4.4}$$

4.3.4. Super Structure Modeling

The buildings are modeled by the 2-D frame element, as illustrated in Figure 4.8. Through standard FEM procedure, the element stiffness matrix corresponding to local coordinate's x-y can be given as:

$$\left[\hat{K}\right]^e = \begin{bmatrix} \frac{EA}{L} & 0 & 0 & -\frac{EA}{L} & 0 & 0 \\ 0 & \frac{12EI}{L^3} & -\frac{6EI}{L^2} & 0 & -\frac{12EI}{L^3} & -\frac{6EI}{L^2} \\ 0 & -\frac{6EI}{L^2} & \frac{4EI}{L^2} & 0 & \frac{6EI}{L^2} & \frac{2EI}{L} \\ -\frac{EA}{L} & 0 & 0 & \frac{EA}{L} & 0 & 0 \\ 0 & -\frac{12EI}{L^3} & \frac{6EI}{L^2} & 0 & \frac{12EI}{L^3} & \frac{6EI}{L^2} \\ 0 & -\frac{6EI}{L^2} & \frac{2EI}{L} & 0 & \frac{6EI}{L^2} & \frac{4EI}{L} \end{bmatrix}$$

Figure 4.9. The element stiffness matrix.

Where E is the young's modulus, A is the cross section area, I is the moment of inertia and L is the length of the element. For a typical element, the transform function can be expressed as

$$[T] = \begin{bmatrix} \cos\varphi & \sin\varphi & 0 & 0 & 0 & 0 \\ -\sin\varphi & \cos\varphi & 0 & 0 & 0 & 0 \\ 0 & 0 & 1 & 0 & 0 & 0 \\ 0 & 0 & 0 & \cos\varphi & \sin\varphi & 0 \\ 0 & 0 & 0 & -\sin\varphi & \cos\varphi & 0 \\ 0 & 0 & 0 & 0 & 0 & 1 \end{bmatrix}$$

Figure 4.10. The transform matrix.

Hence, the element stiffness matrix corresponding to general coordinates can be derived by the following equation:

$$[K]e = [T]T\ [\acute{K}]e\ [T] \tag{4.5}$$

The element mass matrix can be derived either as lumped-mass matrix or as consistent mass matrix. Different mass formulation method has only small affect on the result but; the dynamic analysis of a consistent mass system requires significantly more computational effort than a lumped-mass system does. Thus the lumped-mass method is employed in the finite element modeling in this study.

In lumped-mass system, if more than one translational degree of freedom is specified at any nodal point, the same point mass will be associated with each degree of freedom. On the other hand, the mass associated with any rotational degree of freedom will be zero due to the assumption that the mass is lumped in points which have no rotational inertia. Thus the matrix of a 2-D element can be written as:

$$[M]e = \rho\ A\ L \setminus 2 * [1\ 1\ 0\ 1\ 1\ 0] \tag{4.6}$$

where ρ is the frame's density.

4.3.5. Time Domain Motion Equation

In the FEM analysis, the elastic continuum is approximated as an assemblage of discrete finite elements interconnected only at nodal points on the element boundaries. The governing partial differentiation equations of motions can be written by expressing dynamic equilibrium of the effective forces associated with each element. This procedure derives a system of second order ordinary differential equations in matrix form.

$$[M]\,\ddot{U} + [D]\,\dot{U} + [K]\,U = R(t) \tag{4.7}$$

in which [M], [D] and [K] are the mass, damping and stiffness matrix, respectively, R is the vector of the externally applied load and U is the displacement vector.

Dots indicate derivation with respect to time. It is worth noting from Equation (4.7) that in a dynamic problem, all the forces resulting from motion, including the acceleration-dependent inertial forces, the velocity dependent damping forces and the elastic forces, and the externally applied load should be included in such an equilibrium statement. Especially for the cases where earthquake excitation is applied to the system, the external force vector R can be expressed as $R = -M\,\ddot{U}_g$, where $\ddot{U}_g$ is the input earthquake.

4.3.6. Damping Matrix

The element damping matrix is constructed using Rayleigh method:

$$[D]_q = \alpha_q\,[M]_q + [\beta]_q\,[K]_q \tag{4.8}$$

For each element q, the use of Rayleigh damping results in a frequency dependent damping ratio

$$\lambda_q = \frac{1}{2}\left(\frac{\alpha_q}{\omega} + \beta_q \text{ x } \omega\right) \tag{4.9}$$

Since the damping in both soil and building is not frequency dependent, the selection of α_q and β_q must be made that provides damping values which have the minimum variation over the range of frequencies of interest. Based on the assumption that the first mode of vibration has the highest participation factor among all the modes, the damping should be minimized at the fundamental frequency of the entire soil-structure system, f_1. Furthermore, studies have been performed by using several different earthquakes and several different one-dimensional deposits. The second frequency was chosen as f_2 which is equal to n times f_1.

In light of the response of a shear beam in which of the frequencies of higher modes are odd number of times of the frequency of the fundamental mode of the beam, n was chosen to be an odd integer. The parameter was selected as

n = closest odd integer than f_i / f_1, Where f_i is the dominant frequency of the input motion.

This allows the FEM model to respond to the dominant frequency of the input earthquake motion without experiencing significant over-damping. Thus the damping is set at two frequencies and the values of α_q and β_q can be given as

$$\alpha_q = 2\lambda_q \frac{\omega_1\ \omega_2}{\omega_1 + \omega_2}$$
$$\beta_q = 2\lambda_q \frac{1}{\omega_1 + \omega_2} \tag{4.10}$$

The adoption of this two-frequency scheme results in under damping over the frequency range of ω_1 to ω_2 and over-damping outside the range.

4.3.7. Global Matrices

For the nodes outside the interface as shown in Figure 3.8, their contribution to the global stiffness and mass matrix is the same as in the standard finite element method.

Special attention is required for the nodes at the soil-structure interface. As a node in a 2-D frame element, the node has three degrees of freedom, transverse and axial displacements and a rotation, while a node in a plane strain element has only two degrees of freedom, the horizontal and vertical displacements. In the finite element model, displacement compatibility was applied at the interface nodes, where the rotational degree of freedom is free, and the stiffness of the beams at the ground floor was modified to be larger, so as to ensure that no significantly large rotation exists in the first floor.

Following the same procedure of the global stiffness matrix, the global damping matrix is formulated by an assemblage of the element damping matrix.

4.3.8. Soil – Structure Interaction

Studies relying on soil structure interaction in the past three decades have emphasized three effects: (1) reduction of the resonant frequencies of systems in comparison to those of the fixed-base structure; (2) partial dissipation of the vibration

energy of the structure through wave radiation into the soil; and (3) modification of the actual foundation motion from the free field motion.

Typically, the soil-structure system consists of two distinct parts with different properties. One is the structure with bounded dimensions that consists of the actual structure with its foundation and usually an irregular adjacent soil region. The other part is the soil; unbounded, extending to infinity.

The existing methods for studying the relevant interaction phenomena in dynamic analysis of structures can be classified as a substructure method and a direct method. In direct method, the soil was represented explicitly in the analytical model, and this was completed by merely combining a layer of soil with the model of the structure. While in substructure analysis, the soil-structure interaction system is represented as two independent mathematical models, the connection between them is provided by interaction forces of equal amplitude but acting in opposite directions on the two substructures. It is obvious that the direct method is simpler and easier to implement in computer programs, rendering its extensive use in commercial software packages. However, there is one major deficiency that the bounded soil model does not allow the vibration energy in the structure and soil to propagate away, and thus ignores the effective damping mechanism of the soil half space. To model the radiation condition, a variety of methods have been developed to introduce transmitting boundaries into the finite element models.

Based on various mathematical principles many different local transmitting boundaries have been proposed in the time domain as well as in the frequency range, which include:

1. Use of half-infinite elements (boundary elements).

2. Adaptation of the material properties of elements at the boundary (low stiffness,

high viscosity).

3. Use of viscous boundaries (dampers).

It has been shown that all of them have their advantages and disadvantages, and are problem dependent. Mengi *et al.* (1992) and Bettes *et al.* (1991) have given review of transmitting boundaries and discussion of their limitations. For the implementation of dynamic effects in this FEM model the viscous boundaries method are adopted. The theory of this method is given in the following section.

4.3.9. Transmitting Boundary

In opting for transmitting boundaries, a damper is used instead of applying fixities on the boundary of the computational domain. The damper guarantees that an increase in stress on the boundary is dissipated without rebounding. The implementation of a transmitting base in the finite element model is based on the method described in Lysmer and Kuhlemeyer (1969).

The application of these dampers includes adding damping to each of the nodes which make up the base and sides of the finite element model. Since the finite element model will always be placed over a half space and the influence of the side boundaries can be readily mitigated by increasing the extent of the finite element model, only the base dampers are implemented at present.

Mathematically implementation of these dampers involves adding the transmitting boundary damping terms to the diagonal terms of the corresponding nodes on the transmitting boundary. In this manner, an adjustable force in the x and y direction that are proportional to the velocity of the special nodes are produced. The coefficients added to the diagonal terms are given as:

For direction perpendicular to boundary: $\rho V_p L$

For direction parallel to boundary: $\rho V_s L$

Where V_p and V_s are the velocity of P and S wave corresponding to the material below the finite element model, ρ is the density. L is half the distance of the special node to the next node on both sides.

4.3.10. Time Integration, Newmark Family Method

When inelastic material behavior and/or large deformation and strains are involved in the finite element model, the equations of motion become nonlinear and are usually solved by direct time integration method. The Newmark method is the most widely used method in dynamic analysis.

In order to solve the differential equation for arbitrary variation of forcing function as a function of time, it is necessary to introduce equations regarding the acceleration Ü, velocity Ù and displacement U. Newmark (1959) introduced one of the most widely used methods of numerical integration in earthquake engineering. It consists of the following equations:

$$\begin{aligned} \dot{U}_{t+\Delta t} &= \dot{U}_t + (1-\gamma)\Delta t\ddot{U}_t + \gamma\Delta t\ddot{U}_{t+\Delta t} \\ \dot{U}_{t+\Delta t} &= U_t + \Delta t\dot{U}_t\left(\frac{1}{2}-\beta\right)\Delta t^2\ddot{U}_t + \beta\Delta t^2\ddot{U}_{t+\Delta t} \end{aligned} \tag{4.11}$$

The Newmark family method contains as special cases many well known and widely used methods. Characteristics of some classical methods are summarized in Table 4.1.

It can be observed from Table 3.1 that the acceleration and Fox-Goodwin methods are implicit and conditionally stable. Comparing with implicit and unconditionally stable average acceleration method, they are not economically competitive for large scale systems. Hence, the average acceleration method is employed in the finite element model.

Table 4.1. Characteristics of well-known members of the Newmark family methods (Hughes, 1987).

Method	Type	β	γ	Stability condition	Order of accuracy
Average acceleration (trapezoidal rule)	Implicit	1/4	1/2	Unconditional	2
Linear acceleration	Implicit	1/6	1/2	$\Omega_{crit} = 2\sqrt{3} \equiv 3.464$	2
Fox-Goodwin (royal road)	Implicit	1/12	1/2	$\Omega_{crit} = \sqrt{6} \equiv 2.449$	2
Central difference	Explicit	0	1/2	$\Omega_{crit} = 2$	2

4.3.11. Trapezoidal Rule

Substitute β and γ with 1/4 and 1/2, equation (4.10) can be rewritten as

$$\ddot{U}_{t+\Delta t} = \frac{4}{\Delta t^2}[U_{t+\Delta t} - U_t] - \frac{4}{\Delta t}\dot{U}_t\ddot{U}_t$$
$$\dot{U}_{t+\Delta t} = \dot{U}_t + \frac{\Delta t}{2}[\ddot{U}_t + \ddot{U}_{t+\Delta t}] \quad (4.12)$$

Using equation (4.11), the following equations are derived for solving the displacement, velocity, and acceleration at each time step:

$$U_{t+\Delta t} = [\bar{K}]^{-1}[\bar{R}]_{t+\Delta t}$$
$$[\bar{K}] = \frac{4}{\Delta t^2}[M] + \frac{2}{\Delta t}[C] + [K]$$
$$[\bar{R}]_{t+\Delta t} = [R]_t[M]A_{t+\Delta t} + [C]B_{t+\Delta t}$$
$$A_{t+\Delta t} = \frac{4}{\Delta t^2}(U_t + \Delta t\dot{U}_t + \frac{\Delta t^2}{4}\ddot{U}_t)$$
$$B_{t+\Delta t} = \frac{2}{\Delta t}U_t + \dot{U}_t \quad (4.13)$$

4.4. Experimental and Numerical Modeling Applications

Diana SWANDYNE numerical analysis program has been also used for seismic geotechnical problems (Taylor *et al.*, 1995; Crewe *et al.*, 1995). It is a dynamic interaction and nonlinear 2-D (plane strain and axially symmetric) program which uses the fully coupled biot dynamic equation with the assumptions.

Zarnani and Bathurst (2005) made investigations on geofoam seismic buffers with using FLAC numerical code. They performed physical and numerical tests of wall models with a seismic geofoam buffer inclusion. In this study, large shaking table with 1x1.4x2 m dimensions. The reduced scale wall is modeled with two m long and one m width. The thickness of the EPS geofoam was taken as 150 mm with one m height to match both at numerical and physical models. As a result of set of numerical and physical analysis, it is concluded that the numerical simulation results are also shown to be in quantitative agreement with the relative reduction of the earthquake-induced dynamic earth forces

generated against the rigid wall structures with an EPS geofoam seismic buffer compared to the control case without seismic protection.

Bathurst *et al.* (2006) performed shaking table tests with geofoam seismic buffers. The tests were carried out using 1m high models mounted on a large shaking table. Three different geofoam buffer materials used with 16, 14 and six kg/m³ densities. A rigid box is modeled with 2.5 x 1.4 x 1.3 m dimensions and dynamically tuned over 2.7 x 2.7 m shaking table platform. As a result of this study, it is concluded that the reduction in dynamic load increased with decreasing seismic buffer density. It is found that the maximum dynamic force reduction was 31 per cent at a peak base acceleration of 0.7g.

Bathurst *et al.* (2006) studied on a model for response analysis of EPS geofoam seismic buffers. A wall is modeled with EPS geofoam seismic buffer as a linear elastic material. Four physical reduced-scale model shaking table tests were performed. The dimensions of the shaking table platform were 2.7 x 2.7 m and the EPS geofoam was taken as 150 mm thickness with one m height. The numerical analyses were performed with FLAC numerical code. Four type of EPS geofoam wall were used with 16, 12, 14 and 6 kg/m³. As a result of these investigations, it is seen that the measured peak horizontal force acting on the wall was less for the most compressible buffer compared to the stiffest material. At accelerations higher than 0.7g, there is likely more complex system responses that cannot be captured by the simple displacement model employed. All in all, it is concluded that the model is simple and provides a possible framework for the development of advanced models that can accommodate more complex constitutive laws for the component materials and a wider range of problem geometry.

Zarnani and Bathurst (2008) studied on numerical modeling of EPS seismic buffer shaking table tests. In the numerical analysis, FLAC numerical code was used. Five physical tests constructed with EPS geofoam materials with different material properties. The density of EPS materials were; 16, 14, 12, six and 1.32 kg/m³. The dimensions of shaking table were 1 x 1.4 x 2 m and the EPS geofoam was taken as 150 mm thickness

with one m height. As a result of the study it is seen that the numerical model was able to capture the trend in earth forces with increasing base acceleration for all six models and in most cases quantitative dynamic load–time response of the numerical simulations was in good agreement with measured values.

Pitilakis *et al.* (2008) made investigations on numerical simulation of dynamic soil-structure interaction in shaking table. In this study, they designed a shear stack in 1.2 m long, 0.55 m wide and 0.8 m deep. A shaking table with three m by three m cast-aluminum seismic platform capable of carrying a maximum payload of 21 tons is used. The uniformly graded Dry Hostun S28 sand is used for as test material. The numerical code MISS3D is used to simulate the shaking table tests. The numerical analysis is performed in the frequency range up to 100 Hz with a step of 0.1 Hz. It is concluded that in the higher-frequency range, above 20 Hz, the numerical tool overestimated the response particularly in the vicinity of the resonant frequency of the deposit. The laboratory data exhibited higher damping, primarily within the uppermost soil layers. A close match is found for the response at the top of the structure particularly when converted to spectral accelerations, assuring the correct spectral design. The numerical simulation is not affected by the inability to reliably simulate the soil seismic response above 20 Hz.

Alternative to above detailed QUAD4M software, one of the well known alternatives is FLAC (Zarnani and Bathurst, 2008; Bathurst *et al.*, 2006). It is possible to model 2-D geotechnical problems that consist of several stages, such as sequential excavations, backfilling and loading. Also it is possible to simulate the large strain behavior of three dimensional 3-D structures of soil, rock or other continual materials that undergo plastic flow when their yield limits are reached. It can be used in a mixed discretization scheme to model plastic flow and collapse. Although it is programmed as a finite difference code, the spatial discretization is handled in essentially the same way as for constant strain finite element triangles and we can deduce that reliable results will require a mesh containing large number of small elements. The advantage, for nonlinear problems, is that the computational processes involved in each time step are extremely simple.

Literature study on numerical and experimental modeling tests for geotechnical application under earthquake loadings are summarized in Table 4.2 with further information on shaking table tests and centrifuge tests.

5. STUDY PROGRAM

5.1. General Information

This study presents the preliminary research works on a potential seismic isolation method to dissipate earthquake energy, thus reducing structural response and minimizing the potential damage. Usability of Tire Waste Sand Mixtures (TWSM) as Geotechnical Seismic Isolation (GSI) material is investigated with numerical analyses. It already exist former studies including numerical analysis of shredded rubber and soil mixture placed around structure foundations (Tsang *et al.*, 2007, 2009, 2011). All of these former studies are performed with experimental data obtained by Feng and Sutter (2000), in Resonant Column Tests (RCT) applied on rubber soil mixtures (RSM) composed from sand and tire shreds. All of the previous studies on the mitigation of earthquake hazards using RSM include the use of only one type of tire rubber as GSI material. The static and dynamic properties of RSM are influenced by type of rubber, rubber aspect ratio, rubber/sand ratio in the mixture, sand unit weight, confining pressure, other sand and rubber characteristics, and environmental, experimental conditions as known (Masad *et al.*, 1996; Edinçliler *et al.*, 2004).

Relying on this reason, a series of tests is conducted under different normal/confining stresses. During experiments, two different types of tire, tire buffings (TB) and tire crumbs (TC) were mixed with sand in variable ratios to determine the soil properties of the TWSM (Yıldız, 2012; Çağatay, 2008). The tire types are nominated as buffing rubber and granulated rubber respectively, according to ASTM D6270-08 (2012). Furthermore, cyclic triaxial tests (CTT) are executed with same composite material under three different confining pressures.

The static and dynamic test data of TB-Sand (TBS) and TC-Sand (TCS) mixtures with different mixing ratios have been evaluated regarding their availability to be used as GSI material under low to medium rise reinforced concrete structures. Following, the proper TWSM data is analyzed with QUAD4M; a dynamic, time domain, equivalent

linear, two-dimensional finite element software; capable to do equivalent linear analysis of a soil profile. Numerical analyses cover fourteen numerical analyses. They covered eight scenarios differentiated with soil or TWSM placed in soil layer, earthquake record used during simulation, type of foundation, and structure's number of stories. Results are compared with the former studies, and they are monitored according to normalized horizontal acceleration time histories at the roof and footing levels of the structures and first floor horizontal drift time history. The according peak and root-mean-square values are determined with the first period shift of the structure in each case.

This comparative study concerns use of granulated tire waste material as GSI underneath foundation of low-medium rise structures, under different earthquake ground excitations. The following parts cover present TWSM static and dynamic properties evaluation, deciding to proper GSI material accordingly, and data preparation for numerical modeling.

5.2. TWSM Static and Dynamic Properties Evaluation

Silivri Sand (S), widely found in Istanbul/Turkey is mixed with granulated rubber, tire crumb (TC) and buffing rubber, tire buffing (TB); which were supplied from private providers in Istanbul.

Sand is classified as SP; poorly graded rounded sand relying on Unified Classification System (UCS). It has coefficient of uniformity (C_u) 2.4 and coefficient of curvature (Cc) 1.35. S.

TC is provided from a special company. Material aspect ratio is 1-1.5. TB is obtained as a result of retreading process. They possess an aspect ratio 1/5.

Sand, TC and TB's Specific Gravity values are 2.67, 1.04, and 1.08 respectively. Further static and dynamic properties are given below in more details.

5.2.1. Static Properties of TWSM

A series of test had been conducted with TWSM samples prepared in two groups; first group being a mixture of TB and sand, and second one, TC and sand (Table 5.1). Each group of mixtures had five samples, differentiated with mixing ratio of TC or TB over sand by weight: 5, 10, 20, 30, and 40 per cent.

California Bearing Ratio (CBR) and Direct Shear Tests were performed with all of the TWSM mixture samples and samples of pure sand, TC and TB. In CBR tests, two series of TBSM were included to experiment's scope; TB1-S presented TB2-S with aspect ratio 3.5-4 and with 7.5-8 respectively.

Table 5.1. CBR test results (Çağatay,2008).

Sample	Unit Weight (kN/m³)	Water Content *per cent*	CBR Value
S	15,1	16,0	7,0
TC5	13,0	15,0	6,0
TC10	12,1	14,0	6,0
TC15	11,5	12,0	6,0
TC20	10,7	10,0	5,0
TC30	9,9	10,0	4,0
TC40	9,4	14,0	4,0
TB1-S5	12,2	14,0	7,0
TB1-S10	11,2	13,0	8,0
TB1-S15	10,3	12,0	9,0
TB1-S20	9.0	11,0	10,0
TB1-S30	7,9	11,0	10,0
TB1-S40	6,6	10,0	10,0
TB2-S5	13,9	15,0	8,0
TB2-S10	13,0	14,0	9,0
TB2-S15	12,5	14,0	10,0
TB2-S20	11,8	13,0	12,0
TB2-S30	11,0	12,0	11,0
TB2-S40	10,5	12,0	11,0

Resultantly, The CBR value of sand, which was 7, was decreased to 4.13 as minimum for TCSM with 40 per cent TC/S ratio by weight. Contrarily, sand's CBR tended to be increased due to TB presence. Both TB1 and TB2 inclusions to Sand caused increase in CBR value. TC with angular shape decreased sand's CBR; while TB with fiber shape increased it. These resulted from insufficient frictional surface between TB and Sand granules.

Further, the effect of tire content percentage by weight (TW per cent) in mixtures was investigated. TWSM with TB2 at 20 per cent by weight had the best performance of

shear resistance. The CBR value of TWSM increased up to an optimum TW per cent, exhibiting a peak value. It decreased with further TW per cent increase in TWSM beyond optimum level.

Direct Shear Test (DST) was performed to get TWSM shear strength data with S, TC, TB and TWSM composed of Sand and TB, Sand and TC; both having same mixture rates with CBR test: 5, 10, 15, 20, 30, and 40 per cent (Table 5.2). Each DST is repeated under 10 kPa, 20 kPa, and 40 kPa normal pressures.

Table 5.2. DST summary of TWSM (Çagatay, 2008).

	internal friction angle (°)	**cohesion (kPa)**	**unit weight (kN/m³)**
S	24,0	0,0	16,5
TB5	31,0	12,1	13,2
TB10	27,4	13,2	12,5
TB15	22,2	14,9	11,5
TB20	34,0	14,5	10,3
TB30	30,5	12,0	8,9
TB40	24,0	8,2	7,5
TB	28,0	5,3	4,5
TC5	26,1	2,1	13,7
TC10	35,8	3,5	13,0
TC15	34,2	5,2	12,5
TC20	30,4	4,2	11,8
TC30	29,5	4,2	10,7
TC40	33,0	3,8	10,0
TC	11,3	5,8	6,5

DST results showed that TC or TB inclusion into specimen caused continuously increase in apparent cohesion which was null. Among them, TB was the additive which caused greater apparent cohesion. Furthermore, again both TW material inclusions to soil caused increase in shear strength.

Moreover than DST and CBR, Çagatay (2008) was conducted quick triaxial compression (QTCT) and consolidated drained triaxial (CDTT) tests with similar sand specimen, uniformly graded (SP) with Cu 2.8, the Cc 1.16, and Relative Density (Dr) 0.64.

QTCT is successively performed under cell pressures (confining pressure) 40, 100, and 200 kPa. CDTT was applied on saturated specimen; again, at the compression stage the cell pressure (confining pressure) was set either to 40 kPa, 100 kPa, or 200 kPa. The sample is loaded under a strain rate of 0.5 mm/min.

At TWSM specimens, it was determined that as the per cent TC by weight increased the axial strain value at failure also increased. For the TWSM with 40 per cent TC by weight, no peak stress values were observed, and the deviator stress continued to increase with increasing axial strain. Similarly TWSM prepared with TB, showed peak values in their deviatory stress-strain graphs. Differently, they failed at larger axial strains compared to specimens containing the same percentage of TC. TWSMs with 30 and 40 per cent TB by weight, no peak deviator stress was observed. Again, the shear strength was found using the stress values corresponding to 15 per cent axial strain.

Table 5.3 displays that TWSM had different cohesion values (c) and angle of internal friction (Φ (º)) depending on the percentage by weight of tire waste (TW). An equivalent friction angle was calculated by fitting the experimental shear data with a straight line through the origin, and forcing the cohesion to be zero (regression analysis) to compare and evaluate the test results better. The maximum cohesion value was obtained from the specimen containing 20 per cent TC by weight, and the minimum cohesion value was obtained from the pure TC specimen. Buffing rubbers, tire buffings (TB) leaded to lower cohesion values compared to TC in five per cent, 10 per cent, 20 per cent, and 30 per cent additions, and to higher cohesion values in 40 per cent, and 100 per cent additions. The equivalent friction angle was calculated from the cohesion and friction angle values obtained from the experimental results by using regression analysis. The shear envelope is forced through the origin by reducing the apparent cohesion to zero. The

highest equivalent friction angle which is 43.18 degrees was obtained from the specimen composed of five per cent TB by weight and sand, and the lowest equivalent friction angle which is 17.74 degrees is obtained from the specimen composed of pure TB.

QTCT results indicated that;

1. The addition of fiber shaped material with an aspect ratio 3.5-4 gave higher shear strength parameters compared to the addition of granular material with an aspect ratio of 1-1.5.

2. The shear strength decreased with increasing tire content beyond five per cent of tire inclusions by weight.

3. Greatest shear strength was achieved by adding five per cent TB by weight to sand, which gave a cohesion value of 11.43 kPa, a friction angle of 41.28 degrees, and an equivalent friction angle of 43.18 degrees.

Table 5.3. Quick triaxial compression test results (Çagatay, 2008).

Specimen	c (kPa)	Φ (°)	Φ_{eq} (°)	Unit Weight (kN/m³)
Sand	9.97	41.48	43.02	16.0
TC	8.1	16.89	19.71	6.5
5% TC	15.10	38.19	40.88	15.1
10% TC	21.02	38.16	41.57	14.5
20% TC	24.65	35.12	39.57	13.3
30% TC	14.21	31.02	34.19	12.5
40% TC	9.28	28.69	30.96	11.2
TB	9.54	14.35	17.74	4.6
5% TB	11.43	41.28	43.18	14.7
10% TB	14.98	35.93	38.78	13.7
20% TB	14.04	30.99	34.07	12.1
30% TB	13.63	26.89	30.33	10.3
40% TB	11.18	24.70	27.72	9.1

CDTT were conducted on same specimens set, under 40, 100, and 200 kPa of confining stresses (Table 5.4). Pure Sandy specimen showed peak shear stresses around 5-6 per cent axial strain. Sand specimens had a dilatant volumetric strain behavior. Pure TC and TB specimens showed an approximately linear deviator stress-strain behavior in all confining pressures. No peak deviator stresses were observed for both types of the pure tire specimens, so the shear strength was defined from the shear stress at 15 per cent axial strain.

The volumetric strain behaviors of pure tire waste specimens were also approximately linear and contractive. All TWSM had a dilatant volumetric strain behavior, and peak deviator stresses. TWSM with 30 and 40 per cent by weight of TC showed tire-like stress-strain behavior under high confining pressures, and sand-like stress-strain behavior under low confining pressures. On the other hand, in the experiments with

TWSM with 30 and 40 per cent by weight of TB, no peak deviator stresses were observed, and the deviator stress continued to increase with increasing axial strain at any confining pressure. For both of the tire inclusions, specimens containing 30 per cent TW by weight showed a dilatant volumetric strain behavior. However, TWSM with 40 per cent of TB or TC by weight had a contractive volumetric strain behavior. An initial loss of volume and some dilatant behavior was observed. It was also determined that in the range of these aspect ratios the volumetric strain behaviors of TC and TB had similar characteristics. In all tests a higher confining pressure leaded to a higher deviator stress, and a less dilatant (more contractive) volumetric behavior.

Angle of internal friction decreased and cohesion increased even though apparently as the presence of TB or TC increased in TWSM, similar to QTCT. At both TWSM series prepared with TC and TB, maximum shear strength had been reached by adding five per cent by weight TW in S. Further increase of TW/S ratio, caused a decrease a shear strength despite of other mechanical properties' amelioration. Compared five per cent TB-S and TC-S Direct Shear values, it was observed that the fiber shaped tire inclusions with an aspect ratio of 3.5-4 influenced the shear strength parameters better compared to granular tire inclusions with an aspect ratio of 1-1.5.

The QTCTs were conducted under all levels of confining stresses. A strain rate of 0.5 mm/min was used in the experiments. According to the test results the optimum reinforcement was fiber shaped TB with an amount of five per cent by weight.

Five per cent TB addition to sand leaded to a cohesion value of 11.43 kPa, and an internal friction angle of 41.28 degrees, where the calculated equivalent friction angle was determined as 43.18. Addition of TC was not as effective as addition of TB. Using fiber shaped tire wastes with an aspect ratio of 3.5-4 leads to higher shear strength parameters compared to granular tire wastes with an aspect ratio of 1-1.5. It was also determined that as the TC content increased the axial strain value at failure also increased, but the use of TB instead of TC as tire inclusions resulted even in a larger axial strain value at failure.

Table 5.4. Summary of consolidated drained triaxial tests (Çagatay, 2008).

Specimen	c (kPa)	Φ (°)	Φ $_{eq}$ (°)	Unit Weight (kN/m³)
Sand	1.45	41.49	41.70	16.0
TC	30.17	17.56	25.95	6.5
5 per cent TC	16.13	39.35	41.99	15.1
10 per cent TC	17.38	38.33	41.31	14.5
20 per cent TC	15.60	35.44	38.48	13.3
30 per cent TC	12.72	36.28	38.67	12.5
40 per cent TC	27.85	27.57	33.90	11.2
TB	29.51	16.62	24.89	4.6
5 per cent TB	5.51	41.07	42.02	14.7
10 per cent TB	15.64	35.10	38.12	13.7
20 per cent TB	14.74	33.88	36.78	12.1
30 per cent TB	11.83	30.47	33.12	10.3
40 per cent TB	28.05	24.36	31.27	9.1

Lastly, CDTTs were performed on specimens having same ratios of compositions as the QTCT. Same confining stresses were used, and the tests were conducted at a strain rate of 0.5 mm/min at which the pore pressure remained zero for the duration of the test. The results showed that addition of five per cent TC or five per cent TB both increased the shear strength of sand. However, the greatest shear strength was obtained by adding five per cent TB to sand. The specimen prepared by adding five per cent TB to sand has a cohesion value of 5.51 kPa, and an internal friction angle of 41.07 degrees, where the equivalent internal friction angle can be calculated as 42.02 degrees. The shear strength decreased for tire contents beyond the value five per cent by weight. The results of consolidated drained tests indicated that fiber shaped tire buffings at an amount of five per cent by weight should be added to sand as reinforcement for geotechnical applications. The stress-strain behavior and the volumetric strain behavior of tire waste-sand mixtures changed from sand-like behavior to tire-like behavior at a tire waste content of 40 per cent. It was also determined that in all tests a higher confining pressure leaded to a higher

deviator stress, and a more contractive volumetric behavior. Specimens prepared with both types of tires showed similar volumetric strain behavior in the range of the aspect ratios used in this study (1-1.5 and 3.5-4). It was observed that pure sand specimen and specimen containing fvie, 10, 20, and 30 percent tire waste had dilative volumetric behavior. Pure tire waste specimens and specimens containing 40 per cent tire waste showed contractive volumetric behavior.

QTCT and CDTT results showed that the optimum results are obtained by five per cent TB addition to the sand. It is also concluded that fiber shaped tire inclusions influences the shear strength parameters better compared to granular tire inclusions. The results indicated that use of TB additive will improve the performance of highway embankments under the traffic load. Adding five per cent of fiber shaped TB by weight to sand will form a reinforced lightweight fill composition to be used in geotechnical applications improving the shear strength of soil. Tire shape, tire aspect ratio, and tire content have a significant effect on the shear strength parameters of the composition. Fiber shaped tire inclusions influences the shear strength parameters better compared to granular tire inclusions. The optimum tire content is determined as five per cent from the triaxial test results.

During DSTs, sand was especially predominant at TBS mixtures with low TB content, up to 15 per cent. With the second series, contributive effect of TC was increasing parallel to TC percentage in TCS mixture. Moreover, apparent cohesion of sand had tendency to increase but not in perfect correlation to TW increase in TWSMs. In both TCS and TBS series, maximum apparent cohesion was reached at 15 per cent by weight TW/TWSM mixing ratio. Comparing TW series between them, the apparent cohesion value of TBS was considerably higher than TCS. It can be due to geometrical shape, aspect ratio and density.

Following, it was concluded that both TB and TC inclusion improved TWSM shear strength. The maximum internal friction angle of TC and TB samples were obtained with

mixing ratios 10 per cent and 15 per cent by weight respectively. Further TW inclusion in TWSMs caused decrease in mixtures' shear strength.

When CDTT results were considered the optimum reinforcement should be TBS5. Using TB with higher aspect ratio leaded to reach higher shear strength than TC. Secondly, the axial strain value at failure increased as TC per cent in TCS increased. And use of TB as tire inclusions resulted even in a larger axial strain value at failure.

In the QTCT experiments, the results showed that both addition of five per cent TC and TB into S increased its shear strength. However, the greatest shear strength was seen with TBS5. The shear strength decreased for tire contents beyond the value five per cent by weight.

The stress-strain behavior and the volumetric strain behavior of TWSM change from sand-like behavior to tire-like behavior at a tire waste content of 40 per cent. It was determined that in all tests a higher confining pressure leaded to a higher deviator stress, and a more contractive volumetric behavior. Further, pure sand and TWSM containing 5, 10, 20, and 30 per cent TW showed dilative volumetric behavior. Contrarily, pure tire waste specimens, TBS40, TCS40 showed contractive volumetric behavior.

5.2.2. Dynamic Properties of TWSM

A set of Cyclic Triaxial Tests (CTT) were performed on TWSMs to study their dynamic properties, shear modulus D (per cent) and damping ratio D vs. shear strain γ (per cent) curves (Table 5.5). The collected experimental data is further subject to investigation for potential use in earthquake mitigation effects. CTT apparatus found in Istanbul Technical University Geotechnical Materials Testing Laboratory; following the load-controlled cyclic triaxial technique. Results obtained are relative to several parameters; sample density, strain level, number of cycles, material type, saturation and confining

stress. three levels of mean confining pressure, σ' are preferred; 40, 100 and 200 kPa. Used samples densities are cited in Table 5.5. Percentage deformation, γ level was between 0,5 x 10-4 per cent and 0,5 x 10-2. Being a bit smaller range compared to CTT measurement sensitivity. It can be down to 0,1 x 10-4 per cent and up to 0,1 x 10-1 per cent as underlined in "Principles of Soil Dynamics" by Das and Ramana (1993); that is not bringing any inconvenience for adequate testing. CTT apparatus contains a pneumatic system capable of generating cyclic axial stresses at frequencies between 0,001 Hz and two Hz properly installed CTT apparatus with above-mentioned technique can be used for both fine and coarse grained soils. TWSM Specimens don't show any physical aspect oriented to a categorization out of them. Saturated samples used. Although encountered with previous studies on RCT applied dry specimens as Feng and Kevin (2000); Pitilakis *et al.* (2009), CTT apparatus establishment is adequate for vice versa case.

Experimentally collected data with below explained conditions are considered for probable use in mitigation of earthquake effects on soils. Waste tire type effects, percentage (per cent) by weight of tire waste in TWSM and mean confining pressure σ' effects on CTT results and mixtures' dynamic properties will be discussed.

5.2.3. Modulus and Damping Characteristics of TWSM

To study dynamic properties of TWSM; a series of CTTs is experienced with seven different samples under three different levels of confining pressure.

Focused on Sand and TWSM characteristic D (per cent) vs. γ (per cent) curves; it has seen that between 0,5 x 10-4 per cent and 0,5 x 10-3 γ per cent, D is nearly constant. It begins to increase after reaching this level. Sandy specimens show an increase close to linear whereas TWSM specimens' D has steeper increasing upward behavior (Table 5.5).

Considering mean confining pressure (σ') effect on D (per cent) vs. γ (per cent), such a statement would be valid; curve shits up as σ' increases on S but, it reversibly shifts

down on TWSM specimens. In both TBS and TCS TWSMs, D (per cent) vs. γ (per cent) curves shift up as per cent of waste tire in weight increases.

Second specimens' characteristic curve is Shear Modulus (G) vs. γ (per cent) curves. In all cases G decreases as γ (per cent) increases. On sandy samples, this downward behavior is sharper than on TWSM specimens. σ' causes an upward shift on (G) vs. γ (per cent) curves of every seven specimens. On TWSMs, waste tire presence causes a definite drop on G; TBS10 and TCS10 specimens have much lower G values compared to S specimen under constant σ'. (G) (MPa) vs. γ (per cent) curves still decrease as TB or TC weight (per cent) augments in TWSMs.

Figure 5.1 and Figure 5.2 shows resultant D (per cent) vs. Shear Strain γ (per cent) and shear modulus (G) vs. shear strain (γ) (per cent) curves. Previous studies listed on 2nd section on experimental σ' effect on tire waste sand mixture dynamic properties displayed similar results as Pitilakis *et al.* (2009). Furthermore tire waste effect on sand's dynamic properties is similarly stated in Feng and Sutter (2000); Pitilakis *et al.* (2009).

Table 5.5. Specimen physical properties and CTT program (Yıldız, 2012).

Specimen	Materials by weight	Tire Size	γ(kN/m³)	Confining Pressures (kPa)
S	100 per cent Sand	-	**16,00**	40 - 100 – 200
TCS10	Sand + 10 per cent Tire Crumbs	1 - 2 mm	**14,86**	40 - 100 – 200
TCS20	Sand + 20 per cent Tire Crumbs	1 - 2 mm	**13,72**	40 - 100 – 200
TCS30	Sand + 30 per cent Tire Crumbs	1 - 2 mm	**12,58**	40 - 100 – 200
TBS10	Sand + 10 per cent Tire Buffings	1 - 4 mm	**15,05**	40 - 100 – 200
TBS20	Sand + 20 per cent Tire Buffings	1 - 4 mm	**14,10**	40 - 100 – 200
TBS30	Sand + 30 per cent Tire Buffings	1 - 4 mm	**13,15**	40 - 100 – 200

A series of CTT realized with seven samples composed of S (γ = 16,50 kN/m3), and two different processed tire wastes as TB (γ = 6,50 kN/m3) and TC (γ = 4,60 kN/m3). Tests are applied with three TWSM mixture percentages by weight and under three different levels of σ'. Influence of scrap tire sort, tire over soil ratio by weight in mixture and σ' on shear modulus G (MPa) and damping ratio D (per cent) are studied. Experience results are stated as a whole in Figure 5.3, and Figure 5.4.

As seen from Figure 5.1, Figure 5.2 and Figure 5.4; both processed scrap tires presence in sand reduced sand G (MPa) at all γ (per cent) levels. Furthermore, scrap tire over sand ratio by weight percentage increase in TWSMs causes a further drop of G (MPa) for both tire sorts. But, this time, at a slighter intensity referred to G (MPa) reduction with the first TB and TC – Sand mixings, at 10 per cent.

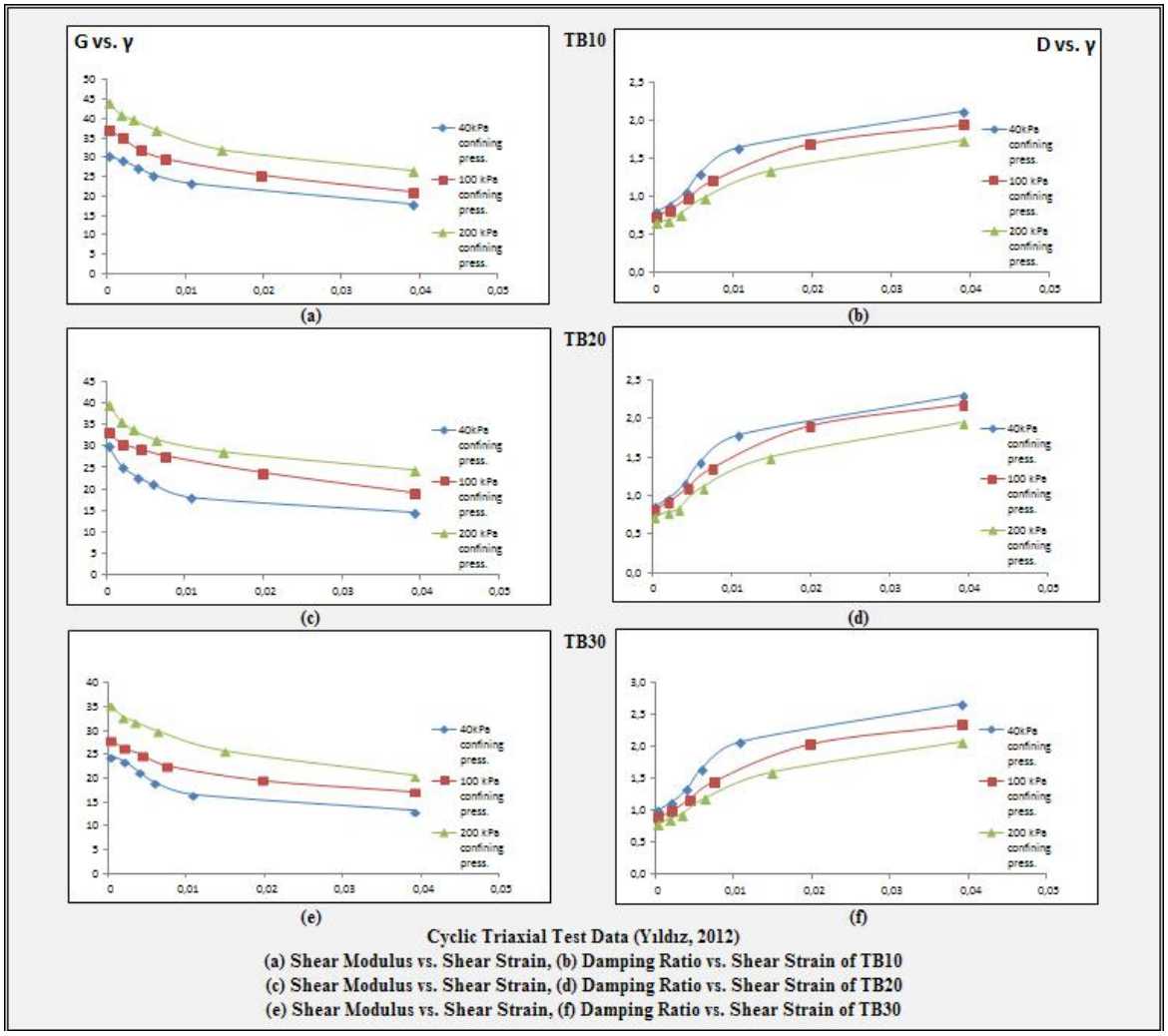

Figure 5.1. TBS D (per cent) vs. γ (per cent) and G (MPa) vs. γ (per cent) curves (Yıldız, 2012).

When G (MPa) vs. γ (per cent) curves of TBS and TCS are compared; under every σ'; TCS samples shows higher G (MPa) than TBS at any arbitrarily chosen γ (per cent). Since increase in σ' causes an upward shift on G (MPa) vs. γ (per cent) plots; TBS10 and TCS10 samples have highest G (MPa) vs. γ (per cent) behavior among all TBS and TCS samples respectively under σ' of 200 kPa.

Evaluation of CTT's concerning D (per cent) vs. γ (per cent) behavior for TBS and TCS samples, indicates that processed scrap tire mixing to sand definitely increases D (per cent) values at all γ (per cent) levels (Figure 5.3, Figure 5.4). And raise in TB/S, TC/S ratio

by weight percentages in TBS and TCS samples respectively results with augmented D (per cent) under all γ (per cent).

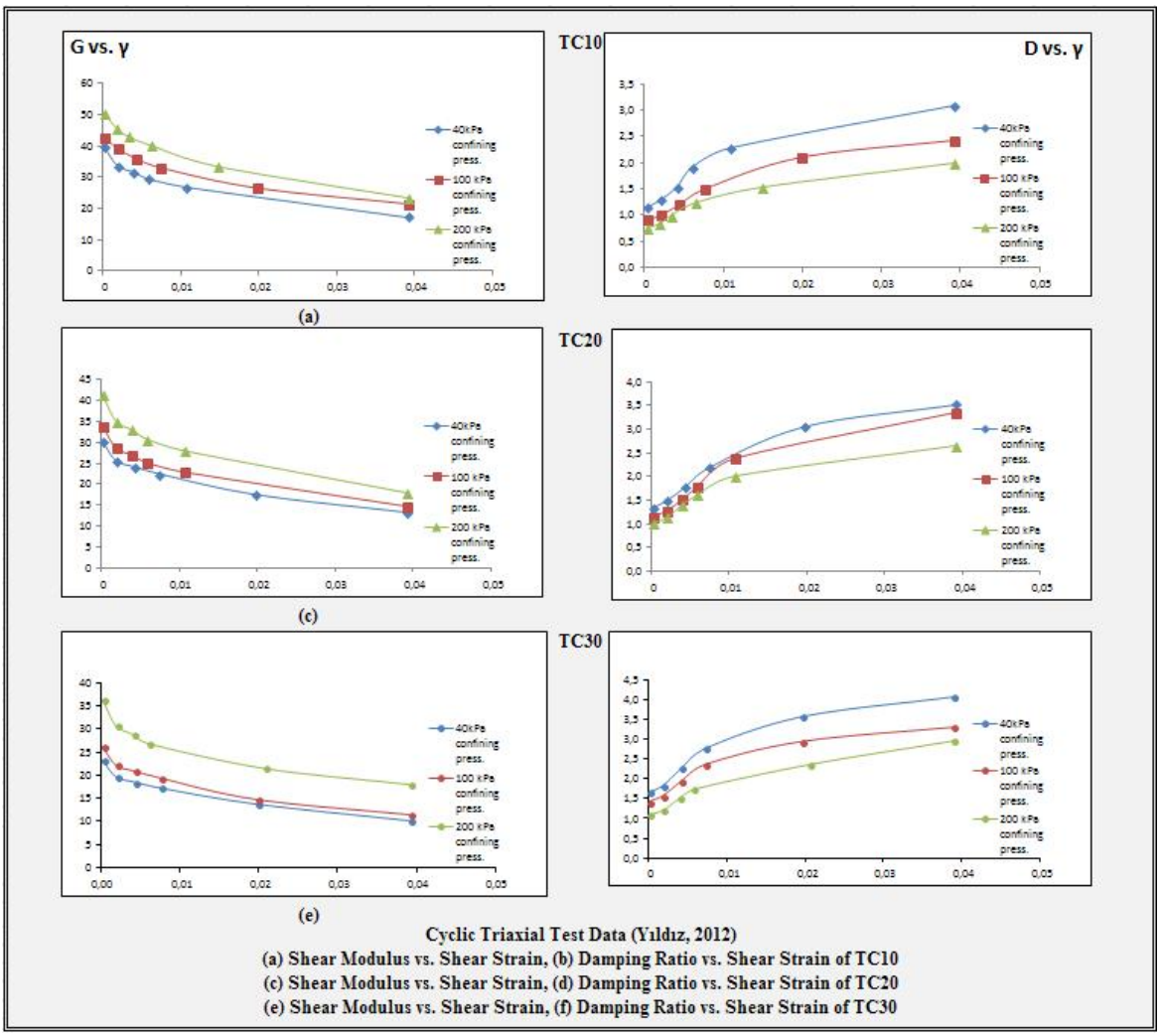

Figure 5.2. TCS D (per cent) vs. γ (per cent) and G (MPa) vs. γ (per cent) curves (Yıldız, 2012).

Sandy samples show D (per cent) behaviors at higher levels under increasing σ'. But, TBS and TCS samples exhibits contrary attitudes. D (per cent) vs. γ (per cent) curves shift down as σ' increases at all tire/sand ratios.

A further try to take a glance at tire shape effect on D (per cent) permits to state that TC mixing in sand results with further amelioration in soil D (per cent) behavior. Under 40 kPa of σ', TCS30 has the highest D (per cent) vs. γ (per cent) curve among 21 CTT results. This conclusion states that Granulated tire wastes have better damping property than Fiber shaped ones.

Concentrated on dynamic behavior of Sandy sample; independent of σ', it showed the lowest damping and highest shear modulus at all shear strain levels (Refer to Figures 5.5, 5.6, 5.7, 5.8). This deduction is in accordance with the recurrently realized experiences since several decades. In case of a strong seismic motion the least predictable characteristics are near site effects. Even though provisions related to them did not appear in building codes up to 1970's; a correlation between near site effects and earthquake damage existed since much earlier. Since Soil Damping characteristics play a significant role in near site conditions; TB and TC usage as a mixture component could be beneficial concerning this situation since their presence in sand raises D (per cent).

DST, QTCT, CDTT, was to reveal the TWSMs' static properties, and last one for dynamic properties respectively. At the end, TWSM behavior displayed different behavior under static and dynamic excitations. The reasons; how different TW influenced differently sand sample, effect of TW amount in total tire-sand mixture will be emphasized with more details in next sections.

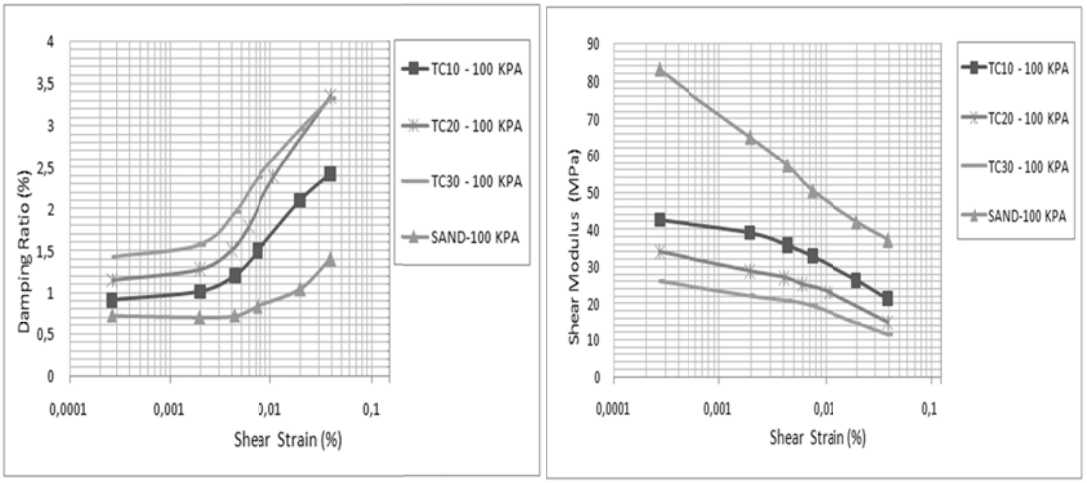

Figure 5.3. D (per cent) vs. γ (per cent) and G (MPa) vs. γ (per cent) curves under 100 kPa σ' (Yıldız, 2012).

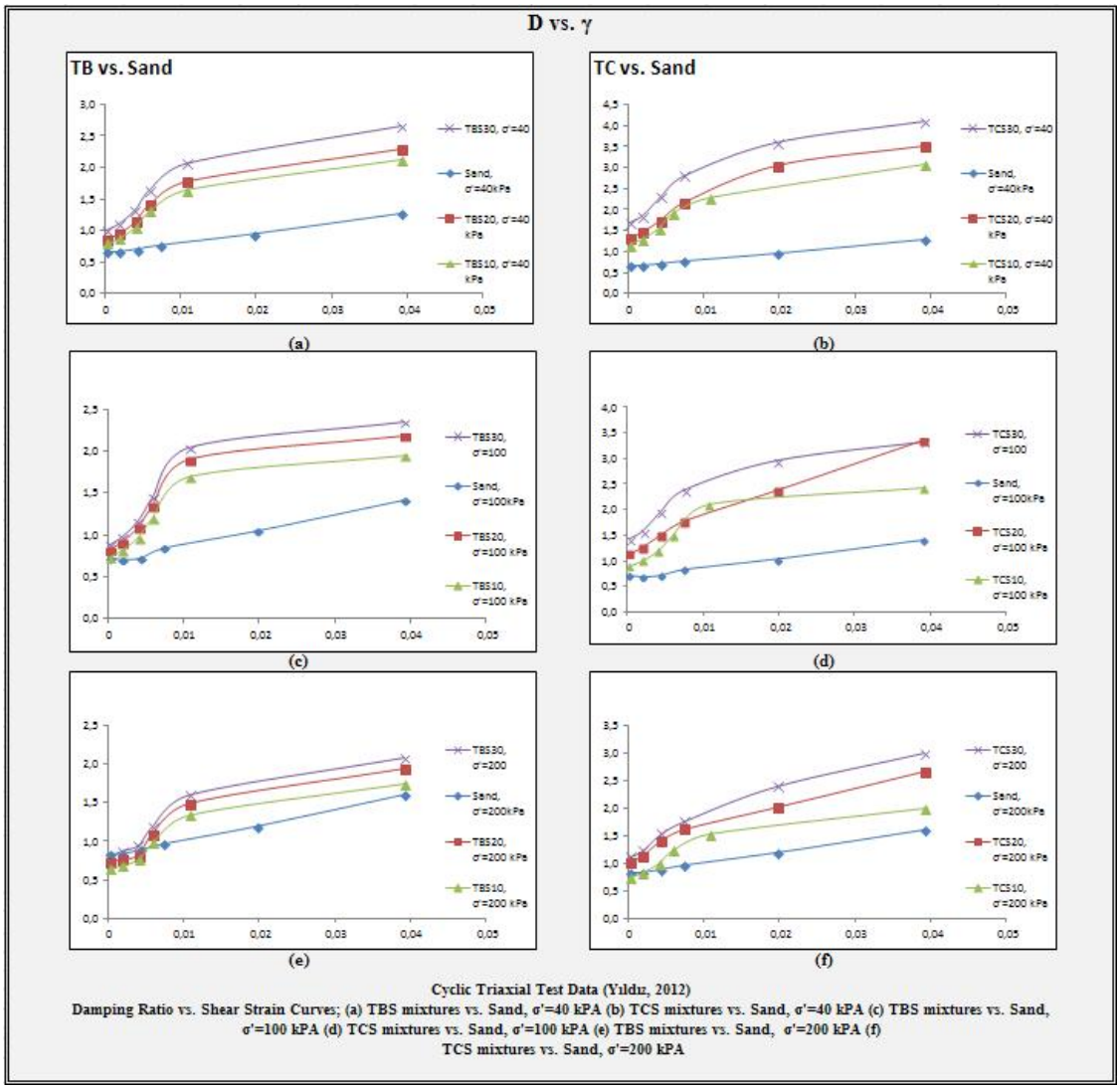

Figure 5.4. D (per cent) vs. γ (per cent) curves under all levels of σ' relying on CTT series (Yıldız, 2012).

5.2.4. Normalized Shear Modulus (G / G_{max})

Seismic ground response analysis always requires soil damping and stiffness information. Whether the test applied to soil specimen is in-situ or in-laboratory condition, explication for the first part is coming from measured damping ratio D at changing shear strain level γ. Average soil stiffness is demonstrated with Normalized Shear Modulus G/G_{max}, which can be obtained from Shear Wave Velocity v_s when conducted test is in-situ or Shear Stress G when test is in-laboratory condition. According to above cited study on TWSM with CTT, revealed G values vs. changing γ will be made use for Normalized Shear Modulus G/G_{max} (Juang *et al.*, 2005).

In Literature, many studies have been conducted so far to characterize the factors influencing G/G_{max} and different resultant G/G_{max} curve models; Sun *et al.* (1988), Idriss (1990), Vucetic and Dobry (1991), Ishibashi and Zhang (1993), Darendeli (2001), Menq *et al.* (2005). It had been found that shear strain γ, mean effective confining stress $\boldsymbol{\sigma}'$, soil type and soil plasticity index PI are the most important factors that influence G/G_{max}. Besides them, Stokoe *et al.* (1995) suggested that grouping test data by geology may be an effective approach to reveal less important factors. These factors were reemphasized by the Darendeli Model and cited as number of loading cycles, loading frequency, overconsolidation ratio, degree of saturation, void ratio, and soil grain characteristics.

G/Gmax curve modeled by Darendeli (2001) was taken as reference in this study since it considered more factors than previous models and since it was more separately used among the two most recent G/G_{max} models.

This model proposed following equation based on the Hardin and Drnevich (1972b) hyperbolic model to represent the general trends of G/G_{max} vs. γ.

$$\frac{G}{G_{\max}} = \frac{1}{1+\left(\frac{\gamma}{\gamma_r}\right)^a} \tag{5.1}$$

This was an empirical, modified hyperbolic soil model representing the normalized modulus reduction curves. It utilized two parameters: reference strain γ_r and curvature coefficient a. γ_r is formulized below and is considered constant 0.9190

$$\gamma_r = \left(\frac{\sigma_o'}{p_a}\right)^{0.3483} \left(0.0352 + 0.0010 PIOCR^{0.3246}\right) \tag{5.2}$$

$\boldsymbol{\sigma_a}$' is mean effective pressure $\boldsymbol{\sigma}$', p_a is atmospheric pressure, PI is plasticity index and OCR is overconsolidation ratio.

Sand, TBS30, TCS30 and the Darendeli Mean Model Curve in different confining pressures are in Figures 5.5, 5.6 and 5.7.

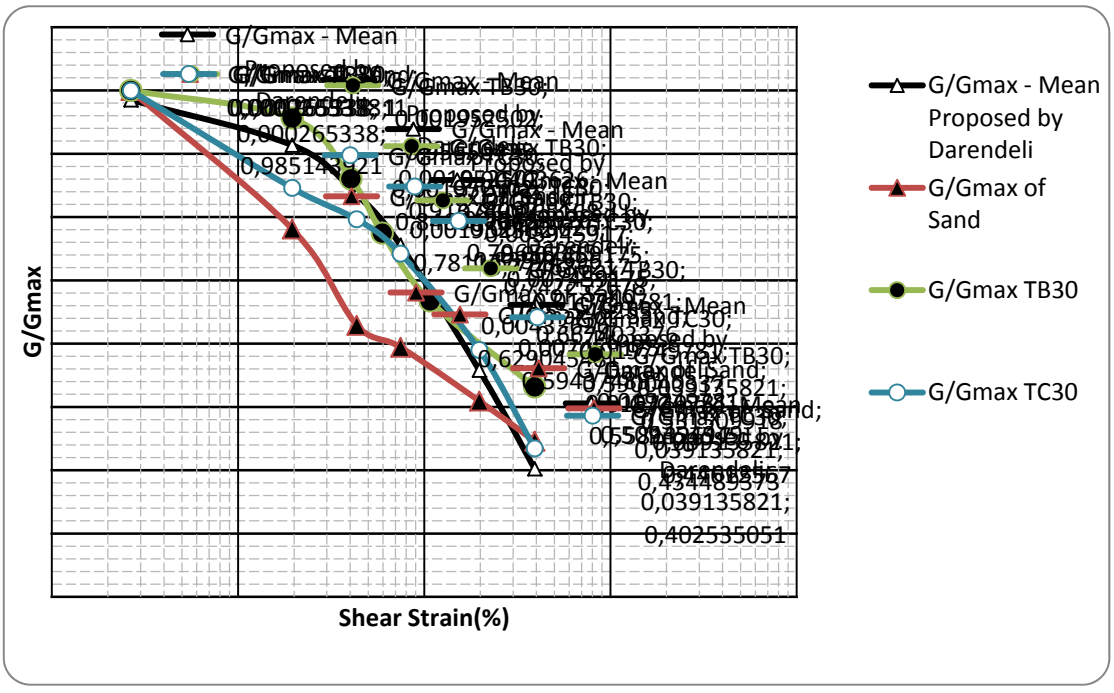

Figure 5.5. G/G_{max} curves of samples vs. Darendeli Model, **σ'**=40 kPa.

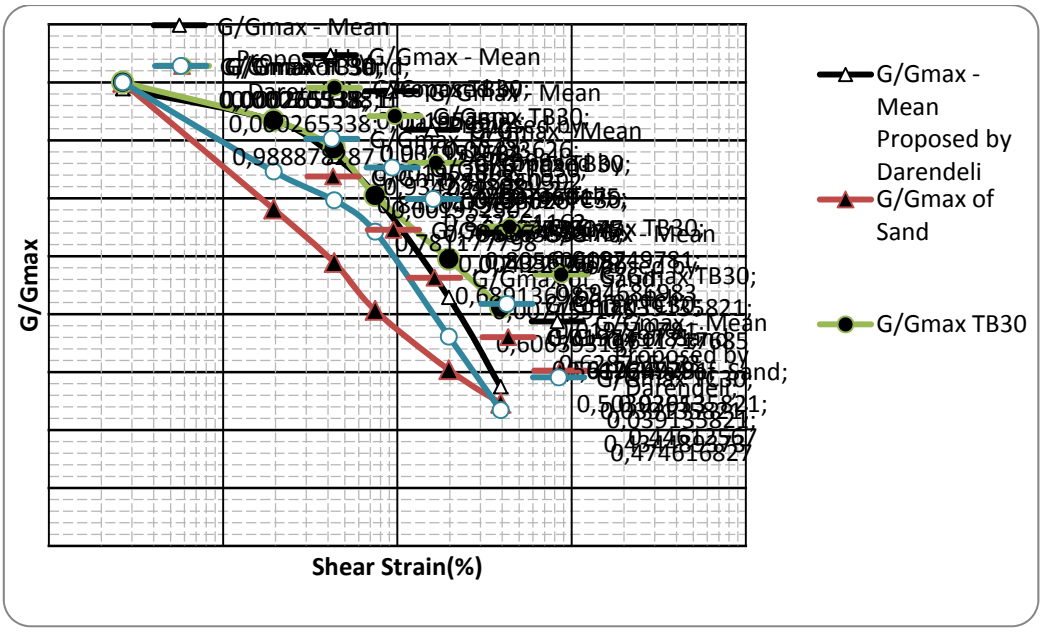

Figure 5.6. G/G_{max} curves of samples vs. Darendeli Model, **σ'**=100 kPa.

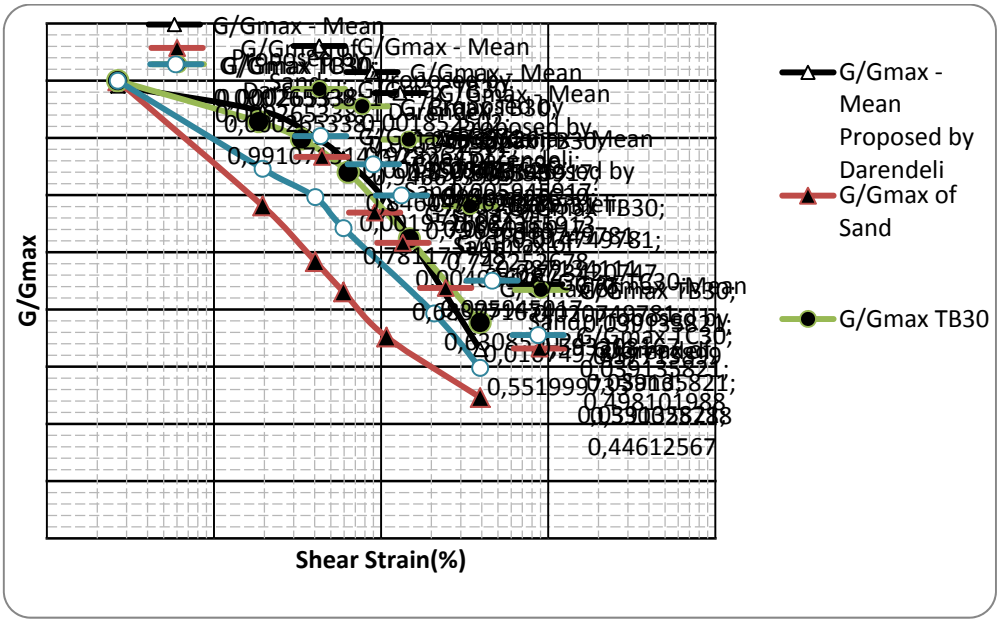

Figure 5.7. G/G_{max} curves of samples vs. Darendeli Model, **σ'**=200 kPa.

5.3. Proper GSI Material Selection and adoption to Numerical Analysis

As summary, CTT Results displayed that soil dynamic properties; Shear Modulus G (MPa) and Damping Ratio D (per cent) were all ameliorated by TW inclusion into sand. The TW/TWSM ratio by weight increase caused continuous decrease in G (MPa), and increase in D (per cent). When focused on confining pressure effect, it caused increase in G (MPa), and decrease in D (per cent) in all sample series TCS and TBS.

When TBS and TCS were compared among them, TCS samples exhibited higher G (MPa) than TBS at each level of TW/TWSM mixing ratio. TCSs also had better D (per cent) performance than TBSs.

Relying on these deductions, it can be said that mixing sand with TW would improve its behavior under dynamic excitations, seismic activities. Moreover TC, granulated TW would be preferred to TB, fiber shaped TW when considered to compose TWSM to mitigate sand against possible earthquake hazards.

Static Stress Tests DST, CDTT, and QCTT did not display similar results with CTT. First of all, TW/TWSM ratio by weight increase did not continuously ameliorate TWSM behavior. During DSTs, maximum internal friction angles of TCS and TBS samples were seen at TCS10 and TBS15 respectively. After these levels, further TW increase in TWSM caused shear strength decrease. The mixing ratio by weight percentage at maximum internal friction angles was even lower at CDTT and QCTT: five per cent.

Secondly, TWSMs composed from TB and sand displayed better soil behavior during static strength measurement tests.

In all DST, CDTT, and QCTT tests a higher confining pressure leaded to a higher deviator stress and a more contractive volumetric behavior lastly.

According to above deductions, among whole TWSMs, TCS mixture would be accepted as best possible alternative for soil mitigation against earthquake hazards and GSI material accordingly. This deduction especially concerns the CTT results.

Besides appropriate TWSM selection, its data amelioration is also required. The experimental data set held has a shear strain range 2.5 * 10-4 – 4 * 10-2 (per cent). But in numerical analysis it is expected to have shear strain up to 0.1 (per cent). Accordingly, it is needed to extrapolate available data.

5.3.1. Possible Methodologies to Extrapolate Data, Hyperbolic Model

To extrapolate the experimental data following methods can be used:

a. Using computer programs, allowing Shake or Quad4M to do hyperbolic. When the shear strain exceeds the maximum value specified in the input material file, the program will get the shear modulus degradation ratio and damping ratio by extrapolation based on the slope of the line between the last two points of the curve on the logarithmic scale of shear strain. This would still give us acceptably reasonable values. But theoretical modeling should be preferred.

b. Keeping shear stress constant in strain larger than maximum experimental strain data. Both tire waste and sand reach higher shear stress values than experimented. Therefore we can't use this option either.

c. Two different material modeling methods. Two kinds of material models have been used to describe the nonlinear stress-strain relations of soils. The first is a four-

parameter model known as the Ramberg-Osgood model (R-0 model). The second is a two-parameter model as represented by the hyperbolic or exponential functions.

In this study the hyperbolic model is used as theoretical model to extrapolate available CTT data. It is logical to assume that any stress-strain curve of soils is bounded by two straight lines which are tangential to it at small strains and at large strains, as illustrated in Figure 5.8. The tangent at small strains denoted by Go represents the elastic modulus at small strains and the horizontal asymptote at large strains indicates the upper limit of the stress τf, namely the strength of soils.

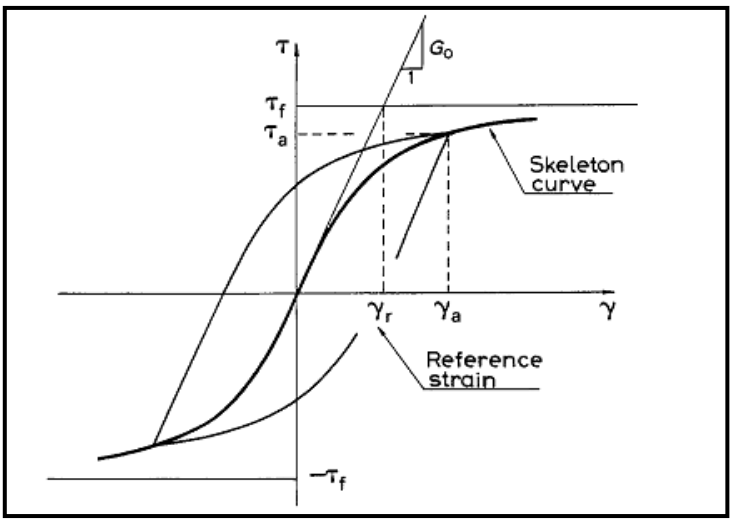

Figure 5.8. Reference shear strain.

The stress-strain curve bounded by these two straight lines may be expressed in differential form as

$$\frac{d\tau}{d\gamma} = G_0\left(1-\frac{\tau}{\tau_f}\right)^n \tag{5.3}$$

where *n* is an arbitrary number. This expression indicates that the tangent to the stress-strain curve takes a value of G_o at $\tau = 0$ and tends to decrease with increasing stress until it becomes equal to zero at $\tau = \tau_i$. Except for the case of $n = 1$, Equation (5.3) can be integrated, as follows, so as to satisfy the condition $\gamma = 0$ when $\tau = 0$,

$$\gamma = \frac{\gamma}{n-1}\left[\frac{1}{(1-\tau/\tau_f)^{n-1}} - 1\right] \tag{5.4}$$

where a new parameter, γ_r, called reference strain is defined as:

$$\gamma_t = \frac{\tau_f}{G_0} \tag{5.5}$$

The reference strain indicates a strain which would be attained at failure stress, if a soil were to behave elastically, as illustrated in Figure 5.8. One of the interesting features of the stress-strain curve as given by Equation (5.3) is that it produces a constant damping ratio of $\mathbf{2/\pi}$ as a limit when the strain becomes large.

If the damping ratio is assumed to take a constant value, D_0, at large strains $\boldsymbol{\tau_a}$ becomes $\boldsymbol{\tau_f}$. Assuming $\tau = \tau_a$, $\gamma = \gamma_a$;

$$\tau = \frac{G_0\gamma}{1+\frac{\gamma}{\gamma_t}} \tag{5.6}$$

The equation for the damping ratio of the hyperbolic model can be derived by applying the Masing rule to the skeleton curve as:

$$D = \frac{4}{\pi}\frac{1}{1-G/G_0}\left[1+\frac{G/G_0}{1-G/G_0}\ln\left(\frac{G}{G_0}\right)\right] - \frac{2}{\pi}. \tag{5.7}$$

This relationship is numerically calculated and plotted in Figure 5.9. In the hyperbolic model as specified above, there are two parameters Go and tf specifying the constitution of the model. In some cases, it is difficult to specify both the strain-dependent shear modulus and damping ratio by means of only two parameters. Particularly inconvenient is the fact that, once the reference strain yr is specified from the strain-dependent characteristics of the secant shear modulus, the value of strain-dependent damping ratio is automatically determined, and there is no choice for any parameter to be adjusted to achieve a good fit to experimentally obtained damping data.

Indicated as dotted area in Figure 5.9 is the approximate range in which lie a majority of test data thus far obtained. It may be seen that, while the model.

Representation is satisfactory in the range of small strains; it tends to deviate from actual behavior of soils with increasing shear strains, thereby overestimating the damping ratio. Another model sometimes used in the theory of plasticity is the exponential function. It is derived by integrating Equation (5.3) with ***n*** = 1 to give;

$$\tau = \tau_f\left(1-e^{-\gamma/\gamma r}\right) \tag{5.8}$$

The expression for the secant modulus for the cyclic loading is obtained as

$$\frac{G}{G_0} = \frac{\gamma t}{\gamma a}\left(1 - e^{-\gamma a/\gamma t}\right). \tag{5.9}$$

The same argument as above holds true as well for the exponential model.

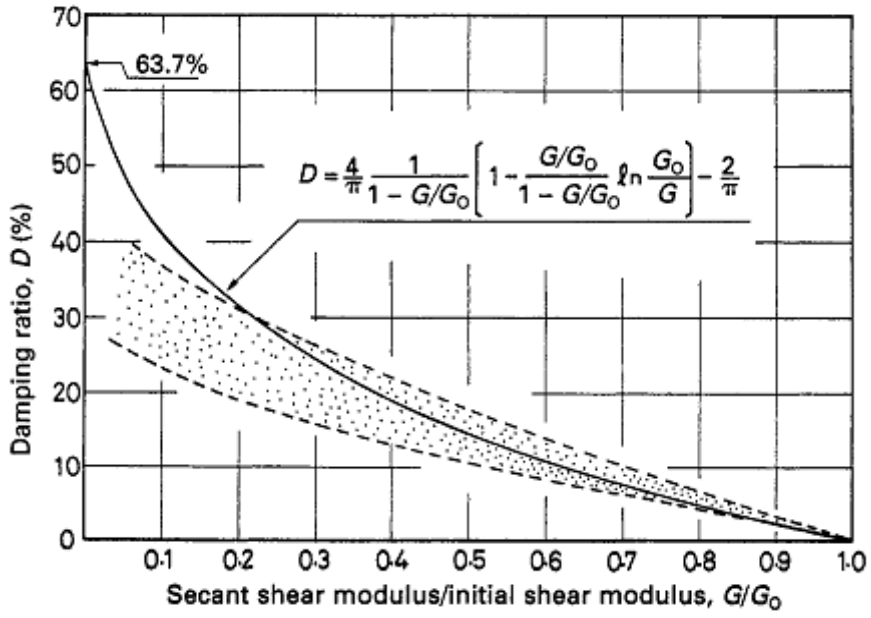

Figure 5.9. Relation between damping ratio and shear modulus ratio.

5.3.2. Elongated Curve Plots, Comparison in the Darendeli Model

The Darendeli G/Gmax model curve (2001) is also used including extrapolated data. If the reference shear strain γr formula is remembered:

$$\gamma_r = \left(\frac{\sigma'_0}{p_a}\right)^{0.3483}\left(0.0352 + 0.0010 PIOCR^{0.3246}\right) \tag{5.10}$$

Where; σa' is effective confining pressure, which is equal to mean effective pressure in CTT setups. PI is Plasticity Index; null since soil is Sand. Pa is atmospheric pressure, 101.325 kPa.

Secondly, slope Δτ/Δγ, 'k' in large shear strains is claimed continued for large strains and data extrapolated with below formula:

$$\tau_{\max} = \frac{\tau_n}{1 - \gamma_n k_n / \tau_n} \tag{5.11}$$

Finally Masing Rule Equation (5.11) is applied to find extrapolated Maximum Shear Modulus and Damping Ratio. Plots are displayed between Figure 5.10 and Figure 5.15.

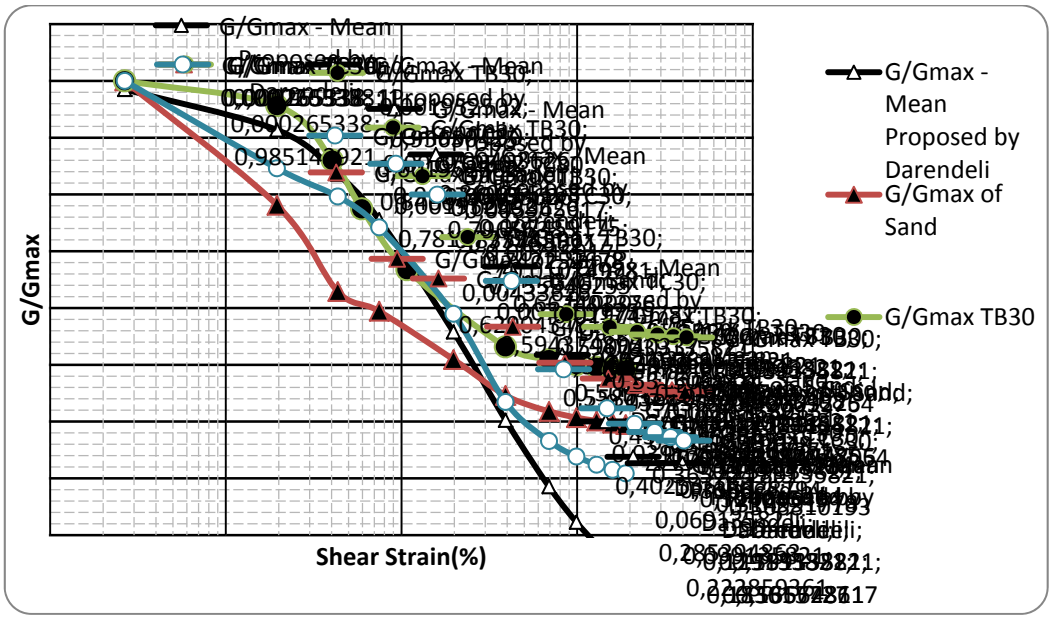

Figure 5.10. Hyperbolic model of G/G_{max} curves and Darendeli Model, σ'=40 kPa.

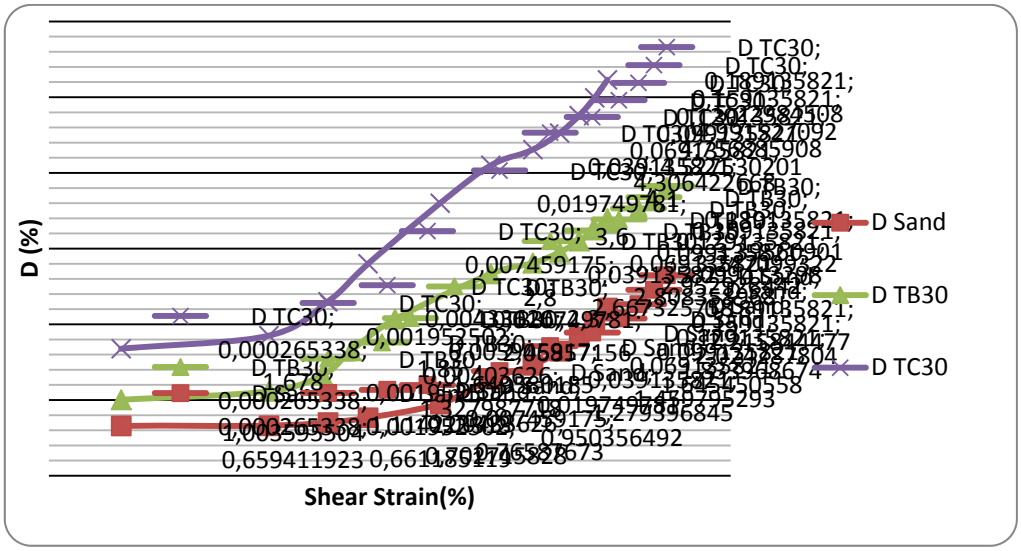

Figure 5.11. Hyperbolic Model of D curves, σ'=40 kPa.

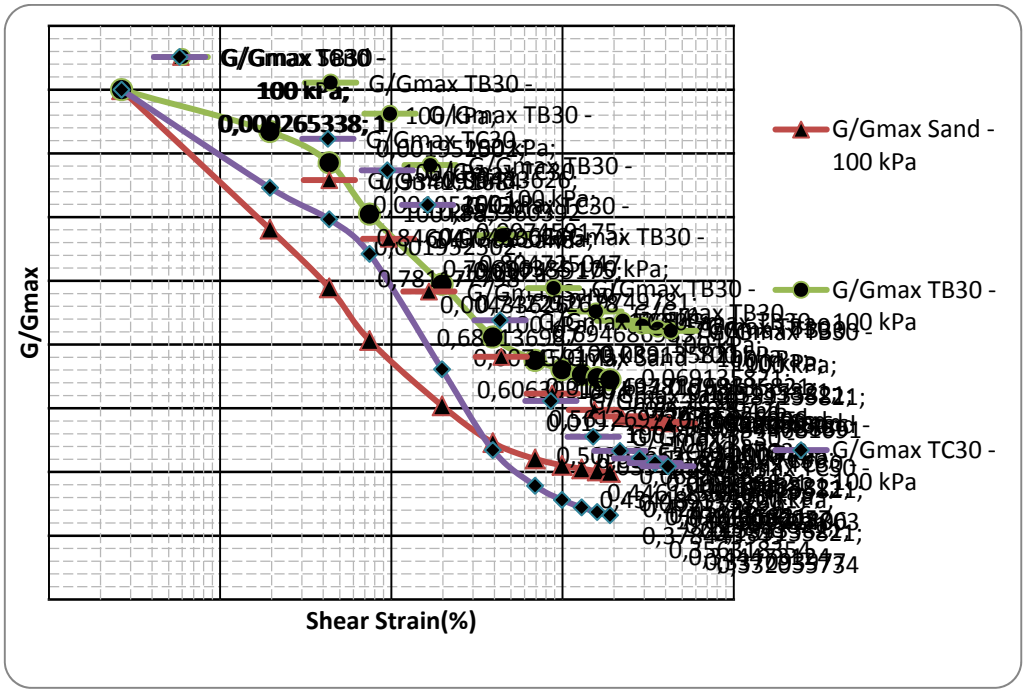

Figure 5.12. Hyperbolic model of G/G_{max} curves and the Darendeli Model, **σ'**=100 kPa.

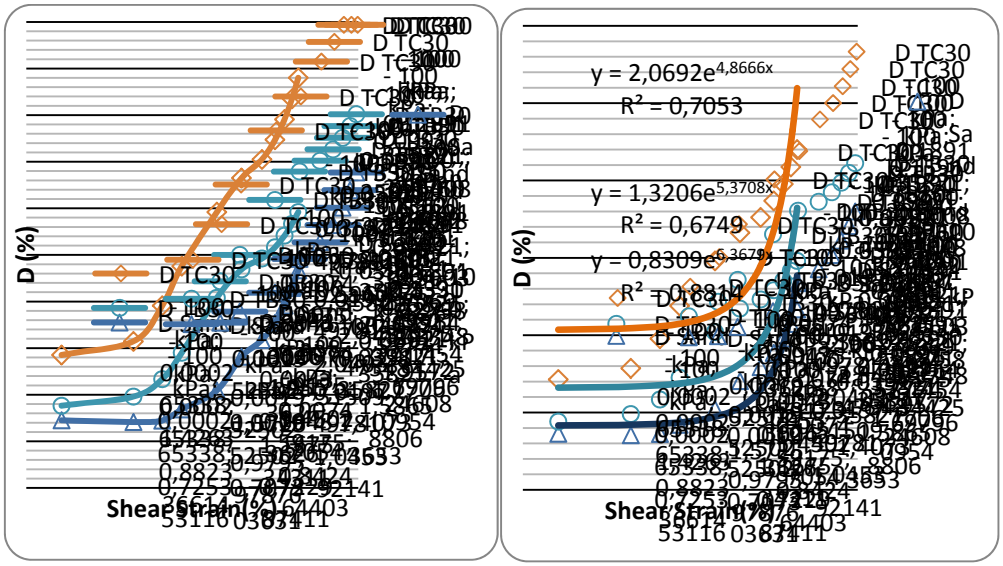

Figure 5.13. Hyperbolic model of D curves, σ'=100 kPa.

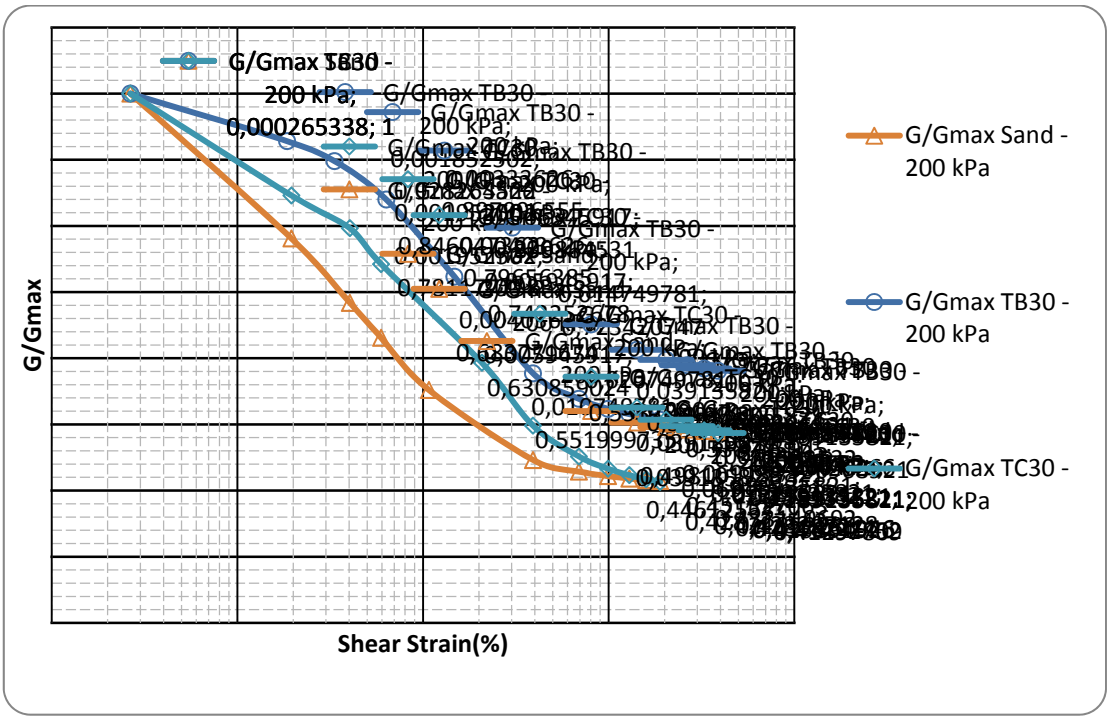

Figure 5.14. Hyperbolic model of G/G_{max} curves and the Darendeli Model, σ'=200 kPa.

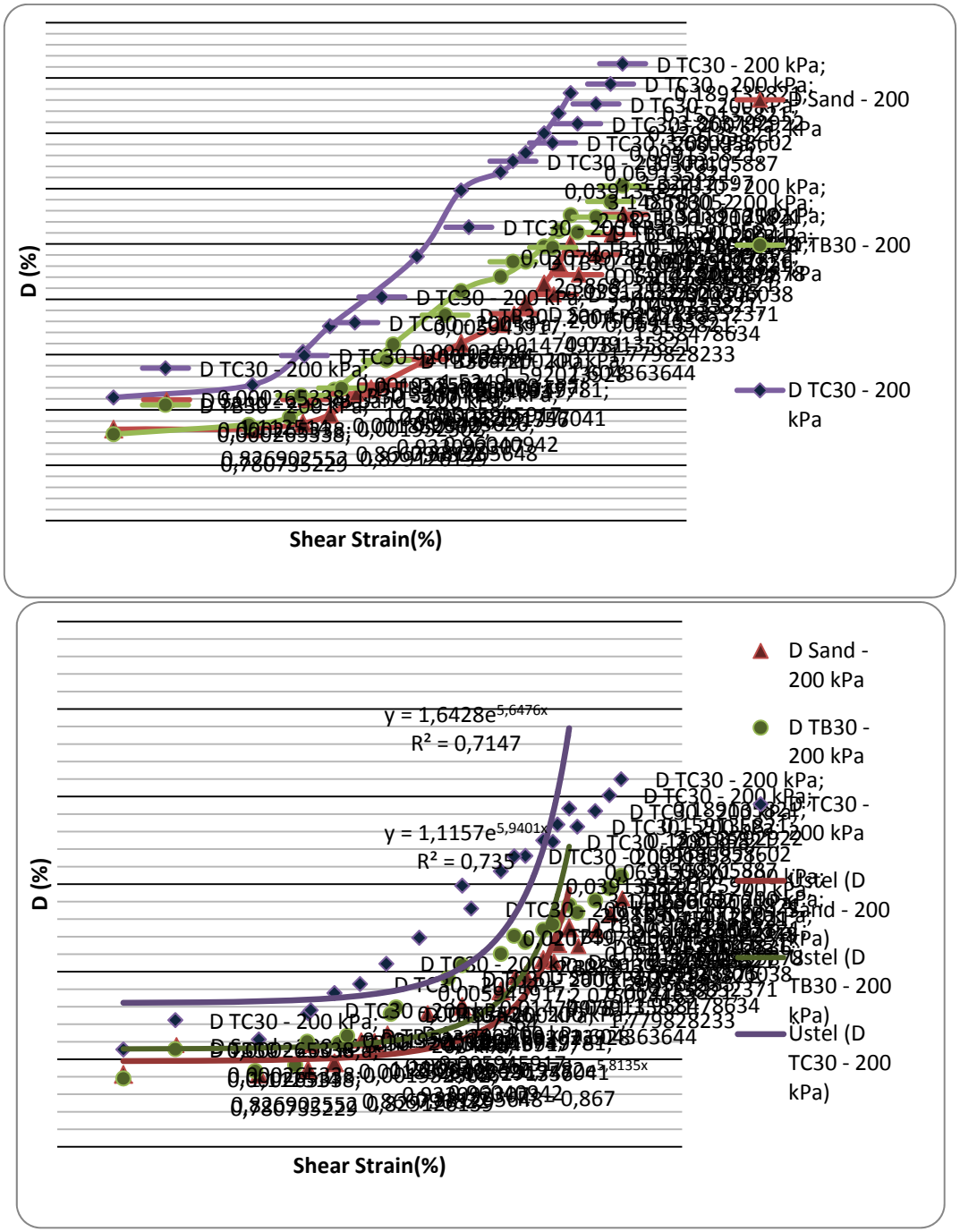

Figure 5.15. Hyperbolic Model of D curves, σ'=200 kPa.

If the shape of the G/Go curves is considered, in comparison with the reference one, it can be observed that the shape differs quite a lot in current case. It is predictable and presumed that there may not be any standard shape, and surely damping curves could even vary more significantly.

5.4. Adapting Structures in Numerical Analysis

Best possible alternative of TWSM citation relying on dynamic properties and available data upgrade for suitable numerical analysis were explained in Section 5.3. Accordingly it was emphasized that TCS samples were more suitable than TBS, and G/G_{max}, D vs. γ curves were elongated.

Further in this study, low to medium rise reinforced concrete structures are included to numerical models where TCS are used as a GSI material, remedy for seismic hazard mitigation.

The proposed Soil – Structure Systems are demonstrated in Figure 5.17. In numerical analyses, structures having same reinforced concrete property and residential functionality but different dimensioning were used. Low to medium rise structures were supposed to have 4, 8, 12, 18-storey (NS) with a typical with dimension; 40 m. TWSM is placed below structure, surrounding the footing or the pile cap (Figure 5.17). During the analyses different TWSM depths (t) of three m or eight m were preferred depending of the structure and foundation type. Dynamic, time domain, equivalent linear, two-dimensional (2-D) FEM, ELA software based on QUAD4M is used during the analyses. Motion Equation is time dependent second order ordinary differential equation. Since inelastic material behavior and large deformation and strains are involved in the FEM, nonlinear equations of motion are usually solved by the Newmark, a direct time integration method. The 4-node plane strain element is utilized to model the subsoil, which is assumed as a plane strain material in 2-D FEM models. The nodes outside the interface are as in the standard finite element method. Connection between soil and structure is provided by interaction forces of equal amplitude but acting in opposite directions on the two substructures. In each element, the stress-strain properties of the soil are defined by a shear modulus and an equivalent damping ratio which depend on the shear strain in ELA. Structure mass is lumped in points which have no rotational inertia. It means that the mass with any rotational degree of freedom will be zero. A damper is used instead of applying

fixities on the boundary of the computational domain. Therefore, an increase in stress on the boundary is dissipated without rebounding.

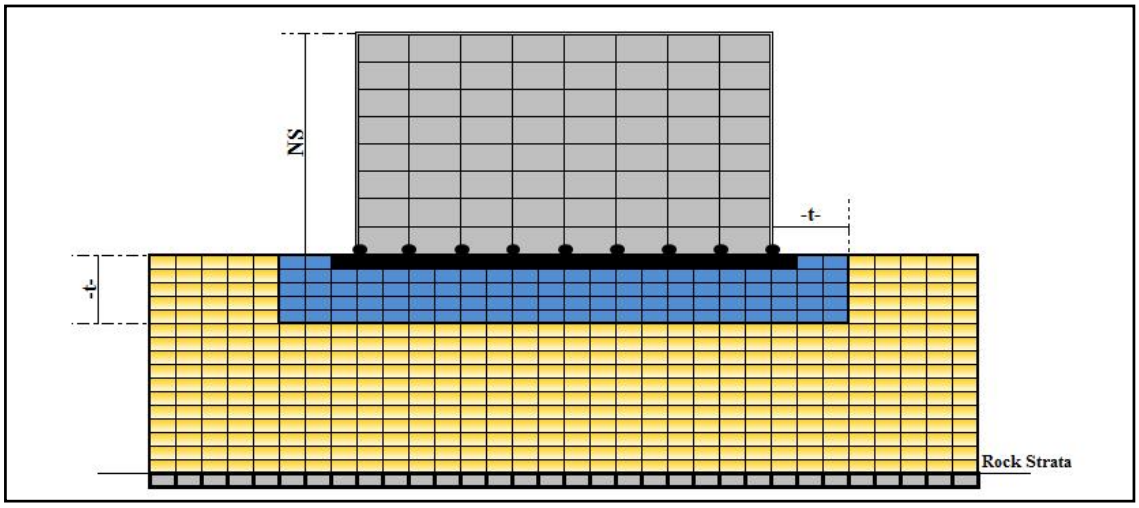

Figure 5.16. Soil – structure system, foundation without pile.

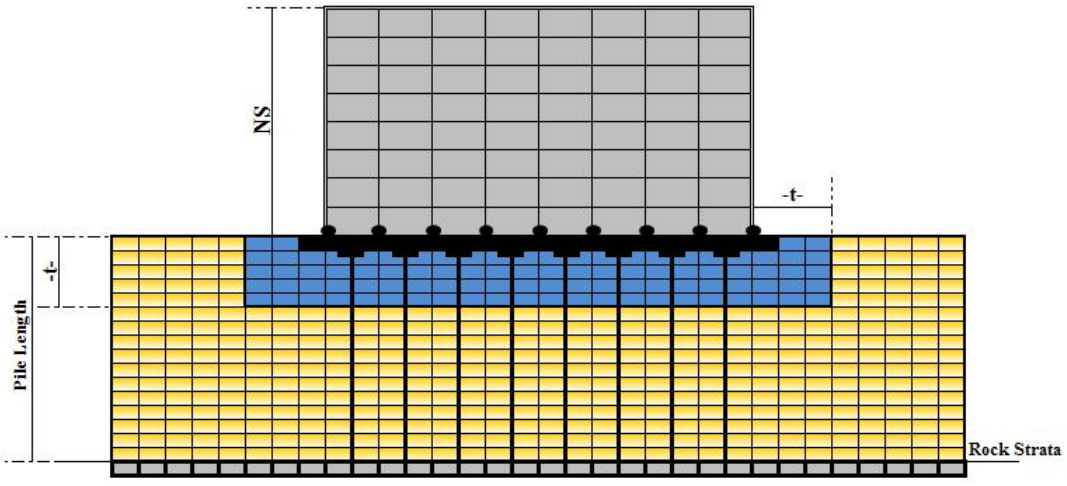

Figure 5.17. Soil – structure system, foundation with pile.

The buildings modeled in this study are supposed to be residential or office buildings. They have typical width of 40 m. The first soil layer surrounding foundation of building is replaced by TWSM. The medium is of thickness (t) in the order of eight m. The total thickness of the subsoil layer is constant at 20 m in all models. The same total

thickness was in the finite element models adopted in studies of Tsang *et al.* (2012) and Ahn and Gould (1992).

The building structure has a constant story height of tree m and bay width of five m. The material for all the beams, columns, floor slabs, and piles is C30 concrete with Young's modulus 30 GPa and density 23,50 kg/m3. The cross sections are 0.3 x 0.4 m and 0.5 x 0.5 m for the beams and columns, respectively. The thickness of floor slab is 0.15 m and the imposed load is eight kN/m2 including live load, and wall weight. The cross-sectional area of each pile is 0.16 m2, and the number of piles for each building model has been designed according to the loadings of the superstructure and the length of the piles. Both shaft friction and end bearing capacity have been taken into account in the pile design.

Special treatment has been made for nodes located at the soil–structure interface. In a two-dimensional frame, they have three DOFs, but it is two when they are in plane strain. In the model, displacement compatibility has been ensured at the interface nodes, where the rotational DOF is free, and the two transformational DOFs as in frame element are coupled with those in the four-node quadrilateral element. Meanwhile, full contact between soil (or TWSM) and piles is assumed.

Moreover, adapting the structure to two dimensional finite element models in plane strain condition was needed. In order to simulate the non-reflective effects of the infinite soil transmitting half-space, the model of viscous boundaries has been assumed as the boundary (transmitting base) of the computational domain.

When combining structures to TWSM samples of different confining pressure, the main focus has been to achieve a total pressure approximately equal to the σ', effective vertical confining pressure at the bottom of soil layer. To explain this principle with a simple numerical example, analysis of 8-storey structure above TCS30 under 100 kPa σ' is considered. Accordingly, it is planned to have a distributed load of eight kPa/m2 - As former claims in similar studies - concerning dead load plus live load combinations vertical components in structural design against earthquake specifications. P_{TCS} = 9.3 kN\m3. If a

soil layer of eight m depth is assumed the confining pressure at bottom becomes 101.2 kPa; quiet close to 100 kPa, the aimed value.

5.4.1. Setting and Adapting Soil Sample Data for Numerical Analysis

In previous sections, it was emphasized that mixing granulated TC to sand provides better soil performance than TWSM prepared with TBS. TC-S mixtures have better stiffness and damping properties than TB-S mixtures. When plotted normalized shear modulus G/G_{max} and damping ratio D against shear strain γ curves are further considered, it has been presumed that G/G_{max} vs. γ (per cent) curves should shift downward as sand is mixed with TW, and as the proportion of TW increases in sand. Contrarily, D vs. γ curve is expected to shift upward as sand is mixing with TW. It is revealed that TC-S curves are properly shaped. The trends of the curves are well apparent. Contrarily, same affirmation can't be claimed for TB-S mixtures' stiffness and damping curves. With experimental results held, not a clear trend can be observed with increasing proportion of TB in sand even when focused only on the actual experimental data with shear strain range up to 0.04 per cent for G/G_{max} vs. γ (per cent) curves. Effective Vertical Pressure, mean confining pressure in experimental data increase causes amplification in G/G_{max}. Therefore lowest G/G_{max} values are seen at lowest mean confining pressure. But even when considering the G/G_{max} vs. γ curve at 40 kPa "Visible difference" can be seen only up to around 0.2 per cent γ. For damping ratio vs. shear strain which is more important, it looks reasonable for strain levels up to 0.04 per cent, yet sand and TBS30 curves at γ (per cent) larger than 0.2 per cent doesn't vary with the same trend as at low-strain. What seems unreliable is that damping ratio curves for sand and TBS30 at strain larger than 0.2 per cent (extrapolated strain levels) do not vary with the same trend as at low-strain. D (per cent) of sand increases substantially, while D (per cent) of TB30 increases at the lowest rate with increasing shear strain. Another unsteady feature is that D (per cent) vs. γ (per cent) TBS10 is larger than sand only up to around 0.2 per cent strain, but the damping ratio of TBS10 is lower than that of sand at large strain.

Excessive use of Experimental instruments and possible sample disturbance are among first reasons leading disoriented data. On the other hand the results with the TC sample series are in accordance with the literature. So the inconvenience can be with the artificially induced extrapolation technique.

Regarding the numerical analysis, it is obvious that it would not be appropriate if TBS series curves were subject to further numerical simulation. When better stiffness and damping properties are also considered, only TCS series are included to numerical simulation program.

Considering that Equivalent Linear Numeric Analysis (ELNA) would give shear strain γ levels up to 10 per cent with increasing layer depth it is preferred to use Feng and Sutter (2000) empirical sand model with the TWSM experimental data. It was also the only data preferred in former studies with very similar scope by Tsang *et al.* (2007, 2009).

5.4.2. Choosing Earthquake Records for Numerical Analysis

For numerical analyses, three earthquake ground excitations were selected. They are, respectively, the 1994 Northridge, California (USA) Earthquake (Mw = 6.7), the 1999 Duzce, Turkey Earthquake (Mw = 7.1), and the 2001 El Salvador Earthquake (Mw = 7.6). The strong motion data were collected from COSMOS Virtual Data Center (website: http://db.cosmos-eq.org/). They cover different frequency contents and a wide range of ground shaking levels, both horizontal and vertical, as shown in Table 5.6 and Figure 5.17.

Table 5.6. Details of earthquake strong-motion data used in the parametric study.

	El Salvador	**Northridge, California (USA)**	**Duzce, Turkey**
Date of Earthquake	13.01.2001	17.01.1994	12.11.1999
Earthquake Magnitude Mw	7.60	6.70	7.10
Peak Horizontal Acceleration (PGAh)	0.72	1.78	1.03
Peak Vertical Acceleration (PGAv)	0.44	1.05	0.33

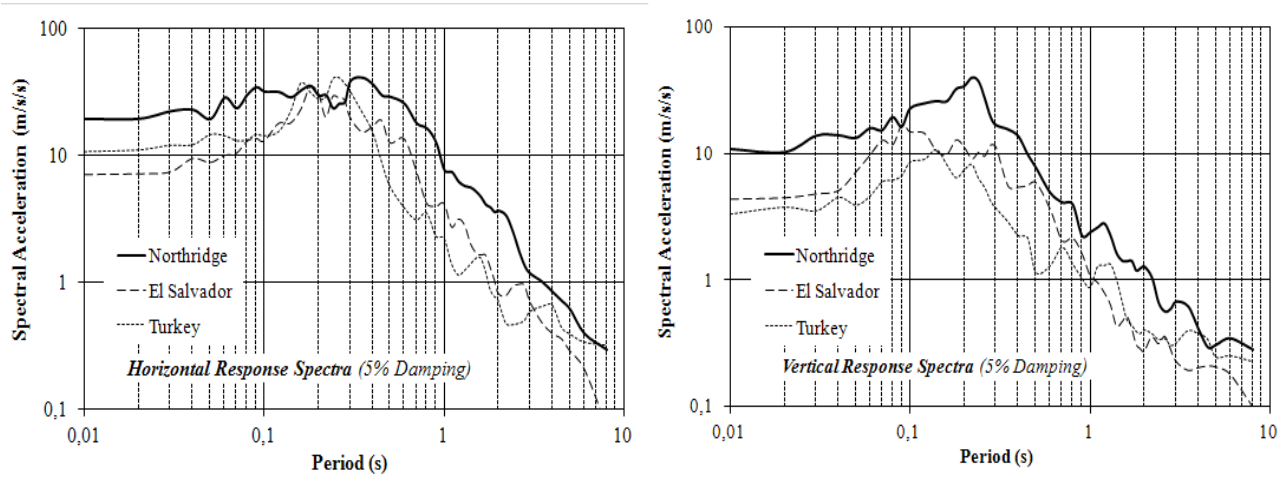

Figure 5.18. Horizontal and vertical response spectra of the above stated earthquake motions.

5.5. Numerical Analyses Study Program

The numerical analyses are classified as case according to seismic motion records used, TCS forming soil layer, structure number of storey (NS) and foundation characteristics (Table 5.7). This part includes analyses results case by case.

Table 5.7. Details of earthquake strong-motion data used in the parametric study.

Ovn fsjdbnfBobnntjt!Dbtft!
!

!!	!!	!!	!!	!!	**Fbsui rvbl f!n pujpot! fyfsufe!**		
Dbtf!	**TpjnfUzqf!' ! Dpog/! Qsfttvsf!**	**Gpvoebujpo! Uzqf!**	**Gpvoebujpo! Efqui !)STN ! Ui jdl oftt*!**	**Gnpps! I fjhi u!**	**Opsui sjehf!)2: : 5*!**	**Uvsl fz!!)2: : : *!**	**Fnh Tbnwbeps!!)3112*!**
2!	UD41!)51! l Qb*!	N bu!	4!	5!	!!	y!	!!
3!	UD21!)211! l Qb*!	N bu!	9!	9!	y!	y!	y!
4!	UD31!)211! l Qb*!	N bu!	9!	9!	y!	y!	y!
5!	UD41!)211! l Qb*!	N bu!	9!	9!	y!	y!	y!
6!	UD41!)211! l Qb*!	N bu!, !Qjnfi!	9!	9!	!!	y!	!!
7!	UD41!)211! l Qb*!	N bu!, !Qjnfi!	9!	23!	!!	y!	!!
8!	UD41!)311! l Qb*!	N bu!, !Qjnfi!	9!	23!	!!	y!	!!
9!	UD41!)311! l Qb*!	N bu!, !Qjnfi!	9!	29!	!!	y!	!!
+!	Qjnfi!Mfohui !jt !tvqqptfe !up!cf !31!n !jo!fbdi !dbtf/!				!!	!!	!!

For evaluating and comparing the effectivity of the TWSM as GSI material into the soil – structure system seismic response, three performance indicators with their peak and root-mean square (RMS) parameters; and fourthly, structures' fundamental periods had been sighted. Considering the structure model as the reference, control model; performance criteria are titled and explained as:

- Structure roof horizontal acceleration – Time History, normalized with reference to the maximum absolute horizontal acceleration at the roof level of the reference model,

- Structure footing horizontal acceleration – Time history, normalized with regard to the maximum absolute horizontal acceleration at the footing level of the control model,

- Structure first floor interstory drift – Time history, normalized with respect to the maximum absolute horizontal drift at the first floor of the control model,

- The ratio between fundamental natural periods of structure's model with TCS, and pure sand.

Since most severe damages are caused by strong ground shaking produced by nearfield earthquakes that are rich in high-frequency seismic wave components, horizontal acceleration response time histories have been collected at the mid-point of the roof of the building (referred to as the roof horizontal acceleration) and at the mid-point at the base of the footing (referred to as the footing horizontal acceleration).

The mid-point of the roof has been chosen because it represents the structure maximum horizontal acceleration response. The other station is considered as the location where earthquake input ground motion is applied in an ordinary structural analysis. The Last parameter is defined as first floor inter-story drift since soft-story mechanism is the major cause of collapse of many buildings in earthquakes. The peak and root-mean-square (abbreviated as RMS) values of the three parameters have been computed; hence, altogether, six parameters have been selected as the performance indicators.

The ‘percentage (per cent) reduction’ parameter is introduced herein to represent the effectiveness of the TWSM–Constructional Frame System in terms of its ability to reduce the acceleration and drift demand in a structure. This parameter is defined as 100 per cent minus the response quantity (i.e., maximum acceleration or inter-story drift) obtained from the proposed model (with TWSM) expressed as a percentage (per cent) of the respective response quantity as obtained from the control model (with sand).

Lastly, to observe energy absorption ability of TWSM, at each numerical analysis, a comparison of structure’s and subsoil’s absolute peak shear strain is considered. Percentage reduction calculated with ratio of the subsoil, structure peak shear strain differences over subsoil peak shear strain. The comparison is done among TWSM and control model.

6. NUMERICAL RESULTS

6.1. Brief Information on Numerical Analysis with QUAD4M

Numerical Analyses were performed with software developed on QUAD4M for a complete dynamic, time domain Equivalent Linear Analysis (ELA) of 2-D soil structure frame in a Finite Element Model FEM (Xuan, 2009). Properties were explained in detail in Chapter 4 and reemphasized in Chapter 5.4.

This comparative study has 14 numerical analyses of eight different scenarios with this software. Three strong earthquake ground motions were used to have different frequency content. Modeled structures were low to medium rise reinforced concrete buildings with residential, commercial functionality. Reinforced concrete foundations with or without pile was proposed. TCS mixture placed around structure's foundation had been investigated for usability as geotechnical seismic isolation (GSI) material, earthquake hazards mitigation solution (Table 5.7).

Consistent with the literature, three main performance indicators and their peak and root-mean square (RMS) parameters and structures' fundamental periods had been chosen as analyses results for evaluating and comparing the affectivity of the TWSM on seismic response of structure. The structure model with pure sand soil layer as the reference was the control model in each case. Performance criteria were chosen as normalized structure roof horizontal acceleration – time history, structure footing horizontal acceleration – time history, structure first floor interstorey drift – time history, structure's fundamental natural period ratio. The numerical analyses were classified as case according to seismic motion records used, TCS forming soil layer, structure number of storey (NS) and foundation characteristics. This chapter shows each case's results.

6.2. Case 1; TCS30 as GSI Material Underneath a 4-storey Reinforced Concrete Building

Numerical analysis Case 1 consists of reference and TCS30 models of four storey concrete building above TWSM layer with three m thickness. Concerning results are displayed in Figure 6.1.

It has seen from Figure 6.1a, Figure 6.1b and Figure 6.1c that response of structure against EQD excitation is in confliction with the expected results. The average of output RMS is negative, that means an amplification of earthquake motion happened when it was transmitted from soil.

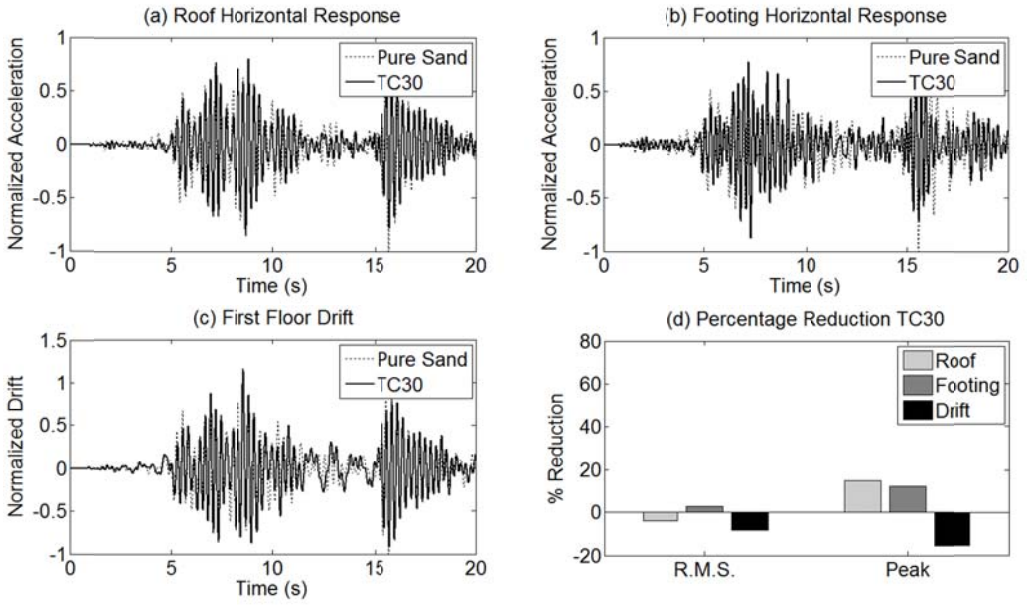

(a) Roof, (b) Footing Horizontal Acceleration, and (c) First-Floor Inter story drift for the TCS10 under Düzce (1999) Earthquake Motion, Normalized Time Histories. (d) (per cent) reduction for roof and footing horizontal acceleration and 1st floor inter-story drift. (RMS, root-mean-square)

Figure 6.1. Numerical analysis results for case 1 under EQD.

6.3. Case 2; TCS10 as GSI Material Underneath an 8-storey Reinforced Concrete Building

TCS10 were numerically analyzed under EQD, EQE, EQN strong ground motions records. Above of eight m. TCS10 or sand layer, an 8-storey reinforced concrete structure was modeled. Results are displayed from Figure 6.2 to Figure 6.4 in terms of first floor drift, roof and foundation accelerations. Figure 6.2a, Figure 6.2b; Figure 6.3a, Figure 6.3b; Figure 6.4a, and Figure 6.4b show the normalized roof and footing horizontal acceleration time histories, and Figure 6.2c, Figure 6.3c, and Figure 6.4c show the time history of the inter-story drift demand of the 1st floor.

As seen from Figure 6.2, Figure 6.3,and Figure 6.4; normalized Acceleration vs. time values at the footing level are lowered when initially higher than 0.5. It can be observed that TCS10 does not show a separated behavior than sand when the horizontal acceleration is relatively low. The minimization of soil seismic response at the footing level shall be a result of improvement at the Damping Ratio.

The roof horizontal acceleration is the structure response to the acceleration emitted at the footing level. The modeled 2-D Frame is based on a mid-rise reinforced concrete structure that poses an effective pressure on soil at the same level of effective confining pressure. As expected, peak acceleration values are subject to decrease and whole structural response is lowered.

First Floor Drift is similarly the 2-D FEM Structure Response to strong motion coming from ground but at the first floor level, not at roof level. The horizontal displacement is also lowered as roof displacement as expected.

Lastly, percentage reduction bar-graph shows the affectivity of improved sand with TW against pure sand profile under same earthquakes. The graphs show that although per

cent10 TC adding in sand soil does not contribute to strict change in soil seismic response to strong ground motions; structural response is visibly ameliorated. The average RMS percentage reduction is around per cent30 with EQN, per cent35 with EQE, per cent50 with EQD. The Period Lengthening ratio is 6.4 per cent, from 0.985 to 1.064.

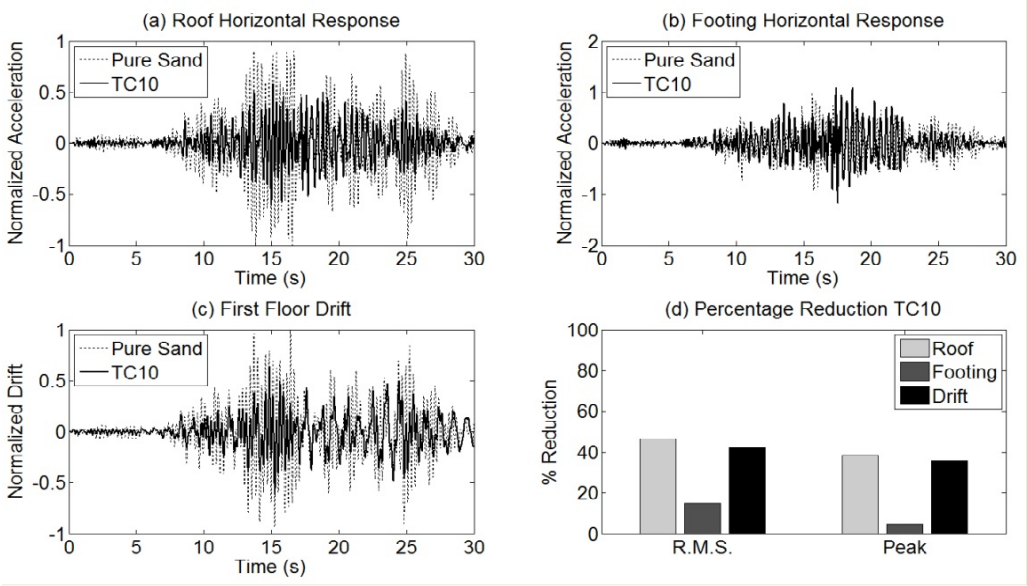

(a) Roof, (b) Footing Horizontal Acceleration, and (c) First-Floor Inter story drift for the TCS10 under El Salvador (2001) Earthquake Motion, Normalized Time Histories. (d) (per cent) reduction for roof and footing horizontal acceleration and 1st floor inter-story drift. (RMS, root-mean-square)

Figure 6.2. Numerical analysis results for case 2 under EQE.

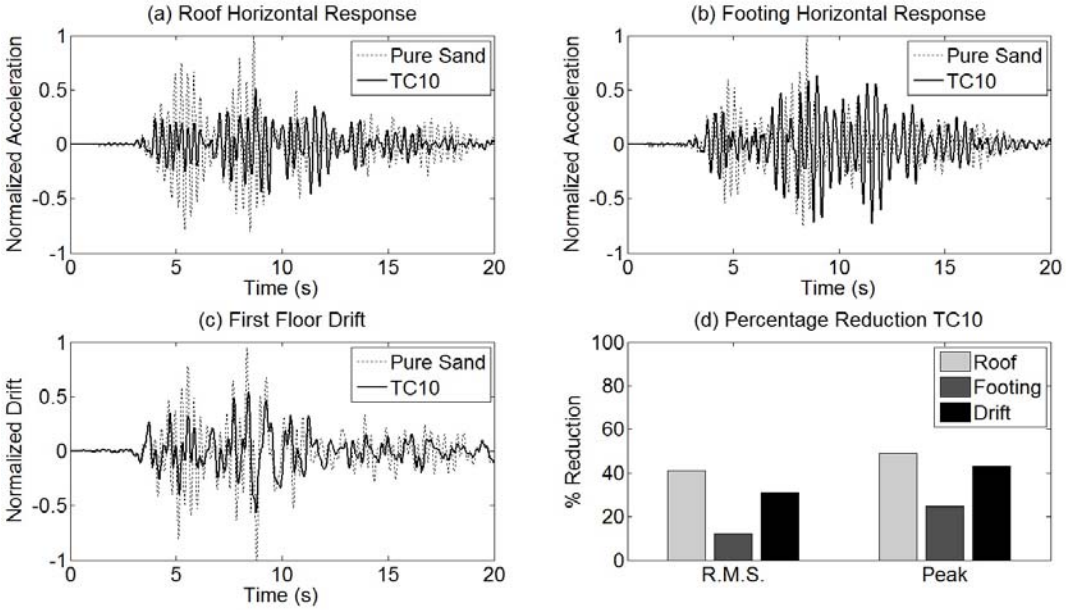

(a) Roof, (b) Footing Horizontal Acceleration, and (c) First-Floor Inter story drift for the TCS10 under Northridge (1994) Earthquake Motion, Normalized Time Histories. (d) (per cent) reduction for roof and footing horizontal acceleration and 1st floor inter-story drift. (RMS, root-mean-square)

Figure 6.3. Numerical analysis results for case 2 under EQN.

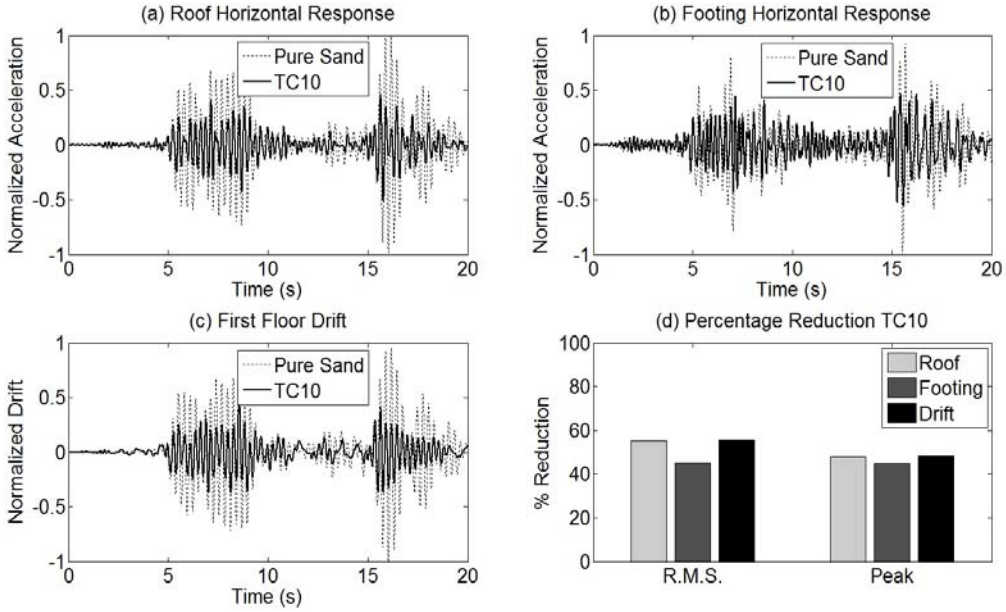

(a) Roof, (b) Footing Horizontal Acceleration, and (c) First-Floor Inter story drift for the TCS10 under Düzce (1999) Earthquake Motion, Normalized Time Histories. (d) (per cent) reduction for roof and footing horizontal acceleration and 1st floor inter-story drift. (RMS, root-mean-square)

Figure 6.4. Numerical analysis results for case 2 under EQD.

6.4. Case 3; TCS20 as GSI Material Underneath an 8-storey Reinforced Concrete Building

Case 3 is the repetition of Case 2 with only one change; use of TCS20 at the soil strata. Similarly, it possesses three numerical analyses under EQD, EQE, and EQN earthquake records. The structure is exactly the same of Case 2, 8-storey structure, with a residential function supposed to be constructed on an eight m depth of soil strata.

Analysis results are displayed from Figure 6.5 to Figure 6.7. The reference model is with the eight m pure sand layer underneath the above cited structure. All of the acceleration and drift data normalization is done according to maximum absolute accelerations at roof and foundation level, and drift at 1st floor level of this control model.

In Figure 6.5a and b; Figure 6.6a, b and Figure 6.7a, b the superposed normalized roof and footing horizontal acceleration time histories of the TCS20 and sand samples are shown. Further, Figure 6.5c, Figure 6.6c and Figure 6.7c display the time history of the inter-story drift demand of the 1st floor. Lastly, Figure 6.5d, Figure 6.6d and Figure 6.7d monitor percentage reduction bar-graphs.

From Figure 6.5, Figure 6.6, and Figure 6.7 it can be observed that normalized acceleration vs. time values at the footing level are more apparently dropped than Case 2. TCS10 caused a percentage reduction up to 50 per cent; whereas this value rose to 60 per cent with TCS20. At time histories, it can be remarked that TC presence in sand at 20 per cent by weight causes a considerable change at the soil behavior especially when we consider the TCS20 behavior after 13th, 14th second at the EGD Case. Same change observed under EQE but after 20th second. The motion duration is approximately 30 sec.

The roof horizontal acceleration vs. time and first floor drift vs. time curves are 2-D FEM structural frame model ought to be a reinforced concrete structure response to

acceleration submitted at the footing level. It is observed considerable change in structure behavior under emitted strong earthquakes when standing on TCS20 soil mixture compared to Pure Sand.

Percentage reduction bar-graph shows that maximum accelerations at the roof and footing levels, lower floor drifts are lowered by half when pure sandy sample is mixed with granulated rubber TC. On average values, 20 per cent presence of TC in sand leads to normalized structural response reduced down to 60 per cent. Following, structure fundamental period lengthens to 1.012.

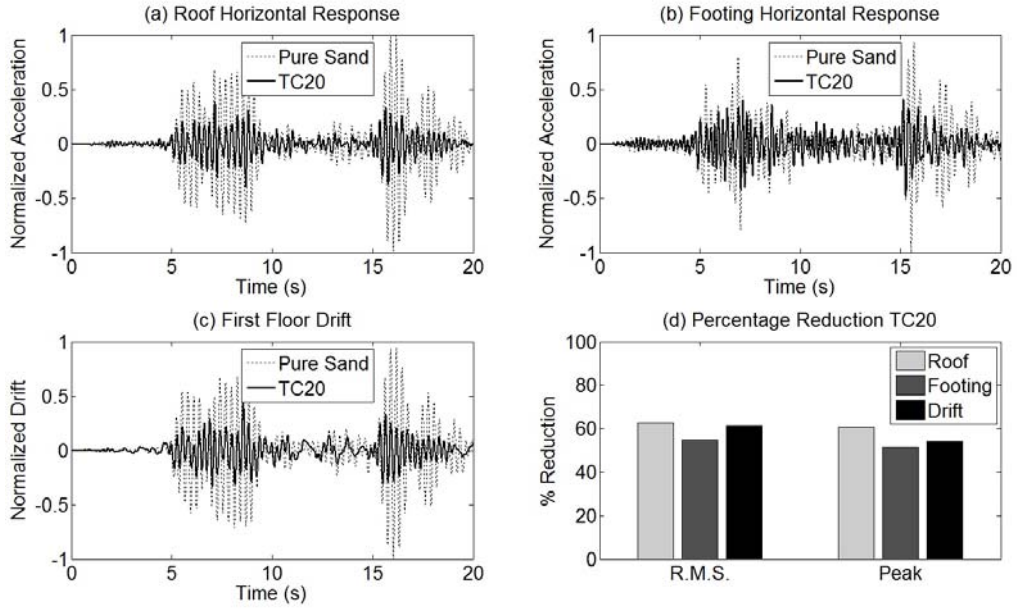

(a) Roof, (b) Footing Horizontal Acceleration, and (c) First-Floor Inter story drift for the TCS20 under Düzce (1999) Earthquake Motion, Normalized Time Histories. (d) (per cent) reduction for roof and footing horizontal acceleration and 1st floor inter-story drift. (RMS, root-mean-square)

Figure 6.5. Numerical analysis results for case 3 under EQD.

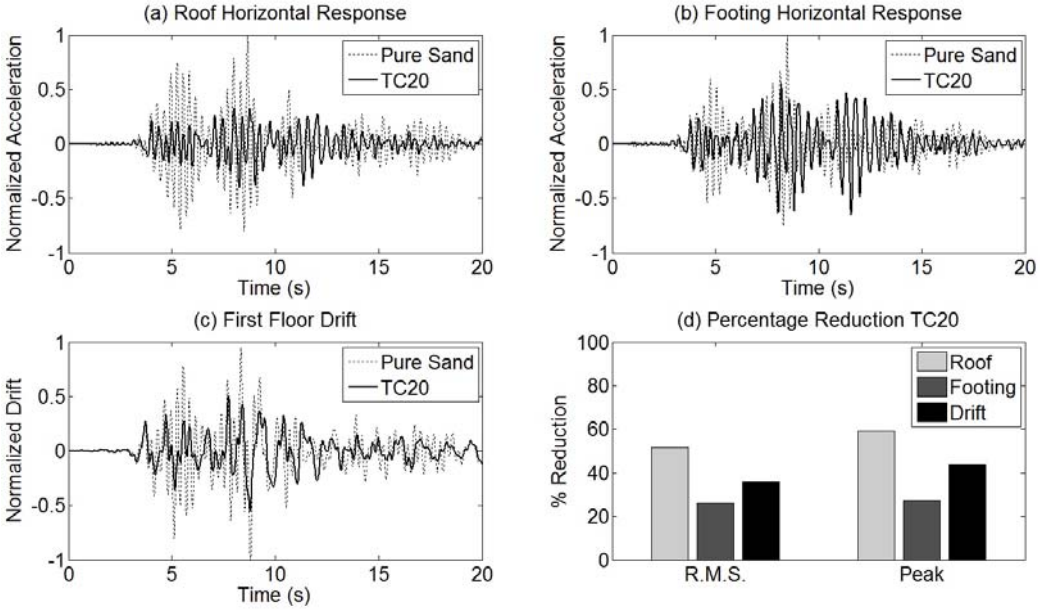

(a) Roof, (b) Footing Horizontal Acceleration, and (c) First-Floor Inter story drift for the TCS20 under Northridge (1994) Earthquake Motion, Normalized Time Histories. (d) (per cent) reduction for roof and footing horizontal acceleration and 1st floor inter-story drift. (RMS, root-mean-square)

Figure 6.6. Numerical analysis results for case 3 under EQN.

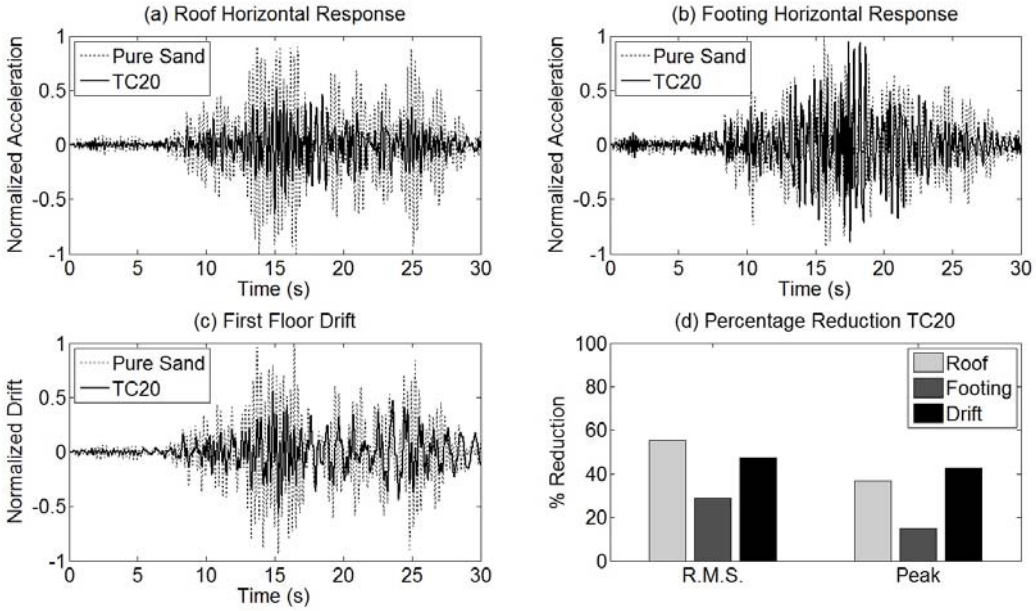

(a) Roof, (b) Footing Horizontal Acceleration, and (c) First-Floor Inter story drift for the TCS20 under El Salvador (2001) Earthquake Motion, Normalized Time Histories. (d) (per cent) reduction for roof and footing horizontal acceleration and 1st floor inter-story drift. (RMS, root-mean-square)

Figure 6.7. Numerical analysis results for case 3 under EQE.

6.5. Case 4; TCS30 as GSI Material Underneath an 8-storey Reinforced Concrete Building

Case 4 is the third repetition of the previous analysis in Case 2 with 30 per cent TC inclusion into sand at soil layer. Regarding to scenario, this case covers simulation of 8-strorey concrete structure on top of eight m depth soil strata with all 3 strong ground excitations EQD, EQE and EQN; similar to Case 2 and Case 3. Same model as Case 2 and Case 3 was taken as reference model. Results are exhibited at Figure 6.8, Figure 6.9, and Figure 6.10.

Figure 6.8a, Figure 6.9a, and Figure 6.10a display the normalized roof acceleration time histories of the 2-D FEM Structural Model against EQN, EQE and EQD respectively. In all three Earthquake Scenarios, structural response at the roof level is lowered down to 67 per cent. It can be observed the influence of TC inclusion ratio increase. Since peak accelerations are below material tolerance limits, acceleration with time is always decreasing.

Figure 6.8b, Figure 6.9b, and Figure 6.10b display the normalized footing acceleration time histories of the 2-D FEM Structural Model against earthquakes EQN, EQE and EQD. The analyses with EQE and EQN show a 15 per cent and 25 per cent normalized footing acceleration. This value is increased up to 55 per cent when EQD is used. Observing time histories of EQE and EQD, it can be remarked that soil behavior is ameliorated under strong ground motion with long duration since reduction in acceleration becomes more obvious after 20th second of the movement.

Figure 6.8c, Figure 6.9c, and Figure 6.10c are 2-D FEM Structural Response to EQN, EQE and EQD respectively at the first floor level. Invariably, significant improvement is observed at each case up to 70 per cent in the most optimistic scenario.

When Figure 6.8d, Figure 6.9d, and Figure 6.10d are monitored; it can be remarked that root mean squares of maximum acceleration and drift values are degraded in each earthquake scenarios. Considering the maximum values only, record with EQN displays a lowered reduction at the footing level. Other time histories display obviously successful results against demand. Normalized accelerations and drift values are reduced to 60 per cent on average with EQD. But this value was limited to 45 per cent with EQN. Structure fundamental period lengthening ratio reaches 14 per cent in Case 4.

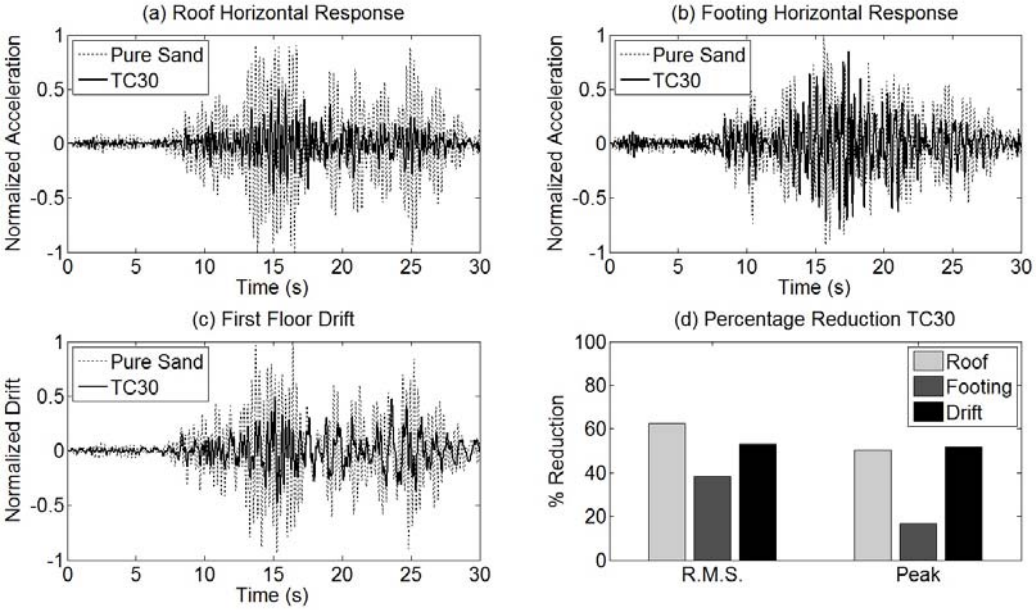

(a) Roof, (b) Footing Horizontal Acceleration, and (c) First-Floor Inter story drift for the TCS30 under El Salvador (2001) Earthquake Motion, Normalized Time Histories. (d) (per cent) reduction for roof and footing horizontal acceleration and 1st floor inter-story drift. (RMS, root-mean-square)

Figure 6.8. Numerical analysis results for case 4 under EQE.

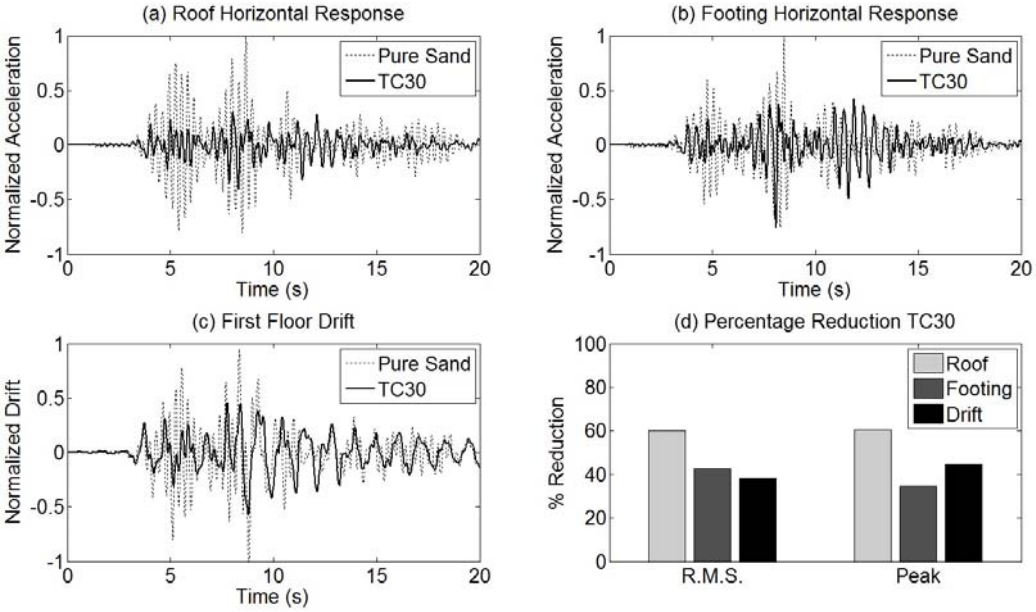

(a) Roof, (b) Footing Horizontal Acceleration, and (c) First-Floor Inter story drift for the TCS30 under Northridge (1994) Earthquake Motion, Normalized Time Histories. (d) (per cent) reduction for roof and footing horizontal acceleration and 1st floor inter-story drift. (RMS, root-mean-square)

Figure 6.9. Numerical analysis results for case 3 under EQN.

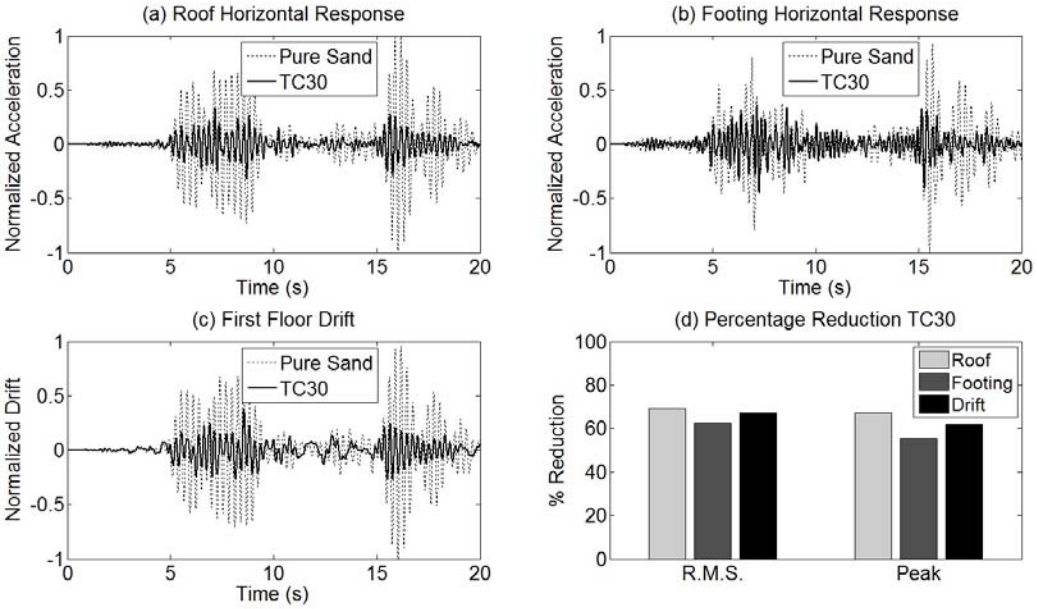

(a) Roof, (b) Footing Horizontal Acceleration, and (c) First-Floor Inter story drift for the TCS30 under Düzce (1999) Earthquake Motion, Normalized Time Histories. (d) (per cent) reduction for roof and footing horizontal acceleration and 1st floor inter-story drift. (RMS, root-mean-square)

Figure 6.10. Numerical analysis results for case 3 under EQD.

6.6. Case 5; TCS30 as GSI Material Underneath an 8-storey Structure with Pile

Case 5 is the numerical analyses of 8-storey reinforced concrete structure with 20 m depth pile. Two analyses were simulated with sand and TCS30 layer separately, with eight m thickness around its foundation, under EQD strong ground motion. Pure sand placed underneath the structure was the reference model. Results are displayed at Figure 6.11 in terms of normalized first floor drift, roof and foundation accelerations.

Peak Normalized Acceleration value at the footing level is lowered 23 per cent. In Case 5, it is seen that the effect of TWSM underneath reinforced structure with pile foundation is low compared to previous cases.

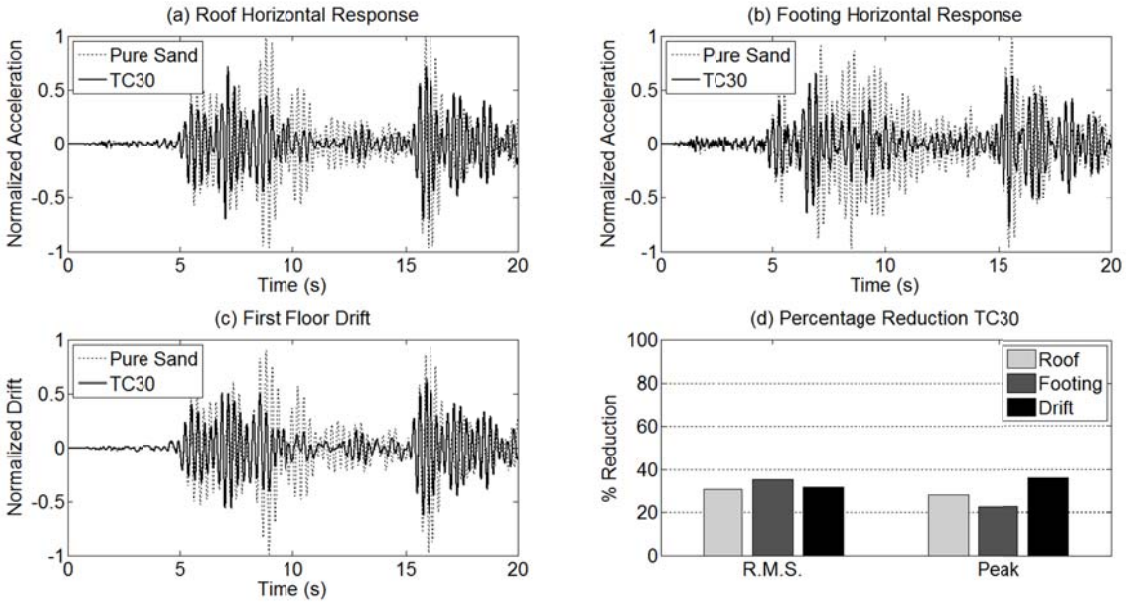

(a) Roof, (b) Footing Horizontal Acceleration, and (c) First-Floor Inter story drift for the TCS30 under Düzce (1999) Earthquake Motion, Normalized Time Histories. (d) (per cent) reduction for roof and footing horizontal acceleration and 1st floor inter-story drift. (RMS, root-mean-square)

Figure 6.11. Numerical analysis results for case 5 under EQD.

The roof horizontal acceleration is the structure response to the acceleration emitted at the footing level. The peak acceleration value is subject to 30 per cent decrease.

First Floor Drift, like the roof horizontal acceleration is still the structure response to strong motion coming from ground, but at the first floor level. The horizontal displacement is lowered at the same level of roof horizontal acceleration in Case 5.

Percentage reduction bar-graph displays the effectivity of improved sand with TW against pure sand profile under same earthquakes. The graphs show that TC inclusion to pure sandy soil does not contribute to strict change in soil and structure responses in this case. At the end, the average reduction of outputs is 33 per cent. Fundamental natural period of the structure becomes 0.931 from 0.914, two per cent.

6.7. Case 6; TCS30 as GSI Material Underneath a 12-storey Structure with Pile

In case 6, structure's number of story increased to 12. Rest of the scenario was similar to case 5; 20m depth pile under foundation which stays on top of eight m soil strata. Again, EQD was used.

Results are displayed at Figure 6.12 in exactly same terms of previous cases; Normalized roof horizontal acceleration, footing horizontal acceleration, and first floor drift. Their time histories are plotted respectively in (a), (b), and (c). The superposed plots are all normalized results with respect to the maximum absolute acceleration/drift of the reference control model.

Further, it is observed that the role of TWSM use instead of pure sand under structure is more sharply exhibited in stabilization than seismic movement deamplification. The percentage reduction at the footing horizontal response is 12 per cent, half of the first floor drift.

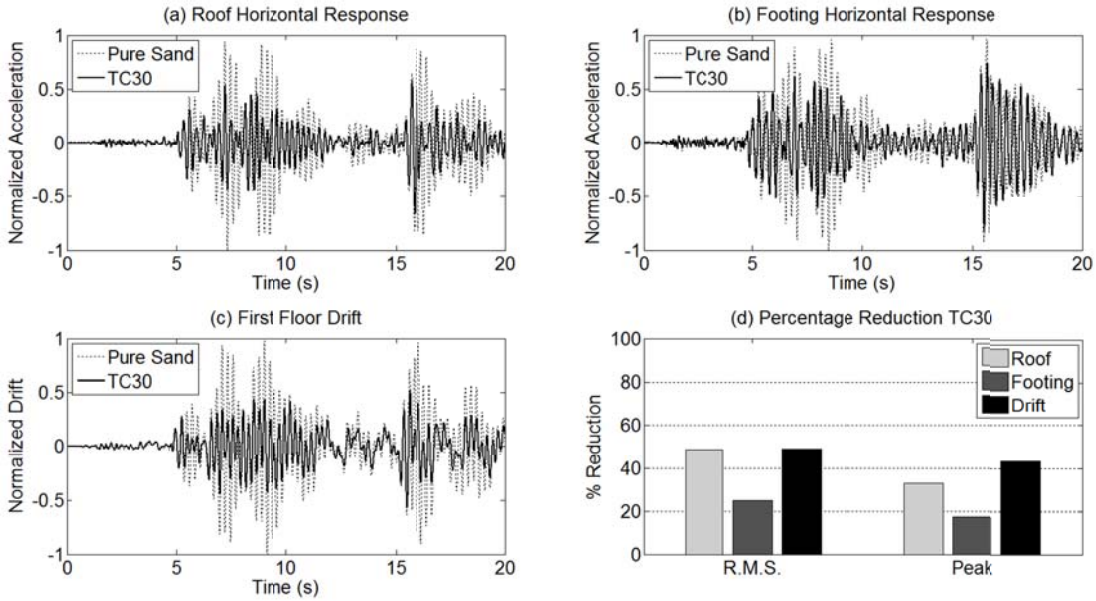

(a) Roof, (b) Footing Horizontal Acceleration, and (c) First-Floor Inter story drift for the TCS30 under Düzce (1999) Earthquake Motion, Normalized Time Histories. (d) (per cent) reduction for roof and footing horizontal acceleration and 1st floor inter-story drift. (RMS, root-mean-square)

Figure 6.12. Numerical analysis results for case 6 under EQD.

The average of three parameter reduction percentage RMS is 40 per cent, higher than previous case. Structure fundamental period slightly changes from 1.36 to 1.38.

6.8. Case 7; TCS30 as GSI Material Underneath a 12-storey Structure with Pile

The seventh case has the exact setup of the sixth case, but the soil layer is presented with the CTT data of TCS30 subject to higher confining pressure **σ'**. Along the same line, the model with sand layer of eight m depth under 12-storey reinforced concrete structure with pile at its foundation level is the control model for the same structure on top of eight m depth TCS30 layer. Results are shown at below Figure 6.14. The superposed plots are all normalized results with respect to the maximum absolute acceleration/drift of the reference control model. The Figure (d) gives the percentage reduction of measured outputs at maximum and average levels.

The effect of TC adding in sand displayed more slightly compared to previous case. Figure 6.13 shows that the RMS average is only 20 per cent. This is half value at Case 6. Peak values of parameters are around 20 per cent likely. The change in fundamental period is the exact of Case 6.

In CTT test, the increase in confining pressure had caused upward and downward shifts in shear modulus (G) and damping ratio (D) of TCS samples. It can be determined that the results are in parallel with this deduction.

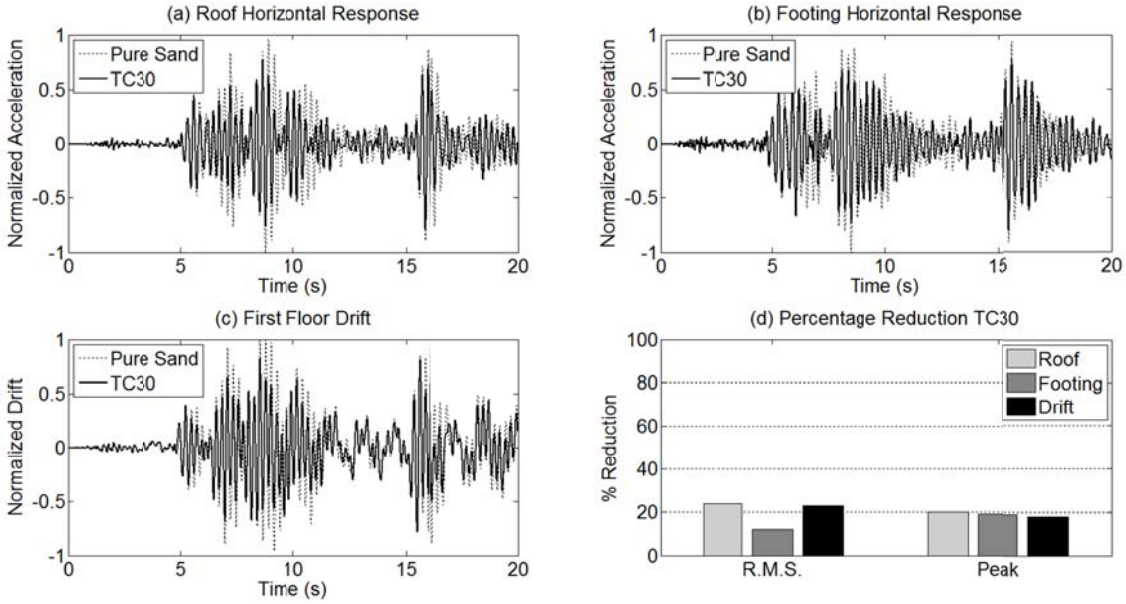

(a) Roof, (b) Footing Horizontal Acceleration, and (c) First-Floor Inter story drift for the TCS30 under Düzce (1999) Earthquake Motion, Normalized Time Histories. (d) (per cent) reduction for roof and footing horizontal acceleration and 1st floor inter-story drift. (RMS, root-mean-square)

Figure 6.13. Numerical analysis results for case 7 under EQD.

6.9. Case 8; TCS30 as GSI Material Underneath an 18-storey Structure with Pile

TCS30 Samples were numerically analyzed under EQD strong ground motion record. Above of eight m. TCS30 or sand layer, an 18-storey reinforced concrete structure with pile at its foundation level was modeled. Results are displayed at Figure 6.14 in terms of first floor drift, roof and foundation accelerations time histories. All parameters are normalized with respect to the maximum absolute acceleration/drift of the reference or control model. Figure 6.15a and Figure 6.15b show roof and footing horizontal accelerations. Figure 6.14c shows the time history of the inter-story drift demand of the 1st floor. Figure 6.14d gives the percentage reduction of measured outputs at maximum and average levels.

Figure 6.14 displays that this case also is one of the analyses where TC inclusion effect is moderately seen referred to other models. Concrete and pile foundation system is supposed to be considered a factor that hides the TCS influence on structure as general

observation. Principally, the constant vertical pressure increase in soil layer which is the rise in the number of stories of the structure lowers the TCS layer resistance against seismic activity as well as Sand layer. Resultantly, peak normalized acceleration at the footing and roof levels are lowered only approximately eight per cent.

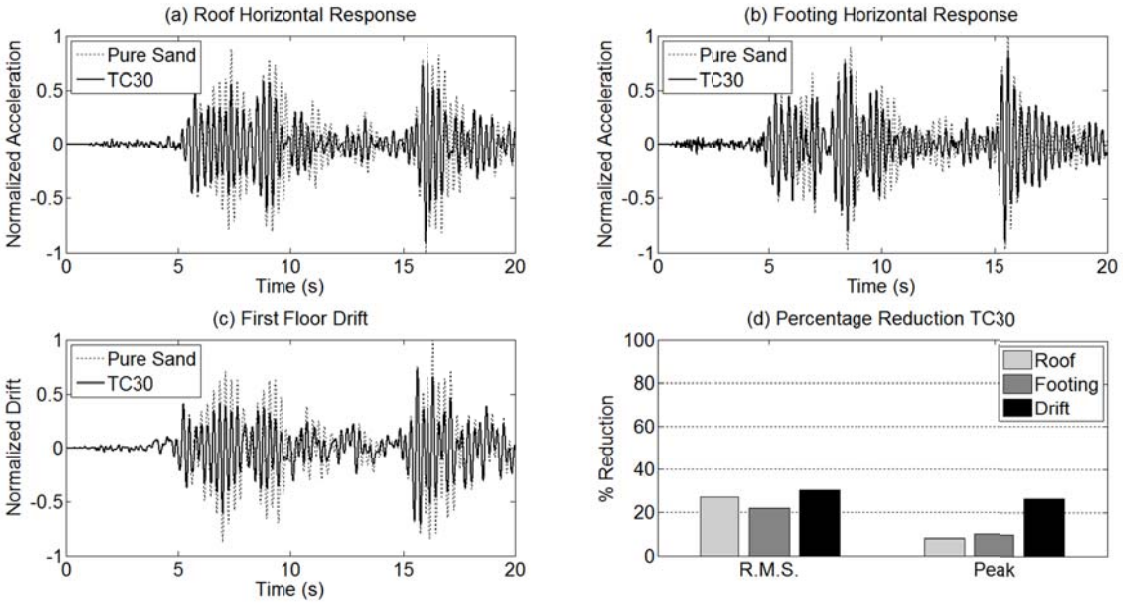

(a) Roof, (b) Footing Horizontal Acceleration, and (c) First-Floor Inter story drift for the TCS30 under Düzce (1999) Earthquake Motion, Normalized Time Histories. (d) (per cent) reduction for roof and footing horizontal acceleration and 1st floor inter-story drift. (RMS, root-mean-square)

Figure 6.14. Numerical analysis results for case eight under EQD.

6.10. Numerical Analyses Results, Discussions

This comparative study included 14 numerical analyses with eight scenarios to investigate the usability of TWSM as Geotechnical Seismic Isolation (GSI) material. Their performance parameters were TWSM (type and ratio) placed underneath foundation, subsoil layer thickness, type of foundation, and structure's number of stories. The main concentration is to determine the behavior of a structure – sub soil system depending on the TWSM use around the foundation of the structure instead of sand.

The CTT results of TWSM formed separately with granulated rubber and buffing rubber inclusion with different proportions are analyzed at the first stage. The Damping Ratio D (per cent) versus Shear Strain γ (per cent) and Shear Modulus over Maximum Shear Modulus, G/G_{max} versus Shear Strain γ (per cent) curves are plotted and evaluated. Briefly, it can be deduced that soil dynamic behavior acquisition for earthquake hazards mitigation is possible due to both granulated and buffing TW usage. G/G_{max} at any arbitrary γ (per cent) level augments with increasing tire waste presence in soil. Accordingly, below conclusions are claimed:

- TB and TC use as improvement material on sand has eminently increased **D** (per cent) up to three times depending on the weight ratio, at all **γ** (per cent) values. Contrarily to **G**; dropping down to ¼ levels at small **γ** (per cent)'s.

- σ' (kPa) change during CTT affected specimen behavior. σ' (kPa) increase has a D (per cent) amplifier effect on sand specimen whereas, acts as a deamplifier on TWSM mixtures. Experimental results show that all seven specimens G (MPa) vs. γ (per cent) curves shifted up with σ' (kPa) increase.

- Different reprocessed tire waste affects sand dynamic properties at different levels. Concerning lowest σ' (kPa) level - 40 kPa and maximum TW/S ratio - 30 per cent; TC30 shows D_{max} (per cent) four per cent at maximum γ (per cent) which is approximately twice higher than D_{max} (per cent) of TB30 at same γ (per cent).

- Focused on G (MPa) vs. γ (per cent) curves of specimens, CTT results indicate that TW presence in S causes an intense reduction in G (MPa) at small γ (per cent) levels; furthermore, TWSMs show more linear behavior compared to S.

The software developed on QUAD4M by Xuang (2009) was preferred in this study as formerly used by Tsang *et al.* (2010, 2012). It is computer software capable to do time

domain, 2-D Equivalent Linear Analysis of soil and structure system modeled with Finite Element Method FEM. The experimental data were reconsidered regarding allowability for numerical analysis with this software. Plotted D and G/G_{max} curves were carefully investigated. Accordingly, all TBS were excluded from numerical analysis since curves do not reflect the ideal shape and soil behavior. TCS experimental data were subject to study. For a reliable numerical analysis, to have an adequate shear strain range of dynamic properties, D and G data were extrapolated and interpolated with hyperbolic curve modeling.

The results are monitored with fundamental natural period ratio of structure's model with TCS and pure sand; the peak and root-mean square (RMS) values of normalized structure roof horizontal acceleration – time history, normalized structure footing horizontal acceleration – time history, normalized structure first floor interstorey drift – time history and lastly structure maximum strain reduction comparison.

The outputs did not belong to a small scale of numerical values. Performance Criteria, which are listed in Table 6.1, influenced the results differently.

Table 6.1. Variable inputs used in the parametric study.

Variable Inputs Used in the Parametric Study	
Number of storey (NS)	4, 8, or 18
Depth of piles below foundation	20m
Effective Confining Pressure (kPa)	40, 100, or 200
TC/TWSM by weight (per cent)	10, 20, or 30
Thickness of TWSM layer (m)	3 or 8
Peak Horizontal Acceleration (g)	0,72 - 1,78
Peak Vertical Acceleration (g)	0,33 - 1,05

Strong ground motions with abbreviations EQE, EQN and EQD represent 2001 El Salvador Earthquake (Mw = 7.6), 1994 Northridge, California (USA) Earthquake (Mw = 6.7), and 1999 Düzce, Turkey Earthquake (Mw = 7.1) respectively. Their horizontal peak ground accelerations are 0.72, 1.78, and 1.03. EQD is used in all of the numerical simulations where as EQE and EQN are included to numerical analyses in Case 2, Case 3, and Case 4. They represented an 8-storey structure on top of an eight m soil layer. The soil layer consisted of TCS10, TCS20, and TCS30 in Case 2, Case 3, and Case 4 respectively. Results show the positive effect of TC inclusion to Sand sample at each strong earthquake motion scenario. Even though structure soil interface acceleration level is moderately lower reduced when TC present in soil sample is less than 20 per cent, or from one earthquake record to another; the structure horizontal acceleration at the roof level and inter story drift at the first floors are significantly decreased especially on TCS30. But at least a 30 per cent TC by weight should be present in soil to observe considerable fundamental period shift. At this point, it can be said that small amount of TC presence in

sand also results in ameliorated structural response during earthquakes (in Figure 6.2 to Figure 6.10). Table 6.3 shows detailed numerical results of the analyses, including all of performance criteria as well.

In all scenarios, TWSM depth between foundation and rock strata had been kept constant, eight m except Case 1 only, 4m. To analyze the effect of soil depth under structure's foundation on analyses results Case 4, Case 8, and Case 1 can be considered. Case 4 had better results than the rest of the whole study in each output parameter. (Figures 6.1, Figure 6.8, Figure 6.9, Figure 6.10, Figure 6.14) The average of normalized acceleration and drift time histories RMS was around 66 per cent. The peak acceleration levels were 70 per cent. The lengthening in fundamental structure period was at maximum of this study, 15 per cent. Results of Case 1 and Case eight were one of the scenarios where TC inclusion to soil layer effect was weakest. Increase of soil layer depth was among the parameters caused performance degradation between three scenarios. A further excessive settlement would be possible to be happened with deeper TCS soil strata. Since this study concentrates on subsoil dynamic response, its vertical settlement under static loading is not analyzed. Yet, it can be claimed preloading and soil compaction to be advised as a remedy.

One of the main goals of this comparative study's investigation is the effect of increase in the TC ratio over TWSM by weight. Case 2, Case 3, and Case 4 have the same scenario: 8-storey residential structure with mat foundation, standing on top of an eight m. depth soil layer. Considering all three earthquake records, TC per cent by weight increase resulted increase at period lengthening shift. All of the peak and RMS normalized parameter values reached their maximum value when used TCS30 as sub soil. The average of normalized accelerations and drift values RMS was 66 per cent in Case 4, when model had been simulated with EQD (in Figure 6.2 to Figure 6.10). This performance was the best of the whole study. Relying on these outcomes, it shall be deduced that TCS/TWSM by weight increase has a positive effect on seismic response of structure. Furthermore, numerical analyses made conclude that at least TCS30 should be used for a considerable change in structure's fundamental period. A similar conclusion was achieved with the analysis of experimental data.

CTT results exhibited that as the TC per cent by weight increased, D and G curves shifted upward. As σ' increased D vs. γ and G vs. γ curve move upward and downward respectively. Especially the increase in damping property had been considered as convenient for probable use as GSI material. The same effect investigated in this study especially through Case 6 and Case 7 (Figure 6.12, and 6.13). They consisted of exactly the same hazard scenario, except that TCS30 with low σ' was used as improved soil layer in Case 6, and TCS30 with high σ' in Case 7. The resulting performance was in contradiction with CTT results. The period lengthening ratio, all of the peak and RMS values of roof horizontal acceleration, footing horizontal acceleration, first floor drift were lower in Case 7 than in Case 6. It is deduced that TCS30 under high σ' resulted in poor GSI performance.

In common practice, foundations strengthened with pile is one of the most common solutions against soft soils, as the study's scope. 20m depth pile was used as foundation support in half of the scenarios. To analyze its effect on seismic performance in numerical analyses, Case 4 and Case 5 should be compared. Simulation with EQD of Case 4 exhibited better seismic performance than Case 5 in all output parameters, including structure's fundamental period (in Figure 6.8 to Figure 6.11). Resultantly, although pile existence covered the effect of TC adding in subsoil strata, it is a possible solution for structure stabilization on weak soils.

The last performance criteria was the number of structure's storey. This soil improvement method was recommended as a method for low to medium rise structures against earthquake movement hazards. When cases 5 – 6 (Figures 6.11, and 6.12), and 7 – 8 (Figures 6.13, and 6.14) were compared separately, average values of normalized acceleration and drift RMS were increased with the increase in structure's NS. The normalized acceleration was reduced when structure's NS increased. Furthermore, the period lengthening ratio was reduced when structure's NS increased similarly. Considering normalized drift and horizontal roof accelerations, it could be stated that, structure height increase did not constitute an inconvenience. But regarding the general drop in overall performances with the increase in structure's height, and since the worst seismic

performance was observed at Case 8 it must be deduced that this technique would have a limited effect when used under medium-high rise structures, and low rise structures must be preferred.

To investigate the damping effect of TC, Reduction of Maximum Absolute Horizontal Strain of Structure over Subsoil Ratio is considered. They are given in Table 6.2. If we focus on cases where piles do not exist under foundation, an average of 30 per cent shear strain reduction is observed at analysis where subsoil was TCS whereas it is 17 per cent at the control models. This result supports the damping and vibration absorption property of TCS.

A series of studies were recently published by Tsang *et. al.,* (2006 to 2012). The numerical analyses were done with QUAD4M, and finally with its recent version developed by Xuan (2009). A 10 storey building, with or without pile foundation and a structure representing underground tunnels were used as the structure model. It was composed of concrete lining surrounded by rubber soil mixture below pavement. The soil samples were adopted from experimental study of Feng and Sutter (2000); RSM with 75 per cent by volume of rubber in mixture were considered as GSI material. The vertical and horizontal acceleration at the footing level were exhibited when QUAD4M had been preferred, and the exact outputs of this study were shown when the recent software of Xuan (2009) had been used for modeling. Former studies with same subject of research are summarized in Table 6.4 with this study. As cited, this comparative study includes several models of upper structure, two types of foundation and different proportions of TCS. Furthermore selected TWSM is different than former studies. When the results of eight and 12 story structures with the former studies, average acceleration RMS is 40-60 per cent, whereas it is 50-70 per cent in previous studies where ten storey building was examined.

Table 6.2. Reduction of maximum horizontal peak strain of structure over subsoil.

		Peak Shear Strain Percentage Reduction (%) – Structure vs. Subsoil	
Cases	**Earthquake Motions**	**Reference Model**	**TWSM Model**
1	**Turkey (1999)**	**0,35**	**0,31**
2	**Northridge (1994)**	**0,21**	**0,33**
	Turkey (1999)	**0,26**	**0,03**
	El Salvador (2001)	**0,41**	**0,01**
3	**Northridge (1994)**	**0,30**	**0,78**
	Turkey (1999)	**0,23**	**0,09**
	El Salvador (2001)	**0,34**	**0,04**
4	**Northridge (1994)**	**0,26**	**0,78**
	Turkey (1999)	**0,30**	**0,00**
	El Salvador (2001)	**0,33**	**0,00**
5	**Turkey (1999)**	**0,06**	**0,00**
6	**Turkey (1999)**	**0,05**	**0,00**
7	**Turkey (1999)**	**0,04**	**0,00**
8	**Turkey (1999)**	**0,03**	**0,00**

Maximum values are observed on representative finite element model nodes whole time history is considered. Accordingly, the strains are seen at the same moment or slightly different; at the 1/100 second scale.

Table 6.3. Numerical analyses result summary.

			CASE 1	CASE 2			CASE 3			CASE 4			CASE 5	CASE 6	CASE 7	CASE 8
Vertical Total Pressure			*40kPa*	*100kPa*	*100kPa*	*100kPa*	*100kPa*	*100kPa*	*100kPa*	*100kPa*	*100kPa*	*100kPa*	*100kPa*	*100kPa*	*200kPa*	*200kPa*
Earthquake			*Turkey*	*North.*	*El. Salva*	*Turkey*	*North.*	*El. Salva*	*Turkey*	*North.*	*El. Salva*	*Turkey*	*Turkey*	*Turkey*	*Turkey*	*Turkey*
Sand & RSM			*TC30*	*TC10*	*TC10*	*TC10*	*TC20*	*TC20*	*TC20*	*TC30*	*TC30*	*TC30*	*TC30*	*TC30*	*TC30*	*TC30*
No. of Building Story			*4*	*8*	*8*	*8*	*8*	*8*	*8*	*8*	*8*	*8*	*8*	*12*	*12*	*18*
Pile Length			*0*	*0*	*0*	*0*	*0*	*0*	*0*	*0*	*0*	*0*	*20 m*	*20 m*	*20 m*	*20 m*
Normalized Accelerations and Drift (%)	**Peak**	**Roof**	18,0	49,0	38,6	48,0	60,6	37,0	60,6	59,2	50,3	67,1	28,2	32,8	20,1	8,0
		Footing	16,0	27,3	1,7	44,7	34,6	4,9	51,5	24,9	14,8	55,5	22,5	17,4	18,8	7,5
		Drift	-17,0	44,0	35,8	48,0	44,7	42,6	54,2	43,0	51,7	61,8	36,1	43,3	17,9	22,3
	R.M.S.	**Roof**	-4,0	40,9	46,5	55,3	51,6	55,4	62,7	60,1	62,6	69,3	30,8	48,3	23,8	25,9
		Footing	-2,0	12,4	15,0	45,0	26,2	28,8	54,7	42,7	38,1	62,4	35,2	24,8	11,7	15,9
		Drift	-8,0	35,8	42,2	55,5	38,6	47,4	61,4	31,1	53,1	67,1	31,7	48,6	22,8	29,3
	R.M.S.(Ave.)		**-4,7**	**29,7**	**34,6**	**51,9**	**38,8**	**43,9**	**59,6**	**44,6**	**51,3**	**66,2**	**32,6**	**40,6**	**19,4**	**23,7**
Fundamental natural period (s)	**Pure sand**		0,48	0,925	0,924	0,925	0,925	0,924	0,925	0,925	0,924	0,925	0,914	1,365	1,366	2,05
	RSM		0,46	0,985	0,985	0,984	1,013	1,012	1,011	1,06	1,058	1,057	0,931	1,382	1,378	2,064
Period Lengthening Ratio				1,065	1,066	1,064	1,095	1,095	1,093	1,146	1,145	1,143	1,019	1,012	1,009	1,007

Table 6. 4. Numerical analyses comparison with literature.

Title	Software Preferred	Rubber - Soil Mixture Data	Modeled Structure	Structure's Foundation	Results
Rubber-Soil CUSHION for Earthquake Protection, Tsang et. al (2006)	Quad4M	Rubber Soil Mixture, with Dynamic Properties adopted from Experimental Data with per cent75 Rubber/Soil by volume published by Feng and Sutter (2000)	10 storey structure	Mat foundation with or without piles	On average, horizontal and vertical accelerations reductions were 30–40 per cent, 10–20 per cent respectively. TWSM acted as a mechanism for passive isolation, especially for near-field earthquakes that are rich in high-frequency wave components.
Utilization of Scrap Tires for Earthquake Hazard Mitigation, Tsang et. al (2006)	Quad4M	Rubber Soil Mixture, with Dynamic Properties adopted from Experimental Data with per cent75 Rubber/Soil by volume published by Feng and Sutter (2000)	10 storey structure	Mat foundation with or without piles	
Seismic Isolation by Rubbersoil Mixtures for Developing Countries, Tsang et. al (2008)	Quad4M	Rubber Soil Mixture, with Dynamic Properties adopted from Experimental Data with per cent75 Rubber/Soil by volume published by Feng and Sutter (2000)	10 storey structure	Mat foundation with or without piles	On average, horizontal and vertical accelerations reductions were 30–40 per cent, 10–20 per cent respectively. Acceleration response of structure could be reduced by more than 70 per cent at low periods. TWSM acted as a mechanism for passive isolation, especially for near-field earthquakes that are rich in high-frequency wave components.
Earthquake Protection by Tire-Soil Mixtures: Numerical Study, Tsang et. al (2009)	Quad4M	Rubber Soil Mixture, with Dynamic Properties adopted from Experimental Data with per cent75 Rubber/Soil by volume published by Feng and Sutter (2000) and Laminated Rubber Bearings as 2nd sample.	10 storey structure	Mat foundation with or without piles	
Protecting Underground Tunnel by Rubber-Soil Mixtures, Tsang et. al (2009)	Quad4M.	Rubber Soil Mixture, with Dynamic Properties adopted from Experimental Data with per cent75 Rubber/Soil by volume published by Feng and Sutter (2000)	**Underground Tunnels**	Concrete lining surrounded by RSM below pavement	On average, horizontal and vertical accelerations reductions were around 70 per cent, 60 per cent when placing TWSM below pavement.

Table 6.4 Numerical analyses comparison with literature (Con't).

Title	Software Preferred	Rubber - Soil Mixture Data	Modeled Structure	Structure's Foundation	Results
Geotechnical Seismic Isolation by Scrap Tire-Soil Mixtures, Tsang et. al (2010)	**New Finite Element Analysis Program Developed on Quad4M by Xuan (2009)**	Rubber Soil Mixture, with Dynamic Properties adopted from Experimental Data with per cent75 Rubber/Soil by volume published by Feng and Sutter (2000)	10 storey structure	Mat foundation with or without piles	On average, horizontal and vertical accelerations reductions were 30–40 per cent, 10–20 per cent respectively. Acceleration response of structure could be reduced by more than 70 per cent at low periods. TWSM acted as a mechanism for passive isolation, especially for near-field earthquakes that are rich in high-frequency wave components.
Seismic Isolation for Low-to-Medium-Rise Buildings Using Granulated Rubber–Soil Mixtures: Numerical Study, Tsang et. al (2012)	New Finite Element Analysis Program Developed on Quad4M by Xuan (2009)	Feng and Sutter (2000) Experimental Data with per cent75 Rubber/Soil by volume in mixture, the CTT data of Promputthangkoon and Hyde (2007), and unpublished results from cyclic simple shear tests Xiong et. al (2009)	10 storey structure	Mat foundation with or without piles	The normalized horizontal acceleration of the roof can be reduced by 50–70 per cent; normalized horizontal acceleration of the footing by 40–60 per cent; and normalized inter-story drift of the first floor by 40–60 per cent.
This Study	New Finite Element Analysis Program Developed on Quad4M by Xuan (2009)	Granulated Rubber Soil Mixture TCS, with changing mixng ratios adopted from Experimental Data published by Yıldız (2012)	4, 8, 12, 18 storey structures	Mat foundation with or without piles	The normalized horizontal acceleration of the roof can be reduced by 40–50 per cent; normalized horizontal acceleration of the footing by 25–30 per cent; and normalized inter-story drift of the first floor by 40–45 per cent.

7. CONCLUSION AND RECOMMENDATIONS

The fixed base design, conventional technique for seismic design of structures, is based on the concept of increasing the resistance capacity against strong ground motions by employing structural elements such as shear walls, braced frames, or moment-resistant frames. However, this strengthening strategy may lead to higher masses and seismic forces successively. More specifically, it may result in high floor accelerations or large interstorey drifts depending on subject structure's height and flexibility.

Accordingly, a methodology using passive and active control mechanisms for structure seismic response against earthquake activity has been developing since two decades nominated as seismic base isolation. It is used with natural rubber bearings, lead-rubber bearings, high damping rubber bearings, lead-rubber bearings, friction pendulum system and etc. These techniques were implemented worldwide in various structures such as residential buildings, bridges, power plants, and storage tanks.

As a newer methodology of using geosynthetic materials as structure isolation material has been proposed by Hushmand and Martin (1991), Kavazanjian *et al.* (1991) and Yegian and Lahlaf (1992). They placed geosynthetic liner underneath foundations of structures to defuse seismic activities' energy. The geosynthetic interface between the isolated structure and underlying soil, would limit transmission of horizontal accelerations. More recently, Tsang *et al.* (2006) proposed a second technique for geotechnical seismic isolation (GSI). They conducted numerical analyses with placing improved sandy soil by mixing of tire rubber, below structure's foundation against seismic movement. They found that structure's acceleration response would be decreased down to 70 per cent at low periods. In addition, they noticed that period lengthening ratio was increased up to 40 per cent in few cases.

This study is focused on use of tire crumb – sand mixture (TCS) GSI material around structures' foundations considering enhanced damping (D) and stiffness (G) properties of tire wastes, to mitigate earthquake hazardous effects. The exerted analyses are the preliminary research works on a potential seismic isolation method to dissipate earthquake energy, thus reducing structural response and minimizing the potential damage. Numerical analyses are conducted with low to medium rise structures under different earthquake records with different frequency content. TCS behavior is interpreted in terms of first floor inter-storey drift; horizontal accelerations at roof and foundation base mid points. Structure's fundamental period shift was also another point of concern.

The experimental data with Cyclic Triaxial Tests (CTT) on TCS and TBS were carefully analyzed for a proper numerical analysis material. The Damping Ratio D (per cent) versus Shear Strain γ (per cent) and Shear Modulus over Maximum Shear Modulus, G/G_{max} versus Shear Strain γ (per cent) curves displayed that soil dynamic behavior acquisition for earthquake hazards mitigation is appropriate due to especially granulated TC use. Their D and G data were extrapolated and interpolated with hyperbolic curve modeling to have a proper shear strain range of dynamic properties in numerical analyses.

The software developed on QUAD4M by Xuang (2009), capable to do time domain, 2-D Equivalent Linear Analysis of soil and structure system modeled with Finite Element Method FEM was used in this study as formerly used by Tsang *et al.* (2010, 2012).

From CTT data, it had been concluded that granulated TC inclusion to sand did considerably increase its D up to three times, and leaded to a considerable decrease of G depending on the TC per cent by weight ratio, at all γ values. TCS showed more linear behavior compared to Sand. Therefore it had been supposed that this TC – Sand mixing would be a remedy for mitigation of sand's earthquake hazards. Similarly, numerical analyses displayed the positive effect of TC inclusion to Sand sample at each strong

earthquake motion scenario. Remarkably, under each earthquake motion scenario, ideal TC per cent by weight for considerable fundamental period shift must be at least 30 per cent.

Considering soil effective confining pressure σ', numerical analyses results were not consistent to CTT results. The period lengthening ratio, all of the peak and RMS values of roof horizontal acceleration, footing horizontal acceleration, first floor drift were lowered under high σ'. Whereas, as the TC per cent by weight increased, D curves had shifted upward in CTT.

In numerical analyses, regarding the general drop in overall performances with the increase in structure's number of storey, structure weight; it must be concluded that this proposed GSI technique would have a limited effect when used under medium-high rise structures, and low-medium rise structures must be preferred in parallel with the literature.

A further conclusion is that, change in period lengthening ratio and peak shear strain percentage reduction with increasing TC ratio in TWSM is not relevant. Whereas the acceleration and horizontal drift reductions are more considerable. Resultantly, it cannot be obviously stated that increase of TC ratio leads to better TWSM subsoil behavior. Accordingly further analyses with lower TC/TCS by weight should be conducted to select the most optimistic TC/TCS value regarding applicability – economic aspects.

To stay consistent with the literature, TCS and pile foundation combination as a solution for weak soil strata had been subject to discussion. In numerical analyses they did not have a better GSI performance compared to TCS performed without piles under structures. Resultantly, this methodology should not be recommended for use underneath foundation with piles.

In the numerical analyses, the subsoil depths were claimed and modeled considering in-situ mixing method, because of the possible difficulties to be up risen with backfilling with increasing TCS subsoil layer depth.

Numerical analyses of eight and 12 story structures gave 40-60 per cent RMS acceleration and drift, whereas it was 50-70 per cent in previous studies where ten storey building was examined. Accordingly the granulated tire use with sandy soils weak against seismic activity can be proposed as a solution for low to medium rise concrete structures.

This comparative study proposes use of TCS as a new GSI material alternative for the first time in the literature. TCS energy absorption property is revealed as previously stated with the laboratory experiments. But the method should be subject to further discussions with numerical and physical modeling considering applicability of method according to in-situ conditions and also with lower TCS/TWSM ratio.

REFERENCES

Ahn K.J., P.L. Gould, 1992, "Interactive Base-Isolation Foundation System: II. Parametric Study", *Journal of Engineering Mechanics (ASCE)*, 118(10):2059–2071.

ASTM D 3999 – 91: *Standard Test Methods for the Determination of the Modulus and Damping Properties of Soils Using the Cyclic Triaxial Apparatus,* American Society for Testing and Materials.

ASTM D 6270-08, 2012*, Standard Practice for Use of Scrap Tires in Civil Engineering Applications*, American Society for Testing and Materials.

Baykal, G., A. Edinçliler, A. Saygılı, 2004, "Highway Embankment Construction Using Fly Ash in Cold", *Resources, Conservation and Recycling, Article in Press*, May 2004, Vol 42.

Bettees P., J.A. Bettees, 1991, "Infinite Elements for Dynamic Problems Pt.1", *Engıneering Computations,* Vol. 8, No.2, pp. 99-124.

Bosscher P. J., T.B. Edil, S. Kuraoka, 1997, "Design of Highway Embankments Using Tire Chips ", *Geotechnical and Geoenvironmental Engineering*, Vol. 123, No. 4, pp. 295-304.

Braja M. D., D. Emeritus, G.V. Ramana, 2010, "*Principles of Soil Dynamics*", Cengage Learning; Second Edition.

Buckle I.G., M. EERI, R.L. Mayes, 1990, "Seismic Isolation: History, Application, and Performance – A World View", *Earthquake Spectra,* Vol.6, No. 2.

Çağatay A., 2008, *Investigation of the Effect of Tire Waste Inclusions on the Shear Strength Parameters of Sand*, M.S. Thesis, Boğaziçi University.

Chopra A.K., 2006, *Dynamics of Structures Third Edition*, Prentice-Hall International, New Jersey.

Constantiou M. C., A. S. Mokha, M. A. Reinhorn, 1991, "Study of Sliding Bearing and Helical-Steel-Spring Isolation System", *Journal of Structural Engineering*, Vol. 117, No.4, April, 1991.

Constantopoulos I. V., J.M. Roesset, J.T. Christian, 1973, "A Comparison of Linear and Exact Nonlinear Analysis of Soil Amplification", *Proc. World Conf.*

COSMOS Virtual Data Center, 2013, *Worldwide Strong Ground Motion Records*, http://www.strongmotioncenter.org/vdc/scripts/default.plx.

Darendeli B. M., 2001, *Developement of a New Family of Normalize Modulus Reduction and Material Damping Curves,* Ph. D. Dissertation, Univ. of Texas at Austin.

Edeskar T., 2006, *Use of Tyre Shreds in Civil Engineering Applications: Technical and Environmental Properties,* Ph. D. Dissertation, Lulea University of Technology.

Edil T. B., P.J. Bosscher, 1994, "Engineering Properties of Tire Chips and Soil Mixtures", *Geotechnical Testing Journal*, Vol. 17, No. 4, pp. 453-464.

Edil, T.B., 2002, "Mechanical Properties and Mass Behavior of Shredded Tire Soil Mixtures", *Proceeding of the International Workshop on Lightweight Geomaterial*, Tokyo.

Edinçliler A., G. Baykal, A. Saygılı, 2010, "Influence of Different Processing Techniques on the Mechanical Properties of Used Tires in Embankment Construction", *Elsevier*.

Edinçliler A., G. Baykal, K. Dengili, 2004, "Determination of Static and Dynamic Behavior of Recycled Materials for Highways", *Elsevier/Resources.*

Feng, Z.Y., K.G. Sutter, 2000, "Dynamic Properties of Granulated Rubber/Sand Mixtures", *Geotechnical Testing Journal*, Vol. 23, No. 3, pp. 338-344.

Garga, V.K., V. O'Shaughnessy, 2000, "Tire Reinforced Earthfill, Construction of a Test Fill, Performance, and Retaining Wall Design", *Canadian Geotechnical Journal*, Vol. 37, pp. 75-96.

Goodarz A., 1995, "Overview of Base Isolation, Passive and Active Vibration Control Strategies for Aseismic Design of Structures", *Scientia Iranica,* Sharif University of Technology, Vol.2, No.2, July 1995.

Hudson M., I.M. Idriss, M. Beikae, 1994, *User's Manual for QUAD4M*, University of California Davis, California.

Humphrey D. N., W. Manion, 1992, “Properties of Tire Chips for Lightweight Fill, Grouting”, *Soil Improvement, and Geosynthetics, ASCE, Geotechnical Special Publication*, No. 30, pp. 1344—1355.

Humphrey D., T. M. Sandford, W. Cribbs, W. Manison, 1993, "Shear Strength and Compressibility of Tire Chips for Use as Retaining Wall Backfill", *Transportation Research Record 1422, Transportation Research Board,* 29-35, Washington.

Humphrey, D. N., L. H. Chen, R. Eaton, 1997, “Laboratory and Field Measurements of Tire Chips for Use as Subgrade Insulation”, *Transportation Research Board 76th Annual Meeting*, Washington.

Hyde A. F. L., P. Panu, 2007, *Compressibility and Liquefaction Potential of Rubber Composite Soils*, University of Sheffield, United Kingdom.

Idriss, I. M., 1990, “Response of Soft Soil Sites During Earthquakes”, *Proceedings, H. Bolton Seed Memorial Symposium*, Vol. 2, pp. 273-289, May,1990, Bolton, England.

Ishibashi, I., X. Zhang, 1993, “Unified Dynamic Shear Moduli and Damping Ratios of Sand and Clay”, *Soils and Foundations*, Vol. 33, No. 1, pp.182-191.

Ishihara, K., 1996, *Soil Behavior in Earthquake Geotechnics,* Oxford University Press Inc., New York.

Jong-Sub L., J. Dodds, J. Carlos Santamarina, 2007, “Behavior of Rigid-Soft Particle Mixtures”, *Journal of Materials in Civil Engineering,* ASCE, February-2007.

Juang C. H., R.D. Andrus, Zhang J., 2005, “Normalized Shear Modulus and Material Damping Ratio Relationships”, Journal of Geotechnical and Geoenvironmental Engineering, Apr.-2005.

Kawamura S., I. Nagashima, K. Kitazawa, M. Hisano, 1988, “Study on a Sliding-Type Base Isolation System, Multi-Dimensional Response Analysis”, *Proceedings of Ninth World Conference on Earthquake Engineering August 2-9,* (Vol. V), Tokyo-Kyoto, JAPAN.

Kelly J. M., 1982, “Aseismic Base Isolation”, *Shock and Vibration Digest,* 14(5):17-25.

Kelly J. M., 1986, “Aseismic Base Isolation, Review and Bibliography”, *Soil Dynamics and Earthquake Engineering,* 5-4:202-217.

Kelly J. M., 1994, "The Implementation of Base Isolation in the United States", *Earthquake Engineering, Tenth World Conference,* Balkerna, Rotterdam.

Kelly J. M., 1998, "Seismic Isolation of Civil Buildings in the USA", *Progress in Structural Engineering and Materials,* Vol I (3): 279-285.

Kelly J. M., S.B. Hodder, 1982, "Experimental Study of Lead and Elastomeric Dampers for Base Isolation Systems in Laminated Neoprene Bearings", *Bulletin of the New Zealand National Society for Earthquake Engineering,* 15-2.

Kim H.K., Santamarina J.C., 2008, "Sand-Rubber Mixtures (Large Rubber Chips)", *Canadian Geotechnical Journal,* 45: 1457 – 1466.

Lee, J. H., R. Salgado, A. Bernal, C. W. Lovell, 1999, "Shredded Tires and Rubber-Sand as Lightweight Backfill", *Journal of Geotechnical and Geoenvironmental Engineering*, Vol. 125, No. 2, pp. 132–141.

Lin Su, G. Ahmadi, I.G. Tadjbakhsh, 1991, "Performance of Sliding Resilient-Friction Base Isolation System", *Journal of Structural Engineering,* Vol.117, No.1, January, 1991.

Lysmer J., R.L. Kuhlemeyer, 1969, "Finite Dynamic Model for Infinite Media", *Journal of the Engineering Mechanics Division,* Vol. 95 No. 4 EM pp.859-877.

Martelli A., 2006, "Modern Seismic Protection Systems for Civil and Industrial Structures", *Samco Final Report.*

Martelli A., M. Forni, 1998, "Seismic Isolation of Civil Buildings in Europe", *Progress in Structural Engineering and Materials,* Vol I (3): 286-294.

Masad E., R. Taha, H. Carlton, T. Papagiannakis, 1996, "Engineering Properties of Tire/Soil Mixtures as a Lightweight Fill Material", *Geotechnical Testing Journal,* September 1996, Vol. 19, No. 3, pp. 297 – 304.

Matsagar V. A., R. S. Jangid, 2008, "Base Isolation for Seismic Retrofitting of Structures", *Practice Periodical on Structural Design and Construction,* vol. 13, No. 4, pp. 175 – 185.

Mengi Y., A.K. Tanrikulu, 1992, "Absorbing Boundary Conditions in Soil-Structure Interaction Analyses", *Development in Dynamic Soil Structure Interaction,* vol. 390 of C: Math and Physical Sciences, Klumer Academic Publishers.

Menq F.Y., 2005, *"Dynamic Properties of Sandy and Gravelly Soils"*, Ph. D. Dissertation, Univ. of Texas Austin.

Mokha A., M.C. Constantinou, A.M. Reinhorn, V.A., 1991, "Experimental Study of Friction-Pendulum Isolation System", *Journal of Structural Engineering*, Vol. 117, No. 4, pp. 1201-1217. Apr. 1991.

Moo-Young H., K. Sellasie, D. Zeroka, G. Sabnis, 2003, "Physical and Chemical Properties of Recycled Tire Shreds for Use in Construction", *Journal of Geotechnical and Geoenvironmental Engineering,* Vol. 129, No. 10, pp. 921-929.

Naeim F., Kelly M.J., 1999, *Design of Seismic Isolated Structures From Theory to Practice*, Wiley, New York.

Promputthangkoon P, A. Hyde, 2007, "Compressibility and Liquefaction Potential of Rubber Composite Soils", *Geomaterials: Opportunities and Challenges: Proceedings of the International Workshop on Scrap Tire Derived Geomaterials*, 23–24 March 2007, Elsevier, Amsterdam.

Ribay, E. D., R. Maigre, R. Cabrillac, D. Gouvenot, 2004, "Shear Modulus and Damping Ratio of Grouted Sand", *Soil Dynamics and Earthquake Engineering,* Vol. 24, pp. 461-471, 2004.

RMA, 2009, *Scrap Tire Markets in the United States, Rubber Manufacturers Association Report*, ttp://www.rma.org/publications/scrap_tires/index.cfm?PublicationID=11517.

Saarazin M., M. Moroni, R. Boroscheck, P. Soto, 1996, "Results from a Base-Isolated Experimental Building in Santiago-Chile", *11th Conference on Earthquake Engineering*, Paper No. 1329, Elsevier Science Ltd.

Sajal K. D., P. K. Dilip, 2000, "Seismic Response of Buildings Isolated By Sliding-Elastomer Bearings Subjected To Bi-Directional Motion", *12World Conference on Earthquake Engineering*, 30 January – 03 February, New Zealand.

Scrap Tire Management Council, 2010, "Used Tire Facts and Information - What To Do With All These Tires?", *http://www.epa.state.il.us/land/tires/used-tires-facts-and-information.html*.

Senetakis K., A. Anastasiadis, K. Pitilakis, 2009, "Dynamic Shear Modulus and Damping Ratio Curves of Sand/Rubber Mixtures", *Earthquake Geotechnical Eng. Satellite Conf.*, 2-3.10.2009.

Senetakis K., A. Anastasiadis, K. Pitilakis, 2011, "Experimental Investigation of The Dynamic Properties of Granular Soil/Rubber Mixtures Using a Resonant Column Device", *5ICEGE*, 10-13, Jan.-2011, Santiago, Chile.

Sun, J.I., R. Golesorkhi, H.B. Seed, 1988, *Dynamic Moduli and Damping Ratios for Cohesive Soils Report*, Univ. of California at Berkeley, UCB/EERC-88/15 48 pp.

T.T. Soong, M. C. Constantinou, 1994, *Passive and Active Structural Vibration Control in Civil Engineering*, Springer New York.

Taylor A. W., T. Igusa, 2004, *Primer on Seismic Isolation,* ASCE, Reston.

Tsang H.H., 2008, "Seismic Isolation by Rubber-Soil Mixtures for Developing Countries", *Earthquake Engineering Structural Dynamics,* 37:283 – 303.

Tsang H.H., H. Fong Fiona, X. Xu, S.H. Lo, 2007, *Utilization of Scrap Tires for Earthquake Hazard Mitigation*, Uni. of Hong Kong, Dept. of Civ. Eng. Research.

Tsang H.H., M. Sheikh, M. Neaz, T.K. Lam Nelson, 2007, *Rubber-Soil CUSHION for Earthquake Protection*, Uni. of Wollongong, Sch. of Civil, Mining and Env. Eng. Research.

Tsang H.H., S.H. Lo, X. Xu, M.N. Sheikh, 2012, "Seismic Isolation for Low-to-Medium Rise Buildings Using Granulated Rubber-Soil Mixtures: Numerical Study", *Earthquake Engng Struct. Dyn*.

Tsang H.H., T.K. Lam Nelson, S. Yaghmaei-Sabegh, M. Sheikh, I.B. Neaz, 2010, "Geotechnical Seismic Isolation by Scrap Tire-Soil Mixtures", *Recent Advances in Geotech. Earthquake Eng. And Soil Dyn.,* 5th Int. Conference, San Diego, California.

Tsang H.H., X. Xu, M.N. Sheikh, 2009, "Earthquake Protection by Tire-Soil Mixtures", *NZSEE Conference*.

UNCTAD Flagship Reports, 1998, *Recycle, Reuse or Disposal Alternatives for Scrap Tires*, http://unctad.org/en/Pages/Publications.aspx.

Vucetic, M., R. Dobry, 1991, "Effect of Soil Plasticity on Cyclic Response", *ASCE, Journal of Geotechnical Engineering*, Vol. 117, No. 1, pp. 89-107.

Wood D. M., 2004, "*Geotechnical Modelling*", Spon Press, New York.

Xu Xuan, 2009, *Earthquake Protection of Low to Medium Rise Buildings Using Rubber-Soil Mixtures*, Ph. D. Dissertation.

Yegian M.K., F. Asce, and U. Kadakal, A.M.ASCE, 2004, "Foundation Isolation for Seismic Protection Using a Smooth Synthetic Liner", *Journal of Geotechnical and Geoenvironmental Engineering*.

Yegian M.K., G. Gazetas, P. Georgarakos, 2005, "In-Ground Isolation Using Geosynthetic Liners", *9th World Seminar on Seismic Isolation, Energy Dissipation and Active Vibration Control of Structures,* Kobe, Japan.

Yegian M.K., L.C. Mullen, C.Y. Chang, G. Mylonakis, 2001, "Soil-Structure Interaction Under Dynamic Loading for both Shallow and Deep Foundations", *4th International Conference on Recent Advances in Geotechnical Earthquake Engineering and Soil Dynamics and Symposium in Honor of Prof. W.D. Liam Finn,* San Diego, California

Yegian M.K., U. Kadakal, 1998, "Geosynthetic Interface Behavior Under Dynamic Loading", *Geosynthetics International, Vol. 5, No. 1-2, pp. 1-16.*

Yegian M.K., U. Kadakal, M. Catan, 1994, "Geosynthetics for Earthquake Hazard Mitigation", *Northeastern University*, Boston, MA.

Yıldız Özgür, 2012, *Investigation on the Mitigation of Earthquake Hazards with Inclusion of Tire Wastes into the Sand,* M.S. Thesis, Boğaziçi University.

Yoon, Y. W., S. B. Heo, K. S. Kim, 2008, "Geotechnical Performance of Tire Wastes for Soil Reinforcement from Chamber Tests", *Geotextiles and Geomembranes,* Vol.26, pp. 100-107

Zhou F.L., 2001, "Seismic Isolation of Civil Buildings in the People's Republic of China", *Prog. Struct. Engng Mater.,* 3: 268d276.

Zhou F.L., P. Tan, Q. Xian, X. Huang, Z. Yang, 2006, "Research and Application of Seismic Isolation System for Building Structures", *Journal of Architecture and Civil Engineering,* Vol.23 No.2.